ADDIS ABABA UNIVERSITY
ADDIS ABABA INSTITUTE OF TECHNOLOGY
AFRICAN RAILWAY CENTER OF EXCELLENCE

Numerical Simulation and Analysis of Railway Tunnel Deformation and Supporting System

A case of Awash-Kombolcha-Hara Gebeya Railway Project (Tunnel T-07)

A Thesis in Railway Engineering (Civil Infrastructure)

By

Ivan NYAKANA

JUNE, 2019

A Thesis to School of Graduate Studies of Addis Ababa Institute of Technology Submitted in Partial Fulfillment of the Requirements for the Degree of Master of Science

Railway Engineering (Civil Infrastructure)

The undersigned have examined the thesis entitled '**Numerical Simulation and Analysis of Railway Tunnel Deformation and Supporting System** presented by **IVAN NYAKANA**, a candidate for the degree of **Master of Science Railway Engineering (Civil Infrastructure)** and hereby certify that it is worthy of acceptance.

Im Soo Been, Ph.D./P.E/PMP		
Advisor	Signature	Date
Henok Fikre, Dr.-Ing		
Internal Examiner	Signature	Date
Tensay Gebremedhin, Dr.		
External Examiner	Signature	Date
Mr. Zewdie Moges		
Chairperson	Signature	Date

DECLARATION

Thesis presented in partial fulfillment of the requirements for the masters of degree at Addis Ababa University.

Following this, I grant the university the nonexclusive royalty-free right to archive, reproduce, distribute and display the thesis in any and/or all forms, including electronic format, via any digital library maintained by AAU/AAiT.

I certify that research work titled "**Numerical Simulation and Analysis of Railway Tunnel Deformation and Supporting System**" is my own work. The work has not been presented elsewhere for assessment. Where material used from other sources, it has been properly acknowledged/referred.

…….....

IVAN NYAKANA

Id No: GSR/1778/10

ivannyakana@gmail.com

ivan.nyakana@aait.et.edu.et

ABSTRACT

Analysis of tunneling requires proper estimation and prediction of deformations and tunnel supporting system forces in both the shotcrete and lining. In most recent years there has been a rapid increase in the calculation power and improvements of most analysis software that allow the use of complex numerical analyses in tunnel design. Tunneling rock mass has demanded a better understanding of the behavior of tunnel excavation and supporting system for stability purposes.

A study on tunnel analysis using numerical finite element method using Structure Medium Analysis Program was explored in this dissertation.

Numerical simulation by finite element analysis using SMAP provides an alternative to answer ground settlement, displacements and lining forces since tunneling induces, ground deformation and shows influence of rock mass overburden and geological conditions on the tunnel deformations and supporting system forces. Thus, the problem of stability requires an independent study for each tunnel rock mass zone. The study revealed analysis by numerical simulation by SMAP reported high values in the result compared to the analytical formulation used. From the results of the maximum displacment predicted at the tunnel crown recorded displacement of 50.23 mm and safety factor 2.19. For tunnel excavation stability, the Saftey Factor greater than 1 was computed. In addition, the ground surface dispalacments varies depending on rock mass condition and is higher in lower over burden rock mass. Using numerical solution by FEM for computed maximum displacements around the tunnel revealed higher values in maximum rock mass overburden but also varied depending on the rock mass conditions.

In this study, an ultimate compressive major principal stress of $2{,}020\ \mathrm{kN/m^2}$ was comuputed for the main tunnel and the corresonding supporting system design forces in the final lining i.e liner bending moment of 107.84 kNm, thrust/axial force of $1{,}265$ kN and Shear force of 450.98 kN was simulate for Tunnel T07 rock mass and the rock bolt pattern for each rock bolt with an ultimate load capacity of $230\ \mathrm{kN/m^2}$, for diameter 26 mm diameter and fully grouted rock bolts was estimated numerically.

Keywords: *Numerical Simulation, Tunnel Deformation, Supporting System and SMAP*

ACKNOWLEDGMENTS

This work has been much challenging me alone to complete and I would like to express my gratitude to those who gave assistance during my work on this thesis. I will give special thanks to the following;

Im Soo Been, Ph.D./P. E/PMP my Advisor - For his guidance and great interest in the tunneling project, which would not have been the same without his interest in Ethiopian geotechnical and geology.

Dr. Kim – For his guidance and inspiration, giving the opportunity to use SMAP "Structure Medium Analysis Program" Software from Comtec Research for modeling and analysis.

Yapi Merkezi Ethiopia Team - For allowance to visit the site for a study tour in November 2018 especially on Tunnel T-07, Awash-Kombolcha-Hara Gebeya Railway Project and for availing and giving me all relevant data related to my work.

Ethiopian Railways Corporation, ERC - For giving me the opportunity as the Client to the Awash-Kombolcha-Hara Gebeya Railway Project and for their interest in the thesis Special thanks to employees of ERC at the Head office and at the project site for helping with the selection of case study and AAiT staffs for support of allowance.

To my colleagues: Thank you all for moral, social and academic support you have rendered throughout this master's program each in your respective capacities. May God bless you for me!

To my Family: Thank you, Mom, for encouraging me. After reading my thesis title, I hope you are not afraid of people driving through underground tunnels. Believe me, when I say, most of them are safe. My Brother Adam Nyakana, Auntie Dr. Jacent K. Asiimwe Ph.D., and Uncle Andrew Muguwa for the support, mentorship, and encouragement throughout the studies.

Finally, I would like to give thanks to God for giving me the strength, wisdom and the opportunity that let me have my thesis

TABLE OF CONTENTS

LIST OF TABLES

LIST OF FIGURES

ABBREVIATIONS

A_s	Area – Steel
c	Cohesion – Soil/Rock
c'_m	Cohesion – Rock mass
D	Tunnel diameter
d_b	Rock bolt diameter
E	Modulus of Elasticity – Soil/Rock
E'_m	Elastic modulus – Rock mass
EA	Axial Stiffness
E_c	Modulus of Elasticity – Concrete
E_s	Modulus of Elasticity – Steel
f_{cd}	Design compressive strength – Concrete
$f_{ck,cube}$	Characteristic cube compressive strength – Concrete
$f_{ck,cyl}$	Characteristic cylindrical compressive strength – Concrete
FEM	Finite Element Model
f_{yd}	Design yield strength – Steel
f_{yk}	Characteristic yield strength – Steel
GRC	Ground Reaction Curve
GSI	Geological Strength Index
k	Hydraulic conductivity
K_0	Coefficient of earth pressure at rest
k_{rb}	Rock bolts stiffness
k_{sc}	Shotcrete stiffness
l	Free length of the bolt
$k_{support}$	Total stiffness of the support
m_b	Resistant coefficient from Hoek-Brown criteria
M_d	Design bending moment
M_k	Characteristic value for bending moment
N_d	Design axial force
N_k	Characteristic value for axial force
H_{OB}	Overburden
p_v	In-situ pressure
p_i	Internal pressure
$p_{max,rb}$	Maximum rock bolts design pressure
$p_{max,sb}$	Maximum supporting beams design pressure
$p_{max,shotcrete}$	Maximum shotcrete design pressure
$p_{max.support}$	Maximum total support design pressure
RMR	Rock Mass Rating
RQD	Rock Quality Designation

s	Resistant coefficient from Hoek-Brown criteria
s_c	Circumferential bolt spacing
SF	Safety factor
T_{bf}	Ultimate bolt load obtained from a pull-out test
t_c	The thickness of the shotcrete layer
t_h	The thickness of the shotcrete layer
ULS	Ultimate Limit State
u_r	Tunnel walls radial displacement
$V_{rd,cd}$	Design shear capacity
g	Unit weight – Soil/Rock
γ_c	Partial factor on concrete
γ_{load}	Coefficient of the load's amplification as per Eurocode 2
γ_s	Partial factor on steel
ϕ	Diameter
ϕ_m	Friction angle – Soil/Rock mass
v	Poisson's ratio – Soil/Rock
v_c	Poisson's ratio – Concrete
v_s	Poisson's ratio – Steel
σ_{cc}	Uniaxial compressive strength – Concrete

CHAPTER 1 INTRODUCTION

1.1 Introduction

The rapid increase in the calculation power and improvements of most analysis software has allowed the use of complex numerical analyses in tunnel design. The aim of such analyses is the prime balance between accuracy and complexity, as the latter increases the time and cost of the design. Additionally, the increasing demand to construct tunnels of large size in relatively difficult ground conditions often under significant overburden heights dictates the need to adopt new approaches in the early stages of design such as using numerical approach by Finite Element Method. [1].

In the early design stage, some tunneling problems are analyzed using simplified approaches including 2-D finite element analyses but certain tunneling problems demand the use of advanced 3-D numerical models to calculate, with reasonable accuracy, and considering critical parameters [2].

Bestowing to the traditional methods of tunnels construction critical decisions the selected supporting system methods and the employed excavation schemes are based mainly on the results of the geotechnical investigation with key interest on rock-mass classifications. These classifications are made based on geological observations, exploration, in-situ tests and reliable laboratory test results, with the use of well-known systems, such as the Rock Mass Rating by Bieniawski 1989 or Geological Strength Index by Hoek and Brown 1997.

The purpose of this study is to present a new approach to geotechnical tunnel analysis in order to estimate and predict the tunnel deformation and failure mechanisms of the excavated rock-mass behavior surrounding an unsupported railway tunnel and the design of the supporting system.

1.2 Problem Statement

Railway transport infrastructures have regained their importance due to their efficiency and environmentally friendly technologies worldwide. This has led to higher axle loads, increasing train speeds, and more frequent train usage. However, these improved service provisions have posed new challenges to railway infrastructure crossing difficult topography in hilly and mountainous areas thus calling for tunnel

construction and engineering need.

However, these transportation tunnel structures are highly prone to failure and collapse. Also, unsuccessful failed tunnel structures give rise to both in social and economic clamor [3]. The main failures and hazards of tunnel and underground structures consistently result from geology-geotechnical conditions/their realistic estimation, construction methodology such as tunnel depth, design and analysis approach with importance predominately related to the profound knowledge of ground conditions, workability issues and contractor experience [3, 4].

Therefore, understanding of geological-geotechnical ground conditions is critical to ensure safe and stable tunnel construction [5]. The instability could occur for four different reasons: block rotation, sliding along a joint, overstressing of the rock mass or horizontal stresses [6, 7]. According to [8], challenging ground varies comprising hard, abrasive, weak, squeezing and swelling material, rock bursts and discontinuities such as faults, fissures and joints; most of which can only be accurately assessed when the ground is exposed during excavation. Additionally, rock mass is naturally very diverse and impossible to generalize its properties, behavior, design and suitable construction methods.

There are many existing classification methods including geomechanics Classification System (RMR, Bieniawski, 1989), the Q-system (Barton et al., 1974 & Barton, 2002), the Geological Strength Index (GSI, Hoek and Brown, 1997), used in many tunnel cases and have been applied in many evaluations about the stability of practical tunnel surrounding rock mass. Nevertheless, the aforementioned methods could not quantitatively calculate the stress redistribution stimulated in tunneling works [9]. On the other hand, the finite element method could offer the displacement of the surrounding rock mass, stress redistribution, the plastic zone distribution, and other useful ground predictions and estimations that can help to quantitatively evaluate the stability of the surrounding rock mass [9, 10].

It was against this background of the aggravated need for understanding capabilities of numerical analysis method through use of adequate tunnel analysis software that this study was undertaken. Comparatively speaking, a new approach of numerical analysis

using Finite Element Method (FEM) to estimate underground tunnel deformation reveals distinct advantage for understanding the response of rock mass behavior and the installed tunnel supporting system behavior during the early stage of project planning and post-construction stage.

1.3 Purpose of the Study

In tunnel design, the need is to ensure adequate stability for a durable and serviceable tunnel. Tunnels deformations and supporting systems of tunnels are studied. However, tunnel stability being an important element in the serviceable tunnel. Tunnel deformations and supporting system need enormous attention and study. The basic inspiration to the research is that the instability problem informs of deformations and the pre-stress support system efficiency in resisting the surrounding rock mass.

Therefore, the assembly of benefits and advantages realized through the better understanding of the surrounding rock mass behavior, geotechnical analysis method and supporting system behavior by numerical method using finite element analysis that could keep the tunnel stability are present in this study. The study presented was limited to relevant literature on tunneling, geotechnical engineering, soil, and rock mechanics principles.

Hence, the significance of the research accounted for an improved understanding of the section parameters, their correlation and their effect on tunnel stability and convergence while suggesting the use of numerical simulation and analysis of railway tunnel deformation and supporting system behavior.

1.4 Objective of the Study

1.4.1 Main objective

The aim of this research is to study tunnel deformations and supporting system forces using numerical method by finite element analysis in order to predict tunnel behavior and check tunnel stability.

To assure a safe balanced state of the main tunnel studied sections, numerical simulation, and analysis by SMAP-S2 Static analysis on all deformations and stress distributions of the main tunnel sections is presented in this study.

1.4.2 Specific objectives

The specific objectives include; -

1. Geological and geotechnical ground conditions of the surrounding rock mass were determined.
2. Static Two-dimension modeling of tunnel excavation and supporting system behavior was simulated using Structure medium analysis program (SMAP).
3. Analysis of factors influencing tunnel behavoir at depth thereby a comparison study of each section for main tunnel stability were undertaken.

1.5 Location

The research presents numerical simulation and analysis of railway tunnel deformation and supporting system a case of Awash-Kombolcha-Hara Gebeya railway project, (Tunnel T07) located in Amhara Region. The project stretched between km 261+380 to 261+760 along the Awash-Kombolcha-Hara Gebaya single-track railway line. Tunnel T07 has a length of about 287 m. It has a maximum cover is about 320 m. For this research, in particular, the overburden is about 20m found at 261+540 for section 4 and 40m found at 261+641and 261+680 for section 2 and section 5 respectively that is and where the research proceeds doing the objective of the study at these sections.

1.6 Scope and Limitation of the study

This study employed use of a static two-dimensional numerical analysis approach by SMAP for modeling of surrounding rock mass and supporting system components namely rock bolt and shotcrete lining. Analytical rock load calculations used in tunneling from the literature were used to validate the tunnel behavior results from the numerical output. Furthermore, an analysis on seismic and water pressure might reveal that stresses and deformations increase in tunnel structures thus rendering them to more instable during and after construction but these were not included in this study.

1.7 Methodology

To perform this study a finite element analysis Structure Medium Analysis Program was utilized. Structure Medium Analysis Program includes special programs TUNA Plus that employs SMAP-S2 developed especially for the static analysis of different kind of tunnels under different geotechnical conditions. Based on selected parameters,

the general tunnel behavior is checked along with some analytical rock load calculations for validation purposes.

1.7.1 Data Collection

- Tunnel geometry, ground condition, and supporting system material properties data taken from the AKH project Tunnel T07

1.7.2 Available Resources

The available resources used include hardware and software for doing the virtual simulations of the developed model. The resources required in achieving this study included:

- Computing hardware/ Personal computer (Laptop)
- Application software SMAP for FE simulation.

1.7.3 Approach

- Description of the geologic architecture of the study area defining geotechnical parameters for the rock mass and the ground type performed herein.
- Exploration data, in situ tests results, laboratory tests and results, geotechnical properties and the design parameters of the excavated underground tunnel acquired.
- Developed numerical 2-D model and simulation of tunnel behaviors and Finite Element Method by SMAP-S2 used for Static analysis and calculation. This section includes at boundary distances, mesh refinement and calibration.
- A summary of output results was developed for all dispalcments, stresses, safety factor and lining member forces include analytical solutions for validation.

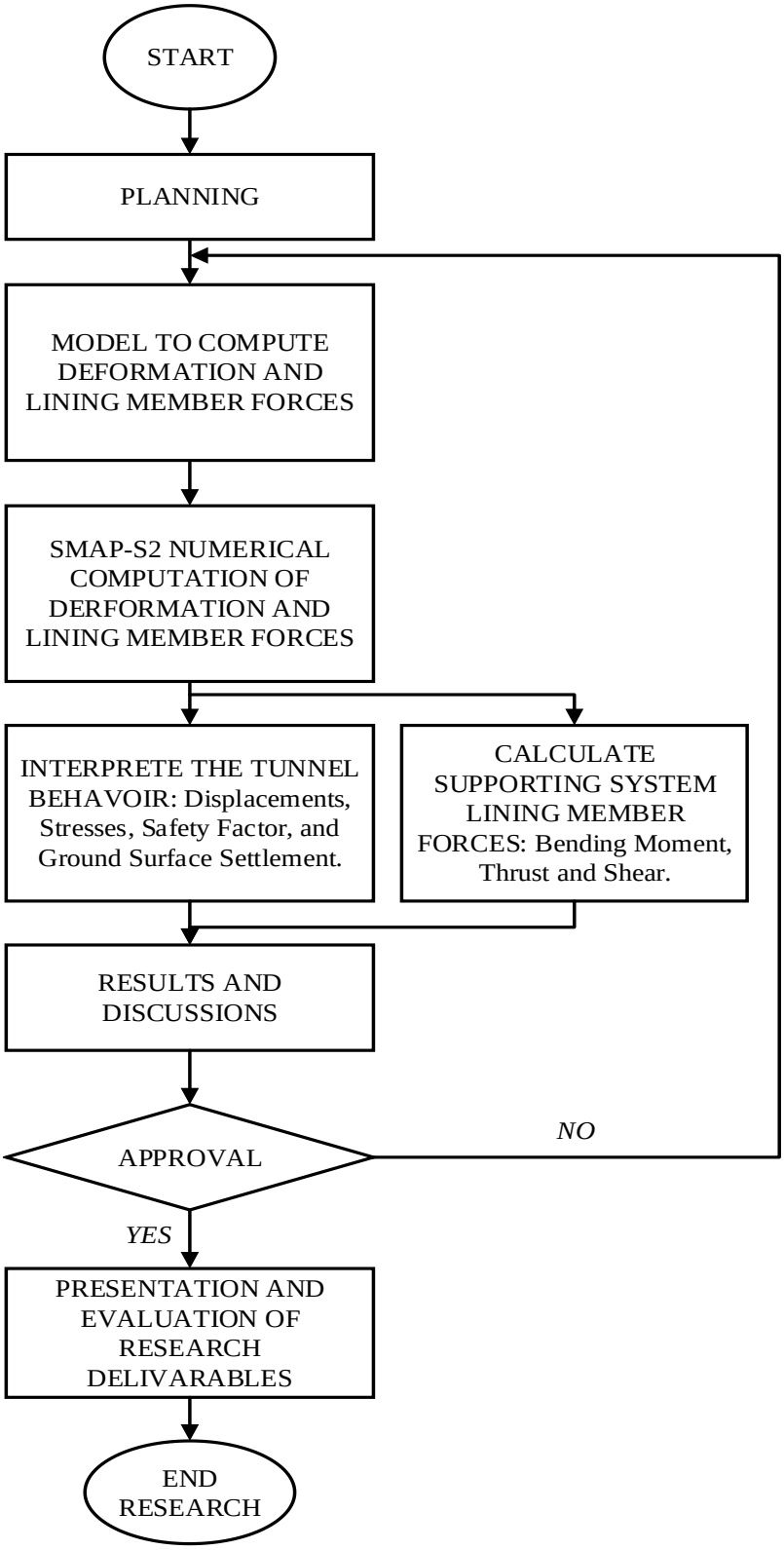

Figure 1- 1 Flow Chart of the basic procedure of Numerical Simulation

1.8 Outline of the Research

The thesis is presented in the following chapters. The arrangement of the thesis is described below.

- Chapter 1 gives a brief introduction and background for the study to the research and arrangement of the thesis. The objective, the scope, and the research methodology are found in this chapter.
- Chapter 2 Literature Review on tunnel excavation behaviors, rock mass and geotechnical studies and tunnel supporting system d. The theoretical background related to other numerical approaches other than the FE approach for analysis of underground structures is reported.
- Chapter 3 discusses the methodology on project analysis and design for Railway Tunnel T07 construction with analytical equations for calculating rock mass loadings and support pressure capacity of the tunnel supporting system are presented herein.
- Chapter 4 discusses modeling using Structure Medium Analysis Program including SMAP-S2 finite element analysis. The FE approach of the numerical simulation of the predicted tunnel behavior including displacements, stresses, safety factor, lining analysis of thrust, bending moment and shear force presented.
- Chapter 5 Results and discussions: this part contains the numerical analysis result of studied tunnel sections along with a discussion on verification of the numerical results have been presented. The behavior of surrounding rock mass on tunnel displacement, stress, and liner forces in the liner on the tunnel done and presented.
- Chapter 6 Conclusions and recommendations, in the final chapter, the study topic has been concluded and further research areas have been suggested.

CHAPTER 2 LITERATURE REVIEW

2.1 Introduction

Underground tunnels are horizontal civil or mining engineering structures whose lengths are either longer than twice the diameter of the tunnel or the sum of both the diameter and height of the tunnel structure [5]. Usually tunnels are underground structures through the ground in topography areas where surface construction is constrained, [11]. Constraints to surface construction are due natural barriers such as hills and mountains and or rivers or lakes, populated municipalities, existing infrastructure or other existing land uses. Underground tunnels reduce the demand for land and can be distinguished by the material and/or structure overlying it. A tunnel overlain by a road or railway may be called a subway, but when it passes underneath a canal it may be referred to as an underpass, aqueduct or a subaqueous tunnel [3].

The first underground constructions were for defense and mining functions. Authors [12] stated that the earliest examples are the salt mine in Hallstatt (B.C. 2500), and flint mines in France and European countries (B.C. 2000). The typical railway tunnel is about 5m x 7m for a single-track tunnel and about 8.5m x 7m high in case of twin tracks. The gradient should be less than 1%. The horseshoe form is the most common type. However, also circular form with segmental concrete cast iron lining also been constructed. [12].

In [13] there was a proposed empirical design tool for tunnels in the rock. Terzaghi assumed a tunnel with a depth greater than 1.5 times (w + h) where w is the width of tunnel and h is the height of the tunnel. He used nine varieties of rock to ascertain this style table. The definitions of those rock sorts are additional qualitative than quantitative. Therefore, this classification system is highly designer dependent. [14].

According to Kastner [15] “support pressure” has been defined as, referring to all effects of the induced state of stress which occur in the rock mass surrounding an unsupported excavation or which are in interaction with support and which load the support system. Thus, support pressure relates to a phenomenon caused by engineering activities but does not apply to virgin stresses. According to Marie [16] rock strength for tunneling purposes is its resistance to deformation. According to Palmstrøm_et.al and Rønning [17, 18], during underground excavation, it is vital to own a detailed visual observation of the rock surface within the whole tunnel edge before the rock is roofed by sprayed concrete. Rock mass

stability is influenced by several parameters, but the following three factors are the most important; - Degree of jointing (block size), Joint friction, and stress.

2.1.1 Rock mass classification

According to [19], rock mass characterization is an integral part of rock engineering practice. Usually, empirical design methods based on rock mass classifications systems provide quick assessments of the support requirements for underground excavations at any stage of a project, even if the available geotechnical data are limited. The underground excavation business tends to adjoin empirical approaches like rock mass classification strategies, which provide a rapid means of assessing rock mass quality and support requirements. There are many different systems for rock mass classification. For natural reasons the Q-system developed between 1971 and 1974 [20] is the one most especially used. In 1974, Bieniawski proposed the Rock Mechanics Rating system developed by assigning rating values to the uniaxial compressive strength of intact rock, Rock quality designation, and Spacing, Orientation, Condition of Discontinuities, and Groundwater conditions [21]. Bieniawski proposed a table in which the recommended support types and the properties of these support types based on these RMR values can be found [14] Another way of determining the stresses at the tunnel is that the one derived from stress distribution around a circular gap. This formula comes by inserting the horizontal stress in tunnels:

$$\sigma_h = K.\sigma_V \qquad (2.1)$$

2.1.2 Geotechnical considerations for tunneling

Researchers including [5, 3] discussed that knowledge on geotechnical engineering analysis methods to design and construct rock tunnels is limited. Geology highlights lithological properties assessed visually and by hand whereas geotechnical engineering emphasizes overall mechanical strength measured by testing materials. Rock loads, structural stability, modes of failure and applicable theoretical failure criterion used in the analysis of underground tunnel deformations, structural supports to maintain stability of the tunnel structure and the rock support interactions.

According to Geol and NEH [22, 23], knowledge of the stress field existing in a particular region prior to tunneling is essential. Measurement of in situ stresses has shown that in many cases measured stresses are anomalous, in the sense that the horizontal stresses cannot be attributed to gravity load, even when allowances are made for variations in surface level.

This anomaly is believed to be a result of tectonic stresses which are caused by movements and strains in the earth "plate" or the "continent" of the region under consideration.

2.1.3 Stresses around Underground structures

During and after excavation a stress release of the rock mass occurs and the rock mass nearest to the tunnel opening takes more loads. During this same process, the rock mass expands into the tunnel opening. Figure 2.2 presents a tunnel section; revealing how the rock mass surrounding the tunnel deforms after excavation has been carried out. The rock mass deforms about 0.5D ahead of the progressing face and reaches its maximum value about 1.5D behind the face [24]

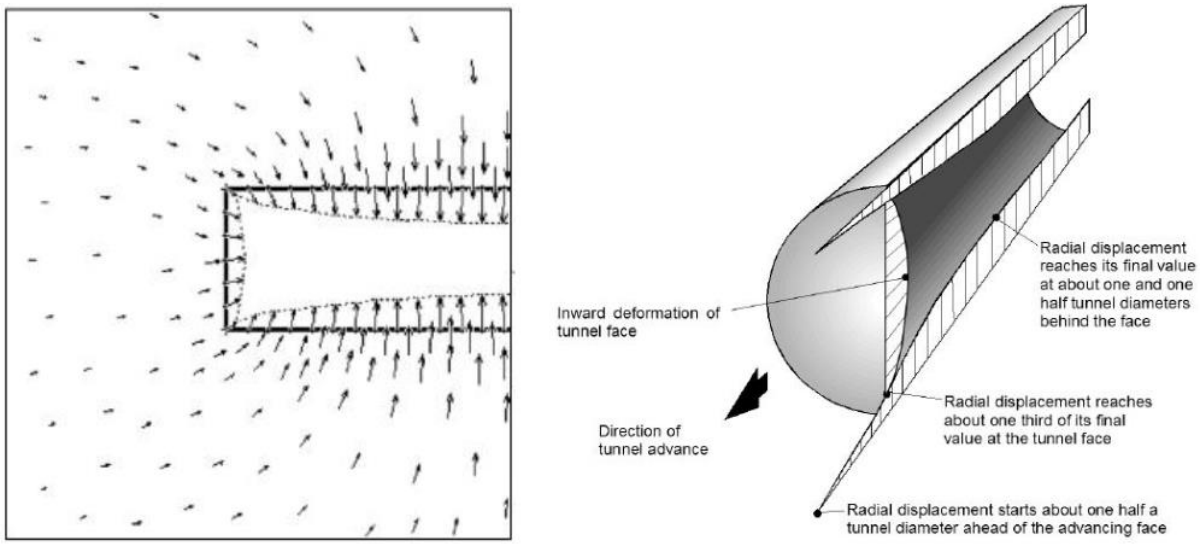

Figure 2-2 Shape of the deformed and the deformation tunnel outline

Figure 2.1 presents an FE Model for a circular tunnel, showing the displacement vectors as well as the shape of the deformed tunnel profile and the deformation in the rock mass surrounding an advancing tunnel excavation. [24].

According to [25], Kirsh's equations for circular openings can be applied giving the radial, tangential, shear stress, and displacements at any point. Usually, the elastic behavior of the rock mass where k is the stress ration in the original rock mass assumed.

In all cases $r \geq r_i$.Thus the displacements can be calculated from them equations below;

$$u_r = \frac{\sigma_v \cdot r_i^2}{4 \cdot G_\gamma} \cdot \left[(1 + k) - (1 - k) \cdot \left(4 \cdot (1 - v) - \frac{r_i^2}{r^2} \right) \cdot \cos 2\theta \right] \qquad (2.2)$$

$$u_\theta = \frac{\sigma_v \cdot r_i^2}{4 \cdot G_\gamma} \cdot \left[(1 - k) \cdot \left(2 \cdot \ (1 - 2 \cdot v) + \frac{r_i^2}{r^2} \right) \cdot \sin 2\theta \right] \quad (2.3)$$

Where r_i is the radius of the tunnel, r is the distance from the axis and θ is the angle, which is referenced to the vertical stress as shown in Figure 2.2. [25]. At the excavation surface σ_r and $\tau_{r,\theta}$ are zero where G_γ the shear stiffness of the rock expressed as

$$G_\gamma = \frac{E}{2 \cdot (1 + v)} \quad (2.4)$$

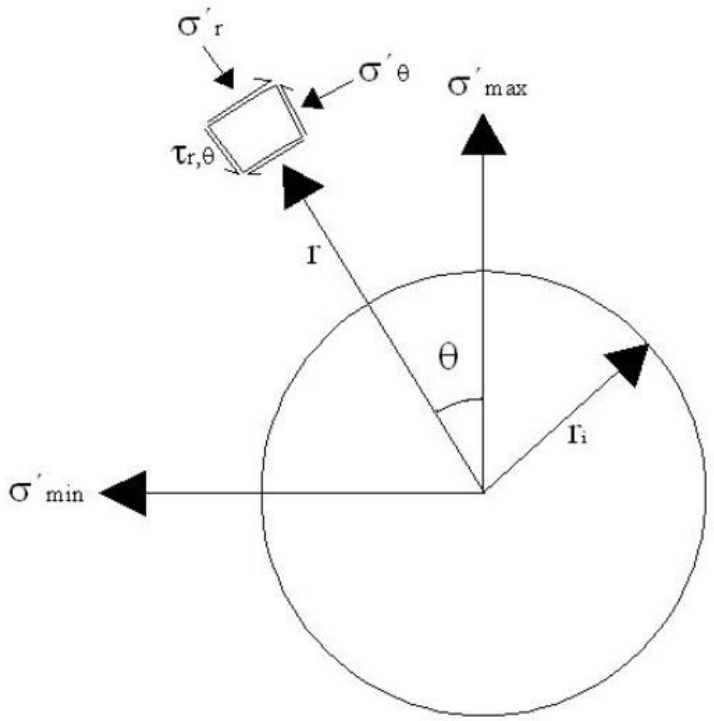

Figure 2-3 Radial, tangential and shear stress given at any point

2.1.4 Criteria of failure

Stress-strain behavior, strength parameters, and failure surfaces are the key features of the stability problems in geotechnical engineering. Several models proposed that reflect the actual soil and rock mass behavior in the literature. Some of these models square measure terribly straightforward just like the ones supported the elastic behavior whereas some square measure, therefore, complicated that they will solely be utilized in numerical calculations and not for practical purposes. [26]**.**

The yield criterion utilized in geotechnical engineering includes Tresca criterion, Mises criterion, Drukle-Plager criterion, and Mohr-Coulomb criterion, and so on. Among them, the Mohr-Coulomb criterion can well reflect the strength effects of soils and is simple and practical. In 1990, Chen and Liu stated that in the Mohr-Coulomb model, the failure of the soil assumed to happen if the shear stress at any point in the soil reaches an associate quantity that is a linear performs of the cohesion, (c) and therefore the traditional stress, (σ). This linear function is

$$\tau = c + \sigma . \tan \emptyset' \qquad (2..5)$$

Where c and $\emptyset'$ are material constants.

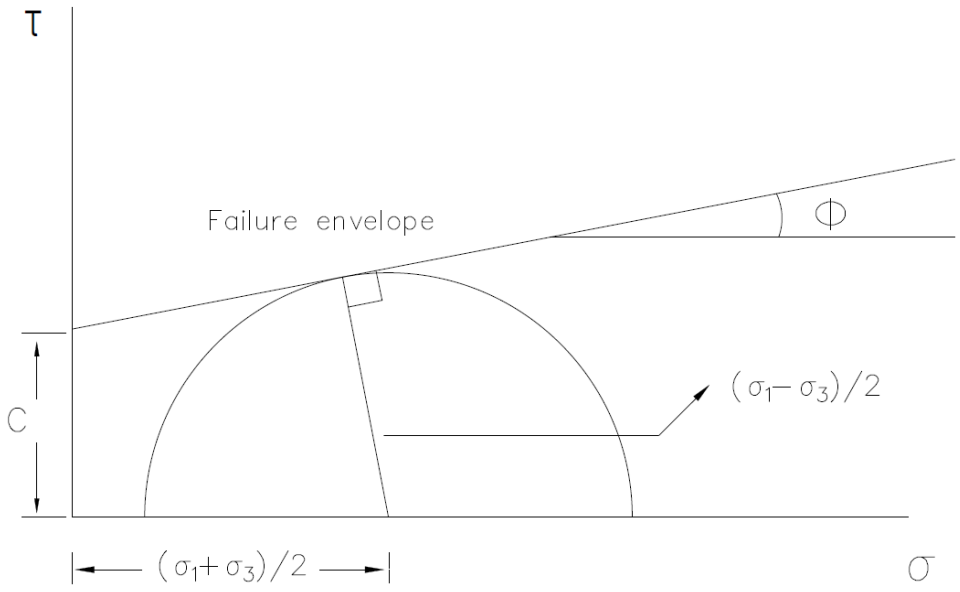

Figure 2-4 Mohr-Coulomb criteria in principal stress space and Mohr's diagram

2.2 Railway Tunnel Supporting System

According to [27], a suitable tunnel support method depends on the site geo-mechanical conditions, project contract, contractor expertise, and availability of the support members. Rock geology and stand-up time decree the possible decisions of temporal or permanent support required to ensure the stability of the immediate rock mass and tunnel construction. In Mohammed [5], the purpose of tunnel support systems is to stabilize the tunnel heading and minimize movements of the surrounding rock mass. However, the emphasis is made on the tunnel roof because it is prone to the peak load [13]. Thus it becomes an ideal region for installation of most support components such as Rock bolts; Steel ribs and Wire mesh reinforced Shotcrete and reinforced concrete lining.

2.2.1 Rock bolts

Rock bolts used to stabilize rock excavations. Rock bolts role is to stabilize rock wedges and prevent movements of the rock mass nearest to the tunnel. A common length of rock bolt is from two to four meters and depends on circumstances at each time. It is very important that the length of the bolts is sufficient to extend into a stable rock beyond the secondary, weak rock. The rock bolts have the capability to tolerate both tensile and shear forces. According to [28]**,** rock bolt is a term specifying a rod or bar-shaped bolt fabricated of steel, tube, etc. and used to support the rock mass. The inclination should be between 15° and 30° which induces the highest shear resistance along the sliding surface. [24]

2.2.2 Shotcrete

Linings comprise wire mesh reinforced Shotcrete and concrete linings. Tunnel support linings selected depending on the geology and extent of rock fracture. Shotcrete can be applied as a temporal or permanent support to provide protection during construction while concrete is commonly applied as a final permanent lining [30]. The most effective way to apply shotcrete on a wall is to begin at the lowest point and move to the sides towards the roof. Often for sound basalt, no support needed, but for moderately broken basalts, 30-40 mm thick shotcrete is needed. Approximately 30-100 mm thick shotcrete used for scoria and sedimentary interbreeds. Where circumstances are very poor e.g. fault zone, 100-150 mm of shotcrete is required.

2.3 Numerical Methods in Tunnel Engineering

Nowadays, the use of numerical methods in geo-mechanics is getting more popular in recent years. Due to the complex nature of tunnel design and analysis, numerical methods are being widely used among tunnel designers, researcher, and experts. The construction of a tunnel as a 3-D problem, but the 2-D approach still dominates the modeling process nowadays.

The software models simulate ground-support interactions including tunnel deformation and construction sequences [5]. The following are just some of those methods [31]; Finite element method (FEM), Finite difference method (FDM), Boundary element method (BEM), Discrete Element Method (DEM) and Beam element method without elastic support. Numerical methods used in tunnel engineering shown in Figure 2.2 below.

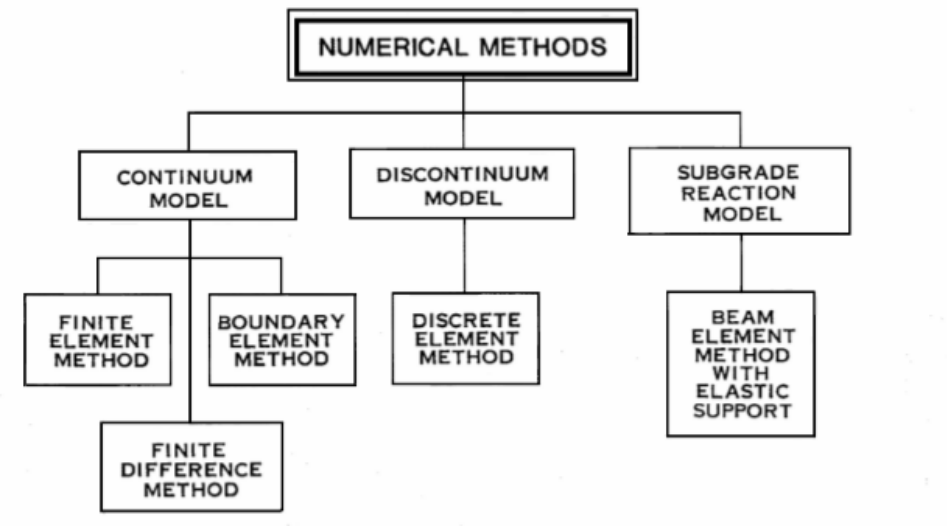

Figure 2-5 Numerical Methods in tunnel engineering (Hoek's Corner. 2016)

In [32]**,** it was stated that the field conditions can be simulated more accurately if the utilized constitutive models can represent the soil behavior accurately in addition, if the boundary conditions set are correct.

2.3.1 Finite Element Method

Finite Element Method is one of the most widely used numerical methods in geo-mechanics and in tunnel engineering. The popularity of FEM is often self-addressed to the very fact that it absolutely was the primary numerical methodology with enough ability to incorporate the fabric non-homogeneity, complex boundary conditions, and non-linear deformability. However, the finite element methodology developed supported time/continuum assumptions. Complete detachment of elements, sliding and large-scale openings cannot be

included. The global stiffness matrix can be ill-conditioned if many fracture elements are incorporated [33].

By exploiting FEM, complex conditions are simulated due to the capability of simulation of advanced constitutive models, non-homogeneities, stage-by-stage construction and time effect.

2.4 Available Software

A FEM commercial package Structure Medium Analysis Program is utilized in order to carry out the analysis. Structure Medium Analysis Program is developed especially for the analysis of the different form of tunnels under different geotechnical conditions.

2.4.1 TUNA "TUNnel Analysis" Program

TUNA is a fully automated computer program developed for TUNnel Analysis by Comtech Research. TUNA Version 7.0 employs a static, two-dimensional, linear elastic finite element method. [34].

2.4.2 TUNA PLUS

TUNA Plus is a fully automated computer program developed for tunnel analysis. TUNA Plus Version 7.0 employs SMAP-S2 which is a static, two-dimensional, nonlinear finite element program developed by Comtech Research. SMAP-S2 is an advanced two-dimensional, static, finite element computer program developed for the geometric and material nonlinear structure-medium interaction analysis.

2.4.3 SMAP-2D SMAP-3D Analysis Programs

SMAP-2D and SMAP-3D are two-dimensional and three-dimensional finite element computer program respectively that continuously improved based on theoretical and experimental works since 1982. Both SMAP-2D and SMAP-3D are state-of-the-art multi-phase nonlinear finite element analysis programs that applied to compute static, consolidation, or dynamic response of dry, saturated, or partially saturated soils and porous rocks. Both have especially useful features for earthquake analysis since they can continuously perform the static analysis followed by dynamic analysis with appropriate boundary change.

CHAPTER 3 METHOLODOGY

3.1 Railway Tunnel T07 Project

According to the dimension, the maximum height and width are summarized in Table 3-1 The corresponding area of excavation is also shown in the same table.

Table 3-1 Excavation data

Typical Cross Section	Excavation height [m]	Excavation width [m]	Excavation area [m^2]
Standard	10.53	9.08	80.3

Underground railway tunnels were the only means to construct a railway line in this hilly region of Ethiopia. The following paragraphs report on Awash – Kombolcha – Hara Gebeya geological and geotechnical conditions explaining both regional and local geological context of the Tunnel T07 site. Ethiopia's seismicity challenges are probable and could be significant stress factors including main tectonic plate boundaries, tectonic regimes or fault lines. The current Ethiopian code for seismic design, EBCS-8 (1995) specifies a peak ground acceleration value, PGA = 0.10g.

At the tunnel site, subsurface investigations consist; four major groups of lithostratigraphic units encountered. These are; Eocene volcanic, Oligocene-Miocene volcanic, Upper Miocene volcanic Quaternary volcanics which are overlain, on the plains and sometimes on the slopes, by associated Quaternary deposits of lacustrine, fluvial and slope debris origin.

According to the geological map from geotechnical and subsurface investigations: -

1. The tunnel was excavated entirely in rock. The rock belongs to Ashangi formation (Tas) of Eocene age, which is composed of aphanitic to coarse-grained basalt / trachybasalt and volcaniclastics.
2. The rock encountered in the boreholes was very weak to weak, with very closely spaced joints, and highly weathered at the top. The rock quality gradually improved with depth.
3. From the hydrogeological analysis, no groundwater encountered in the boreholes drilled for this tunnel. The geomorphological attitude of the tunnel ruled out the possibility of rising of the groundwater level in the rainy season. However, local seepage from the surface may occur after prolonged periods of precipitation.

Table 3. 1 Summary table for Geotechnical profile, Tunnel T-07

Geometrical characteristics	**Chainage (Km)**	261+380	261+450	261+470	261+536	261+584	261+605	261+641	261+661	261+701	261+737	261+737	261+760
	Section length (m)	70		20	66	48	21	36	20	40	36		
	Description	ENTRANCE				**SECTION 4**			**SECTION 2**	**SECTION 5**		EXIT	
	Overburden (m)			15	20	20	20	40	40	40	15		
geology Lithology	**Rock Type**			C2	C2	Av. (B-C)	C2	Av. (B-C)	C2	Av. (B-C)	C2		
	Groundwater condition			WET	WET	WET	WET	WET	WET	WET	WET		
Mechanical behavior intact rock	**Unit Weight (kN/m^3)**			23	23	24	23	24	23	24	23		
	Uniaxial Compressive Strength UCS (Mpa)			10	10	25	10	25	10	25	10		
	Modulus of Deformation (GPa)			3.5	3.5	4	3.5	4	3.5	4	3.5		
	Poisson's Ratio (V)			0.25	0.25	0.2	0.25	0.2	0.25	0.2	0.25		
Rock mass Classification and design parameters	**Rock mass rating, RMR**			40-45	40.45	45-55	40-45	45-55	40-45	45-55	40-45		
	Rock mass class			Poor Rock IV	Poor Rock IV	Fair Rock III	Fair Rock IV	Fair Rock III	Poor Rock IV	Fair Rock III	Poo Rock IV		
	Geological Strength Index			35	35	40	35	40	35	40	35		
	Cohesion (KPa)			60	60	110	60	150	110	150	60		
	Internal frictional Angle			40	40	48	40	44	33	44	40		
	Modulus of Deformation (Mpa)			140	140	200	140	200	140	200	140		
Project	**Total Tunnel length (m)**			287									

Source: Geotechnical Report, Tunnel T-07 (Km:261+450 – 261+737)

3.3.1 Rock Mass Quality Zoning

In the approach adopted for rock mass quality zoning, all the rock/soil condition were subdivided into different classes designated as A, B, C2, C1, and D.

Table 3-2 Rock mass quality, Tunnel T07 rock/soil classes (zoning).

Class	A	B	C2	C1	D
Description	Slightly weathered to fresh, jointed but relatively undisturbed rock mass	Moderately to highly weathered and fractured rock mass	Highly disturbed, highly weathered rock mass (typically in the fault zones).	Rock mass turning into the soil through weathering (typically near the ground surface, e.g. portal areas).	Soil (colluvium).

Table 3-3 Rock mass parameters for the body of Tunnel T-07

Rock Mass class	Expected Formation and Rock Mass Description	Est. Rock Mass Quality		Reference Overburden [m]	c'_m [kPa]	Φ'_m [^{o}]	E'_m [mpa]	ν [-]
		RMR	GSI					
B-C	Ashangi Fm. (Tas) Basalt, Trachybasalt,tuff	45-55	40	20	100	45	200	0.20
				40	150	44	200	0.20
C2	Ashangi Fm. (Tas) Basalt,trachybasalt,tuff	40-45	35	15	60	40	140	0.25
				20	60	40	140	0.25
				40	110	33	140	0.25

3.3.2 Geological Condition and Characterization

Tunnel T07 crosses a single rock formation identified as" Ashangi Formation - Tas" (Eocene Period) composed by black and dark grey, fine-grained to coarse-grained Basalt and Volcanic clastic sediments. The formation characterized by different geo-mechanical conditions, ranging from very good to very poor rock mass or soil. Rock mass characterizations based on the geological report, geological profile, and borehole results, and from direct inspection of the alignment, in particular of tunnel portal areas.

To each sub-zone, a design rock mass quality assigned and Rock mass quality was assessed according to the "GSI approach" (Geological Strength Index) and "RMR approach". These two indexes evaluated by using the ordinary procedure indicated

respectively by Hoek and Brown (1997) for GSI and Bieniawski 1989 for RMR. The value of GSI estimated by using the GSI chart. See Appendix 5.

RMR (Rock Mass Rating) approach carried out by giving ratings for each homogenous part of each interested boreholes of the relevant tunnel. In order to give ratings properly, borehole logs, laboratory results, and borehole-outcrops photos are adopted. Ratings for each index selected from the classic "RMR (Rock Mass Rating) Classification System chart - Bieniawski 1989 herein attached. See Appendix 4

Ratings for Strength of Intact Rock, ratings for RQD and ratings for Discontinuity Spacing obtained through the charts commonly used (Bieniawsky, 1989). The obtained values of RMR and GSI were tested through the following correlation (Hoek and Brown, 1997) to verify the correspondence (order of magnitude) between the two values from Equation 1 earlier stated. Correlation between RMR and rock mass deformation modulus E_i proposed by Galera et al (2005) using expression shown below.

$$E_m \text{ (GPa)} = 0.0876 \text{ RMR for RMR} \leq 50 \tag{3.1}$$

$$E_m = E_i \, e^{(RMR-100)/36} \tag{3.2}$$

For each sub-zone the following parameters of the equivalent continuous were defined according to the local covers, which represent the initial state of stress, and to the Mohr-Coulomb resistance criteria: unit weight of rock/soil (kN/m^3), rock mass cohesion (kPa), rock mass friction angle (°), and Ypung's modulus of the rock mass (MPa)

For calculating the rock mass parameters, as equivalent continuous, the formulations shown in equations below for definition of rock mass or ground behavior model were used. In these calculations, Hoek-Brown disturbance factor D, = 0.8, is chosen (drill and blast in conventional excavation).

$$\sigma' = \sigma'_3 + \sigma_{ci}\left(m_b \, . \, \frac{\sigma'_3}{\sigma_{ci}} + (s)\right)^a \tag{3.3}$$

$$m_b = m_i \, . \, \exp^{\left(\frac{GSI-100}{28-14D}\right)} \tag{3.4}$$

$$\dot{s} = \exp^{\left(\frac{GSI-100}{9-3D}\right)} \tag{3.5}$$

$$\dot{a} = \frac{1}{2} + \frac{1}{6}\left(e^{\frac{-GSI}{15}} - e^{\frac{-20}{3}}\right) \quad (3.6)$$

$$C' = \frac{\sigma_{ci}\,[(1+2a)s + (1-a)\,m_b\sigma'_{3n}]\,(s + m_b\sigma'_{3n})^{a-1}}{(1+2a)(1-a)\sqrt{1 + \frac{\left(6\,a\,m_b\,((s + m_b\sigma'_{3n})^{a-1})\right)}{\left((1+a)(2+a)\right)}}} \quad (3.7)$$

For each sub-zone, the Hoek and Brown's resistance coefficients (m_b, and $\dot{s}$) were estimated by using GSI. Then for each range of overburden, the estimation of the Mohr Coulomb parameters was calculated, according to the construction.

3.2 Construction Method and Support Types

3.2.1 Construction Method

Conventional excavation method was considered as the method of execution for tunnel T07. The conventional excavation method consists of sequential-section advancement combined, if required, with pre-support and/or pre-confining technique ahead of the tunnel face. The excavation was performed by "using drill and blast method" and, depending on local formation geo-mechanical characteristics, where the quality of the rock mass was low, with machinery like shovel diggers to impact hammers.

The excavation is in only one-step (full-face excavation) and in different steps (partial excavation). The decision to work either with a full-face or with a top heading and benching excavation for every stretch of tunnel T07 depended on the considered support class, i.e. on the typology of the adopted support section.

The final dimension for over-excavation defined according to actual convergence measurements during the excavation phase. For standard sections, five support classes were considered depending on the RMR rock mass classification. The definition of each supported class is detailed in the following paragraph.

Table 3-4 Summarize the support classes planned for the T07 Tunnel.

	A1	A2	A3	A4	A5
Support class	**(RMR>81)**	**(61<RMR<80)**	**(41<RMR<60)**	**(21<RMR<40)**	**(RMR<20)**

3.2.2 Primary Support

Support Classes for section A1, A2 and A3 referred to the massive self-supporting rock mass with different degree of fracturing, while section A4 and A5 referred to poor-very poor rock mass conditions, generally not self-supporting after each step of excavation especially under a high initial state of stress. Support section A5 almost coincides with up the supports section A4 (corresponding to "Poor Rock condition (21<RMR<40).

Table 3-5 Support Classes for Tunnel T07

Studied sections	Chainage		Length	Geol.	Expected	Expected	Support Class		Section
			(m)	Form.	Average RMR range	Average GSI range	(% of the Length)		Type
No.	From	To					A3	A4	
Section 4	261+536	261+584	48	"Tas"	45-55	40	38	10	Standard
Section 2	261+641	261+661	20	"Tas"	40-45	35	4	16	Standard(**)
Section 5	261+661	261+701	40	"Tas"	45-55	40	28	12	Standard
Tunnel Length (m)			108				70	38	

(**) Note that for Fault Zones, Type A4 Support Class was used independently by the real conditions of the surrounding rock mass.

According to the Detailed Design Manual for Tunnels and the description of the typologies of the supports previously described, along the T07 Tunnel, the following primary support types were planned for application Table 3.8.

An exception to this classification is given for the starting stretch of the natural tunnel (after the entrance and before the exit of the tunnel). For safety reasons, an A5 standard section was considered from the starting of the tunnel regardless of either foreseen or actual ground conditions (RMR value). During the tunnel execution, when the tunnel is excavated under difficult rock mass conditions, special attention must be paid to the stability of the tunnel face.

3.3 Analytical studies

To acquire the sensitivity on the reaction of the excavated rock mass along the tunnel, for each identified tunnel section with similar covers and similar geotechnical parameter, some analytical studies are performed. This step allows verifying if rock class support linked to the rock mass quality, represented by RMR and GSI, is adequate, and to define those situations which require more detailed studies for dimensioning the lining.

For each tunnel section, the following data are analytically calculated as described in the methodology.

- The general behavior of the unsupported cavity by using the Characteristic Curves (Ground Reaction Curve-GRC).

3.3.1 General Behavior of the Unsupported Cavity and Support Reaction

The general behavior of the unsupported cavity was efficiently expressed by using the "Characteristic Curve" of the unsupported cavity (GRC-Ground Reaction Curve). This is a common approach to study the behavior of tunnels in rock and soils. It is an analytical solution strictly valid for circular tunnels in an elastic-plastic rock mass under a hydrostatic stress field. In spite of its conceptual simplicity, it is a very useful tool for acquiring sensitivity of the reaction of a rock mass (tunnel deformation) subjected to excavation, and for verifying the support in the simpler cases, using, for example, the convergence-confinement method.

In this case, the tunnel characteristic curve relates the internal pressure provided by the installed supports "$\mathbf{P_i}$" to the tunnel walls radial displacement "$\mathbf{U_r}$". In this way the approach gives an estimation of the interaction between the supports reaction and the ground reaction, estimating both the final ground deformations and the pressure acting on the installed supports. For a given tunnel radius and in-situ stress, the shape of the tunnel characteristic curve depends on the assumed rock mass failure criterion, the specific rock mass strength, and deformability parameters.

Once the support is installed and becomes effective, it starts to deform elastically as shown in Figure 3.10, equilibrium is reached if the support characteristic curve intersects the tunnel characteristic curve before either of these curves has progressed too far. As anticipated, with the characteristic line method it is possible to verify the adequacy of the support even without any further detailed analysis.

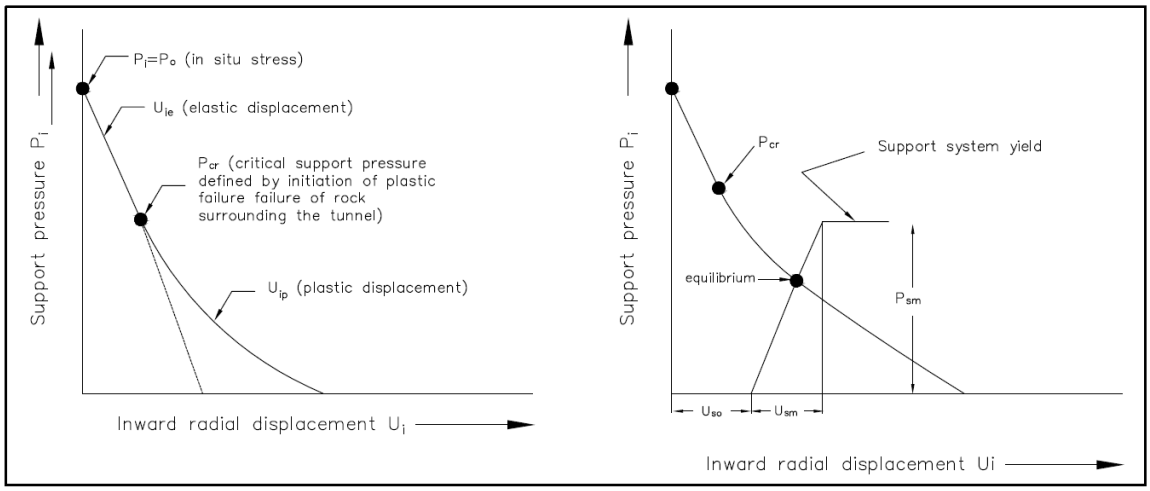

Figure 3-6 Characteristic Curve

The tunnel characteristic curves, at considered studied sections, were determined the Duncan-Fama closed-form solution based on the Mohr-Coulomb failure criteria was considered. The characteristic curves that describe the proposed support types were computed according to the AFTES recommendation "The Convergence-Confinement Method" [35]

3.3.2 Support Characteristic Curves

In order to determine the shape of the proposed support section characteristic curve (i.e. the maximum ground pressure that can be resisted by the supports and the supports stiffness), the following equations have been applied as per document [35]. According to the previous equations, for the support class adopted for Tunnel 07, the main characteristic of the support system is summarized in Table 3.9

Table 3-6 Parameters of the supporting system

Studied Section type	**Support type**	
	A3	**A4**
Standard Section Type	Rock bolts 100 mm shotcrete	Rock bolts 200 mm shotcrete

3.3.3 Geometry and material parameters of studied sections

In order to study the Tunnel 07 behavior, three sections were considered among the alignment of 287 m wide segment of the tunnel with the overburden height and span of approximately 9.1 m. A rigorous study of each of these sections leads to a complete knowledge of all the predicate excavated tunnel behavior. [36]

Table 3-7 Geotechnical Parameters (Yepi Merkezi, 2015)

Studied Sections	Soil/Rock Type	OB [m]	γ [kN/m^3]	C_m [kPa]	∅ [°]	E_m [MPa]	V
Section 2	Rock C2 in fault zone (Highly fractured)	40	23	110	33	140	0.25
Section 4	Rock B-C rock in Transition to fault zone (Moderately fractured)	20	24	100	45	200	0.20
Section 5		40		150	44		

In summary, as specified in detail in the previous paragraph Table 3.8 above to each rock mass classes for the studied section aforementioned above correspond to the following support system:

For Support Class A4, corresponding to 21<RMR<40 and to the support system for "Poor to very poor rock mass quality conditions". These were encountered corresponding to the transition between Fault material and fractured material or faults with relatively good core material. Along tunnel T07, a total length of about 20 m of this studied Section 2.

Support Class A3, corresponding to 41<RMR<60 and to the support system for "Fair to Poor rock mass quality". These were encountered in fractured slightly weathered part of the rock mass. Along tunnel T07, a total length of about 48 m and 40 m for section 4 and section 5 respectively and of this situation was found, mainly where passages between different conditions of the rock mass have been foreseen.

3.4 Pre-dimensioning with the Ground Reaction Curve

3.4.1 Vertical stress distribution around the tunnel

The vertical stress distribution obtained from the simulation by Plaxis FEM model shows the vertical stress induced on the tunnel is between $400\ \mathrm{kN/m^2}$ – $2000\ \mathrm{kN/m^2}$ for Section 2. [36].

3.4.2 Radial displacement on the tunnel walls

As an approximate analysis, shotcrete thickness of 200 mm and an unsupported length of 1 m for A4 Standard section type. All displacements were compatible with the tunnel excavation safely, with a safety factor range between 5.38 and 8.37.

This pre dimensioning suggested that an elastic behavior was expected at the front in this section. Even thought, the previous pre-dimensioning verified with a refined analysis in order to take into account other variables such as the closeness of the hillside.

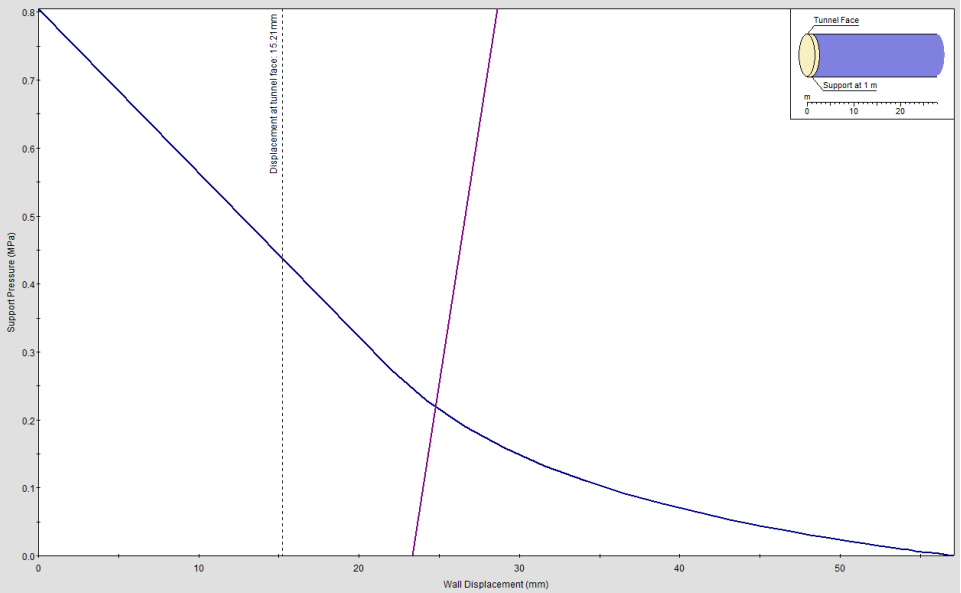

Figure 3-7 Section 2 Radial displacement on the tunnel wall.

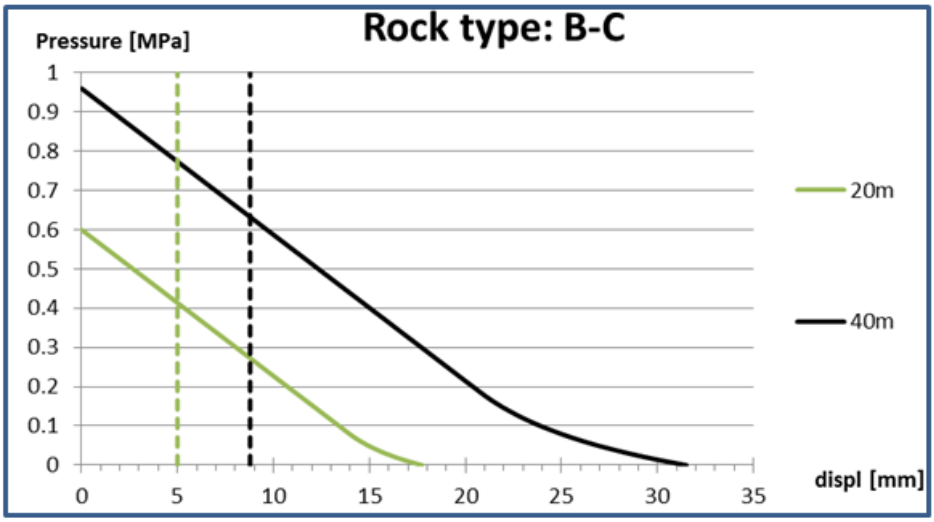

Figure 3-8 Section 4 and 5 Radial displacements on the tunnel wall.

3.5 Validation of the predicated tunnel behavior

3.5.1 Vertical stress from the surrounding rock mass

$$P_v = OB \cdot \gamma \tag{3.8}$$

$$P_v = (40 \times 23)$$

$$\mathbf{P_v = 920\ kN/m^2}$$

$$\textbf{Horizontal stress, } \mathbf{P_h} = \frac{1}{3}.(920)$$

$$\mathbf{P_h = 307\ kN/m^2}$$

3.5.2 Displacement of the excavation wall

Assuming the rock at tunnel face provides an initial support equal to the in-situ pressure inside. The vertical pressure, P_v gradually reduce until it reaches zero at some distance behind tunnel face. The tunnel of radius $r_o = 4.55$ m subjected to vertical stress $p_v = 920\ kN/m^2$on the crown and $p_h = 307 kN/m^2$. Checking for main tunnel stability, rock mass surrounding the tunnel occurs when the internal pressure p_i is less than a critical support pressure, p_{cr} calculated from Equation 3.12, where σ_{ci} is the compressive strength of rock mass..

$$p_{cr} = \frac{2p_v - \sigma_{ci}}{(1-k)}, \quad \text{for } k = 0 \tag{3.9}$$

$$p_{cr} = \frac{2(0.92) - 0.405}{(1)}$$

$$\mathbf{p_{cr} = 1.435\ MPa}$$

$$\text{But, } \sigma_{ci} = \frac{2C\prime\cos\emptyset\prime}{(1-\sin\emptyset\prime)}$$

$$= \frac{2 \times (110)\cos(33)}{(1-\sin(33))}$$

$$= \frac{184.508}{0.4554}$$

$$\mathbf{\sigma_{ci} = 405.156\ kN/m^2}$$

$$u_r = \frac{r_o \cdot (1+v)}{E} \cdot (p_v - p_i) \tag{3.10}$$

$$u_{ie} = \frac{(4.55 \times 10^3) \times (1+0.25)}{140} \times (0.92)$$

$$\mathbf{u_{ie} = 37.4\ mm}$$

$$u_{ip} = \frac{r_o \cdot (1+v)}{E} \cdot \left[2(1-v) \cdot (p_v - p_{cr}) \cdot \frac{r_p^2}{r_0^2} \cdot -(1-2v) \cdot (p_o - p_i)\right] \tag{3.11}$$

$$u_{ip} = \frac{(4.55 \times 10^3) \times (1.25)}{140} \times \left[(1.5) \times (-0.51) \times \frac{4.55^2}{4.55^2} \times -(0.5) \times (0.92)\right]$$

$$\mathbf{u_{ip} = 14.3\ mm}$$

Thus, final radial displacement, u_r observed inside the tunnel is 23.1 mm from computed using the existing elastic rock mass mathematical and analytical calculations. When the internal support pressure, p_i is less than the critical support pressure, p_{cr} failure occurs and the radius r_p of the plastic zone around the tunnel is can be calculated from Equation 3.15 below.

$$r_p = r_o \left[\frac{2(P_v \cdot (k-1) + \sigma_{cm})}{(1+k) \cdot (k-1) \cdot p_i + \sigma_{cm}}\right] \tag{3.12}$$

3.6 Validation for internal support pressure

3.6.1 Length of rock bolt

The length of the rock bolts is verified using $L_b \geq 1.25\left(\frac{1}{3}\cdot \text{Span}\right)$ where L_b is the length of the rock bolt.

Thus;

$$L_b \geq 1.25\left(\frac{1}{3}\cdot 9.1\text{ m}\right)$$

$$\mathbf{L_b \geq 3.79\text{ m} \approx 4\text{ m}}$$

3.6.1.1 Spacing of rock bolt

For spacing S_c between rocks bolts termed as circumferential spacing validation was carried based on rock mass rating (RMR) values.

According to rock mass with $20 \leq \text{RMR} \leq 85$, the rock mass is identified as fair rock Class III according to Bienkwaiski 1987 with RMR values range 40-55, the following expression can be used for very poor highly weathered rock masses in faults.

$$S_c = 0.5\text{ m} + 2.5\text{ m}\cdot\left(\frac{\text{RMR}-20}{60}\right) = 0.5\text{ m} + 2.5\text{ m}\cdot\left(\frac{40-20}{60}\right)$$

$$\mathbf{S_c = 1.27\text{ m} \approx 1.5\text{ m}}$$

This study, considered longitudinal spacing equal to one meter.

$$S_l \approx \mathbf{1\text{ m}}$$

3.6.1.2 Estimation of rock bolt support capacity

The following analysis is limited to the support provided by grouted mechanically or chemically anchored rock bolt. More detailed numerical analysis of the interaction of rock bolts and failing rock masses provided in next chapters in these notes. The maximum support pressure $P_{max_{rb}}$ and the elastic stiffness K_{rb} provided a rock bolt given pattern below.

$$P_{max_{rb}} = \frac{T_{b_f}}{(S_c \cdot S_b \cdot \gamma_{loan})}$$

$$= \frac{230\text{ kN}}{(1.5\text{m} \times 1\text{ m} \times 1.35)}$$

$$\mathbf{P_{max_{rb}} = 113.58\ kN/m^2}$$

$$K_{rb} = \frac{E_s \cdot \pi \cdot d_b^2}{(4 \cdot l \cdot S_c \cdot S_b)}$$

$$= \frac{1.33 \times 10^3 \times \pi \times 0.026^2 \text{ m}}{(4 \times 4 \text{ m} \times 1.5 \text{ m} \times 1 \text{ m})}$$

$$K_{rb} = \mathbf{17,653.39\ kN/m^3}$$

3.6.2 Shotcrete verification

Hoek and Brown (1980a) and Brady and Brown (1985) published equations calculating the capacity of steel sets, shotcrete or concrete linings and rock bolts for a circular tunnel in an in-situ stress field.

3.6.2.1 Estimation of Shotcrete support capacity

$$P_{max\,sb} = \frac{\sigma_{cc}}{(2 \cdot \gamma_{loan})} \cdot \left[1 - \frac{(r_o - t_c)^2}{r_o^2}\right] = \frac{25 \times 10^3}{(2 \times 1.35)} \cdot \left[1 - \frac{(4.55 - 0.2)^2}{(4.55)^2}\right]$$

$$P_{sc_{max}} = \mathbf{796.11\ kN/m^2}$$

$$K_{sc} = \frac{E_s \cdot (r_o^2 - (r_o - t_c)^2)\pi \cdot d_b^2}{2 \cdot (1 - v^2)(r_o - t_c) \cdot r_o^2} = \frac{1.5 \times 10^7 \times (4.55^2 - (4.55 - 0.2)^2)}{2 \times (1 - 0.2^2)(4.55 - 0.2) \times 4.55^2}$$

$$K_{sc} = \mathbf{1.54 \times 10^5\ kN/m^3}$$

3.6.2.2 Estimation of final lining support capacity

$$P_{lc_{max}} = \frac{\sigma_{cc}}{(2 \cdot \gamma_{loan})} \cdot \left[1 - \frac{(r_o - t_c)^2}{r_o^2}\right] = \frac{25 \times 10^3}{(2 \times 1.35)} \cdot \left[1 - \frac{(4.55 - 0.3)^2}{(4.55)^2}\right]$$

$$P_{sc_{max}} = \mathbf{1,133.66\ kN/m^2}$$

$$K_{sl} = \frac{E_s \cdot (r_o^2 - (r_o - t_c)^2)\pi \cdot d_b^2}{2 \cdot (1 - v^2)(r_o - t_c) \cdot r_o^2} = \frac{3.1 \times 10^7 \times (4.55^2 - (4.55 - 0.3)^2)}{2 \times (1 - 0.2^2)(4.55 - 0.3) \times 4.55^2}$$

$$K_{sl} = \mathbf{4.84 \times 10^5\ \ kN/m^3}$$

The value of the tensile strength T used in this study can be compared to the allowable stresses proposed by Euro code 2 of mass concrete for a mass concrete using the expression in Equation 3.17

$$T = \frac{0.3 \cdot f_{c_k}^{\frac{1}{3}}}{1.5} \tag{3.13}$$

Where f_{c_k} is the Characteristic Strength value of concrete in (mPa)

In Table 3.9, two Section 4 (20 m of overburden) and Section 5 (40 m of overburden) are examined for A3 support verification. In Figure 3.3, the dashed lines indicate the expected displacement at tunnel face given by Vlachopoulos and Diederichs (2009) longitudinal deformation profile formulation. The expected radial displacement inside the tunnel until the complete de-confinement of the rock mass is then determined.

Table 3. 2 Expected radial displacement inside the tunnel

Studied Tunnel Section	Overburden	Expected radial displacement inside the tunnel
Section 4	20 m	12 mm
Section 5	40 m	22 mm

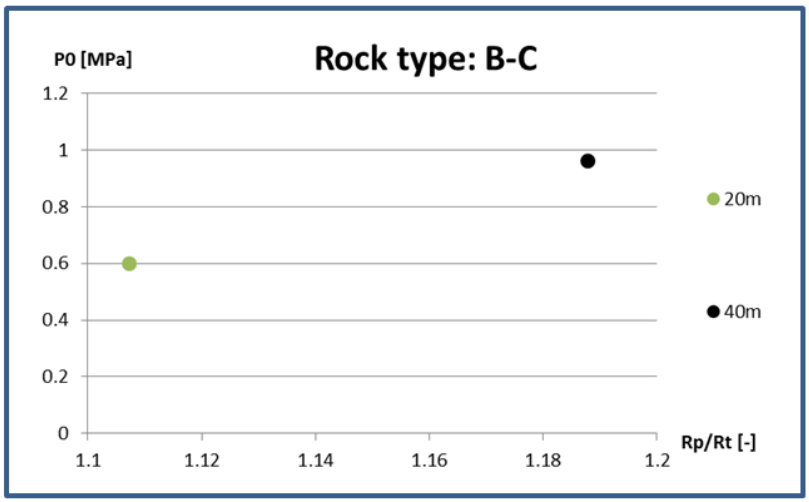

Figure 3-9 Plastic radii with respect to the tunnel in-situ pressure

Therefore, the elastic theory for estimating the surrounding rock mass displacements around tunnel excavations in any rock mass is used for validation. The estimated radial displacement at a point around an excavation in elastic rock is given in Equation 2.3. Study on the plastic radius, Figure 3.4 plots it is a dimensionalized value with respect to the tunnel in-situ pressure. The plot defines the linear relation between the in-situ pressure and the radius of the plastic area induced by the excavation.

The behavior of that plastic area is related to the in-situ pressure (P_0) in a linear way. Hence, more overburden means more in-situ pressure and so, higher values of the plastic radius, which it is consistent with what, experience displays. Using the reaction curve suggested an elastic behavior was expected at the front in these sections.

3.6.2.3 Tunnel stability and support pressure validation

Table 3-8 Summary of radial displacement inside the tunnel

Section	Overburden (OB) m	P_i, MPa	P_{cr}, MPa	u_{ie}, m	u_{ie}, mm	Remark
2	40	0.92	1.44	0.0374	37	Unstable
4	20	0.48	0.43	0.0131	13	Unstable
5	40	0.92	1.12	0.0251	25	Unstable

From the analytical studies, the results obtained from analytical solutions of the ground reaction curve well represent instability problem. Since the internal support pressure, P_i is less than the critical support pressure, P_{cr}, failure occurs thus tunnel support is required.

Table 3-9 Radial displacement inside the tunnel for plastic failure

Section	P_v (MPa)	r_o (m)	σ_{ie} (m)	P_v (MPa)	P_{cr} (MPa)	v	U_{ip} (mm)
2	0.92	4.55	0.41	140	1.44	0.25	14
4	0.48	4.55	0.43	200	0.43	0.20	-0.6
5	0.92	4.55	0.72	200	1.12	0.20	4.8

These deformations induce stability problems in the tunnel depending upon the ratio of rock mass strength to the in situ pressure. The same principle of determining the deformation of the circular tunnel is used to analytically analyze the behavior of the rock mass surrounding the horseshoe with curved sidewalls. For simplicity, see Figure 3.5 the radius of the plastic zone should be greater or equal to the radius of the tunnel, [25]. For this analysis was assumed for all cases $r_p = r_0$.

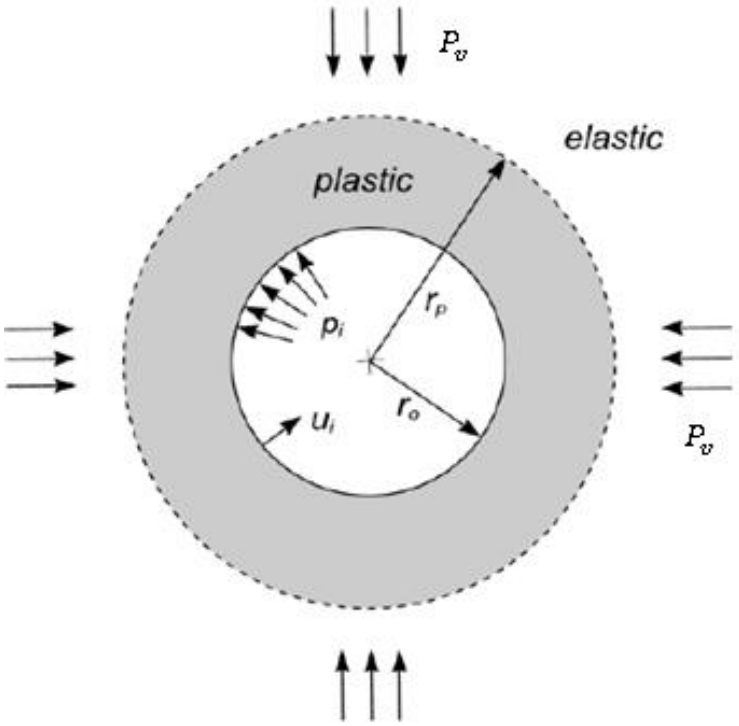

Figure 3- 1 Plastic zone surrounding a circular tunnel in-situ pressure

3.6.3 Summary on tunnel stability

The total maximum internal support pressure provided by the combination of tunnel support components is $2{,}043.35\ \mathrm{kN/m^2}$ which greater than the critical support pressures of 1.4 MPa (Section 2), 0.43 (Section 4), and 1.13 (Section 5) in the rock mass. In addition, Table 3.10 shows the internal support pressure, P_i in Section 2 and Section 5 being less than the critical support pressure, P_{cr}, thus failure is expected to occur. Therefore, an adequate tunnel support system combination capable of resisting the induced deformations and stresses is required. However, the case is different for Section 4 with a lower overburden compared to the other studied sections.

The total maximum elastic stiffness $6.55 \times 10^5 \mathrm{kN/m^3}$ of a combination of rock bolt, shotcrete and final lining is computed since it is vital to provide a flexible and ductile tunnel supporting system capable to meet the requirements of allowable stress design and limit state design for an optimum design method of the support.

CHAPTER 4 MODELLING

4.1 Introduction

In order to achieve the objective, the study employs the numerical modeling and analysis. The data are analyzed using Structure Medium Analysis Program (SMAP) for tunnel Analysis TUNA Plus Version 7.0.

4.1.1 Tunnel Analysis Boundary

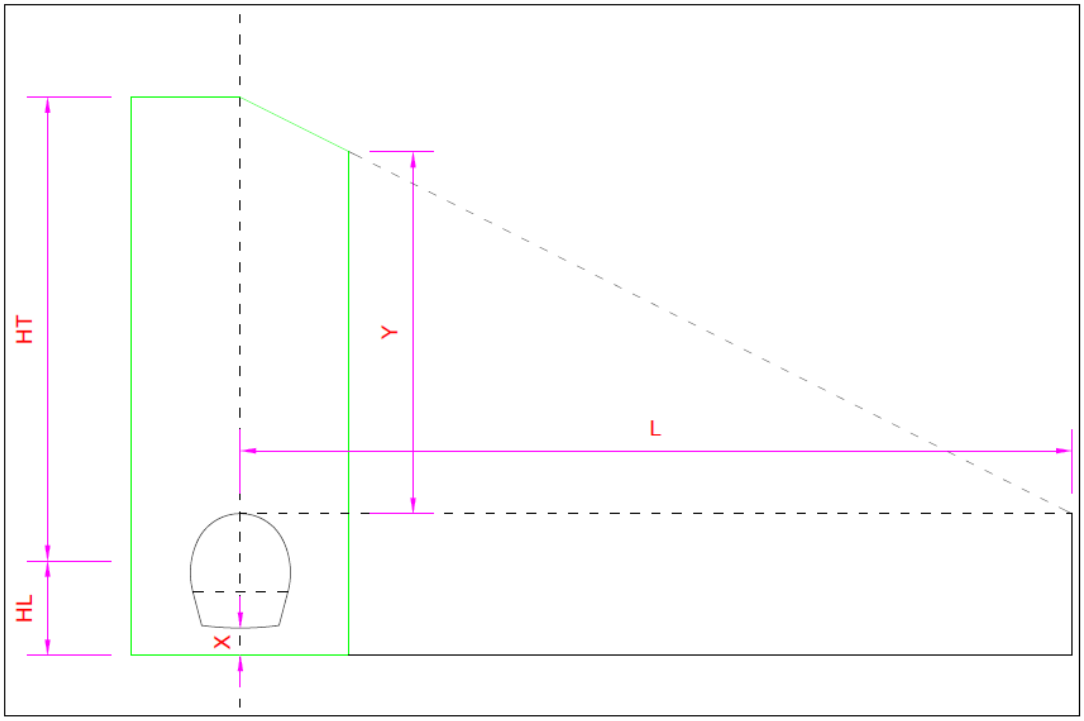

Figure 4-10 Schematic tunnel section boundary model.

4.1.2 Soil/Rock layer Material Properties

Table 4-10 Geological data for studied sections (Yepi Merkezi 2015)

Studied Sections	Soil/Rock Type	H [m]	γ [kN/m^3]	E [MPa]	V	Ø [^{0}]	C [kPa]	K_0
Section 2	Rock C2 in fault zone (Highly fractured)	40	23	140	0.25	33	110	0.33
Section 4	Rock B-C rock in Transition to fault zone (Moderately fractured)	20	24	200	0.20	45	110	
Section 5		40			0.20	44	150	

4.1.3 Shotcrete and Lining and Rock Bolt Material Properties

Table 4-11 Supporting System component properties (Yepi Merkezi 2015)

Studied Sections	t_c [m]	γ [kN/m^3]	E [kPa]	V	Ø [^{0}]	C [kPa]	T [kPa]
Shotcrete	0.2	24	1.5×10^6	0.2	9	5×10^3	1710
Final Lining	0.3	24	3.1×10^6	0.2	9	5×10^3	1710

Table 4-122 Rock bolt properties (Yepi Merkezi 2015)

Property data	**Analyses sections**
	Section 2
Rock bolt diameter, Ø (m)	0.026
Cross section area, A (mm^2)	5.31×10^{-4}
Weight per unit length of rock bolt, WL (kg/m)	2.9
Young's Modulus, E [kPa]	133×10^6
Initial stress, STRSI [kPa]	0.0
Yield stress, [MPa]	265
Strain at the rapture (For $e_f < \frac{\text{yeild stress}}{e_f}$, e_f represents yield starin at tension	0.13
Ultimate Capacity (kN)	230
EA (kN/m)	7.08×10^4

Table 4-133 C25 Concrete and Steel BR500 Rebar properties (Yepi Merkezi 2015)

C25 concrete properties		**Steel BR500B rebar properties**	
fck,cube [MPa]	30	fyk [MPa]	500
fck,cyl [MPa]	25	fyd [MPa]	435
fcd [MPa]	16.67	As [mm2]	S2: 2126
Ec [GPa]	31	Es [MPa]	200000
νc [-]	0.2	νs [-]	0.3

Table 4-144 Partial factors for materials in ULS (Yepi Merkezi 2015)

Material Factor		
Material	**Permanent**	**Accidental/Seismic**
Concrete	1.5	1.2
Steel	1.15	1

Table 4-155 Concrete lining parameters properties (Yepi Merkezi 2015)

Property data	Supporting System	
	Initial support	**Final lining**
Shotcrete modulus of elasticity Ec (GPa)	15	31
Shotcrete Poisson's coefficient νc (-)	0.2	0.2
Internal friction angle of Concrete, $\emptyset$ (^{0})	9-35	9-35
Cohesion of concrete, C[kPa]	387-500	387-500
Unit weight, $\boldsymbol{\gamma}$ (kN/m^3)	22.6	24
Shotcrete layer thickness, th (m)	0.1	0.1
Axial stiffness (MN/m)	3,000	9,300
Flexional stiffness (MNm^2/m)	10	69.75
Self-weight (kN/m/m)	6.25	7.5
Tensile strength of Concrete (kN/m^2)	1,216-1,710	1,216-1,710
Young's Modulus of Reinforcing Bar, E_r	n/a	200,000
Poisson's Ratio of Reinforcing Bars,v_r	n/a	0.3

4.1.4 Assumptions for Tunnel analysis

For this study, tunnel analysis considers the following assumptions:

Plain strain condition in the longitudinal tunnel direction, Excavation stage involves three steps; the stress release before placing shotcrete or rock bolts, Shotcrete remains in the soft state, and Shotcrete remains in the hard state, liners installed when the tunnel excavation is completed. Liner deformations are due to self-weight, groundwater pressure, loosening load and degradation. The surrounding medium and shotcrete modeled by continuum element with the Mohr-Coulomb Material model to analyze the rock mass behavior and response to tunnel excavation. Rock bolts modeled by nonlinear truss elements and Liners are modeled by reinforced layered beam elements with Mohr-Coulomb Material Models while the Interface between the liner and the surrounding medium (rock mass) is modeled by joint element with Mohr-Coulomb material modeled.

The numerical FEM model has been defined for analysis and computation of the member forces; - Bending Moment, Thrust and Shear acting in the liner supporting system both in the initial support and in the final lining and of the force; - Axial stresses acting in the rock bolt.

4.2 Tunnel dimensions

Areas: - $A_1 = 64.5^0$, $A_2 = 25.5^0$ and radii: - $R_1 = 4.05$ m, $R_2 = 3.05$ m from the Yapi Merkezie design, Manual area $A_3$and radius R_3 computed following the design principle in SMAP. The exact values for the dimension of area A_4 and rathe dius R_4 also calculated following the trigonometry.

4.2.1 Description

Compute for $k = \frac{d}{h}$, where h is the invert half width and d is the assumed invert depth. For this study, consider $A_1 + A_2 = 90^0$ and $d = 0.5$ m.

4.2.2 Coordinate at spring line.

$$X_{S.L} = (X_2 + R_2) \tag{4.1}$$

$$= [(R_1 \ \text{Sin}\ A_1 + R_2 \ \text{Cos}\ A_2) + R_2\ ] = 3.953 \text{ m}$$

4.2.3 For coordinates at Invert half width

$$\text{But, } A_3 = \tan^{-1}\left(\frac{\text{Internal tunnel diameter}}{\text{Distance at coodinate } X_{S.L}}\right) \tag{4.2}$$

$$= \frac{8.1}{3.953} = 26^0$$

$$\text{Then, } R_3 = \left(\frac{\text{Internal tunnel diameter}}{\text{Cos } A_3}\right) \tag{4.3}$$

$$= \frac{8.1}{\text{Cos } 26^0} = 9.012 \text{ m}$$

At node no.20, $h = R_3 \ \text{Cas}\ A_3 - \left(R_3 - (X_2 + R_2)\right) = 3.041$ m

Thus $k = 6.081$, where

$$R_4 \ \text{Sin}\ A_4 = h \tag{4.4}$$

$$R_4(1 - \text{Cos}\ A_4) = d \tag{4.5}$$

$$\text{Solving for } A_4 = \text{Cos}^{-1}\left(\frac{k^2-1}{k^2+1}\right) \cong 18.675^{\ 0}$$

$$R_4 = \frac{h}{\text{Sin } A_4} = 9.497 \text{ m}$$

CHAPTER 5 RESULTS AND DISCUSSIONS

5.1 Introduction

For this research, a fully automated Structure Medium Analysis Program (SMAP) for section two tunnel analysis was used to model and analyzes a horseshoe tunnel following the NATM (New Austrian Tunneling Method).

5.1.1 Excavation and external load steps

Table 5-16 Excavation load and lining subjected to external load steps Load Steps

STEP	Description
5	Excavation of Upper Left Core
8	Excavation of Upper Right Core
11	Excavation of Lower left Core
14	Excavation of Lower right Core
15	Lining Subjected to: Self Weight
18	Lining Subjected to: Self Weight and Water Pressure
21	Lining Subjected to: Self Weight and Water Pressure, and Loosening load
22	Lining Subjected to: Self Weight and Water Pressure, Loosening Load, Rock bolt deactivation and shotcrete degradation

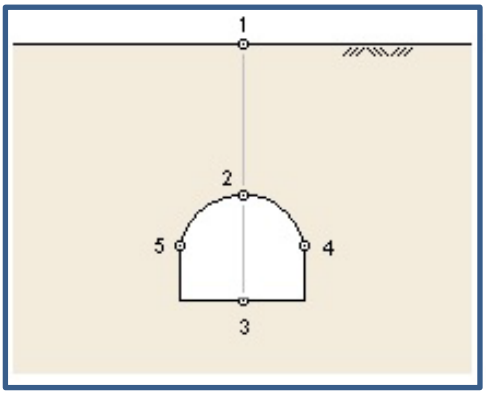

Figure 5-11 Location for displacement history ploy by PLOT XY

- Displacement History at Location: 1 - Ground surface settlement
- Displacement History at Location: 2 – Tunnel Crown
- Displacement History at Location: 3 – Tunnel Invert
- Displacement History at Location: 4 – Spring line (Right Curved Side Wall)
- Displacement History at Location: 5 – Spring line (Left Curved Side Wall)

5.2 Finite element mesh

5.2.1 2-D Mesh dimension and Boundary Conditions

A base mesh for mesh selected for each section under study with the width and height and element size defined from the Base Mesh Window.

For this research, providing a distance at least 4 to 5 times the tunnel diameter from the center to the vertical mesh boundaries is used and a distance about 5 times the tunnel diameter from the tunnel center to the bottom mesh boundary. For the horizontal distance from the left to the right boundary and modified from a recommendation by Moller [37], the following calculation for the mesh dimension was used

$$w = 3D\left(1 + \frac{H_{OB}}{D}\right) \tag{5.1}$$

Where w = the horizontal distance from the left to the right boundary, D is the tunnel diameter and H_{OB} is the overburden height from the ground surface to the top tunnel crown at Location 2.

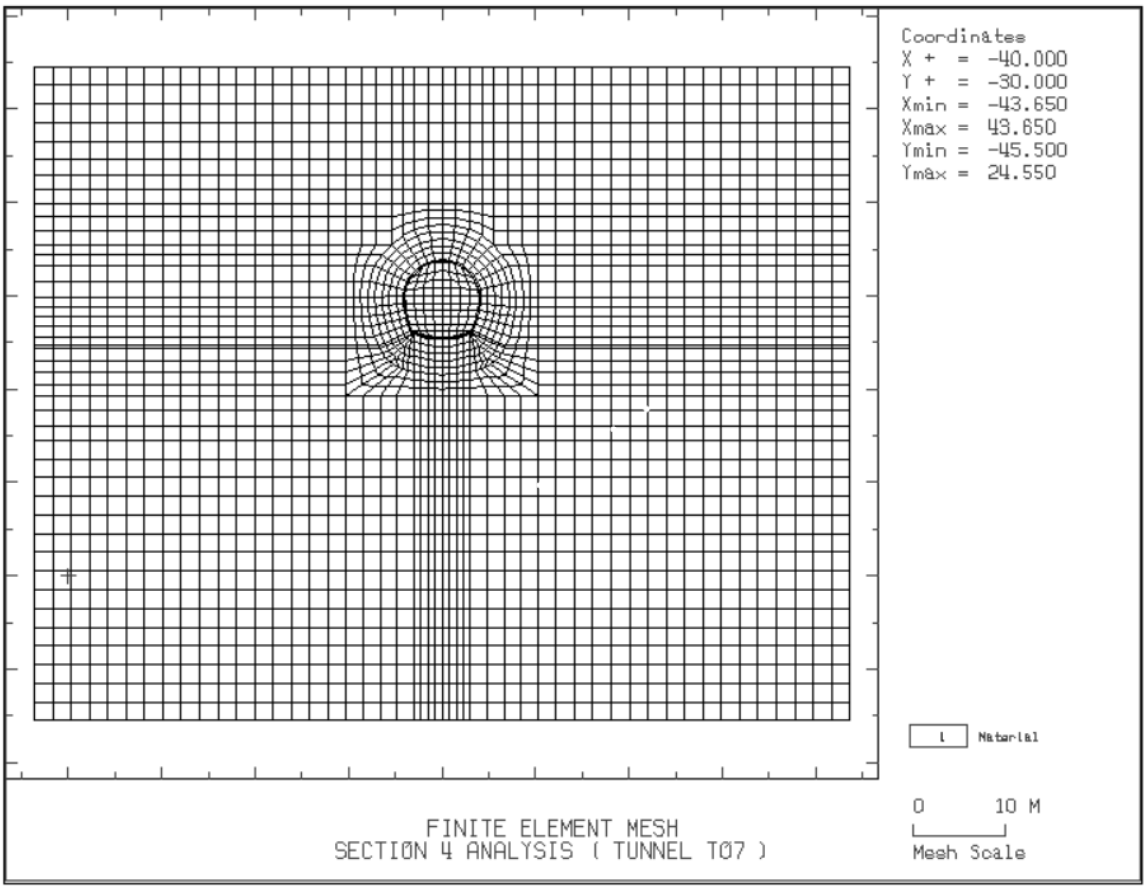

Figure 5-12 Finite Element Mesh Section 4

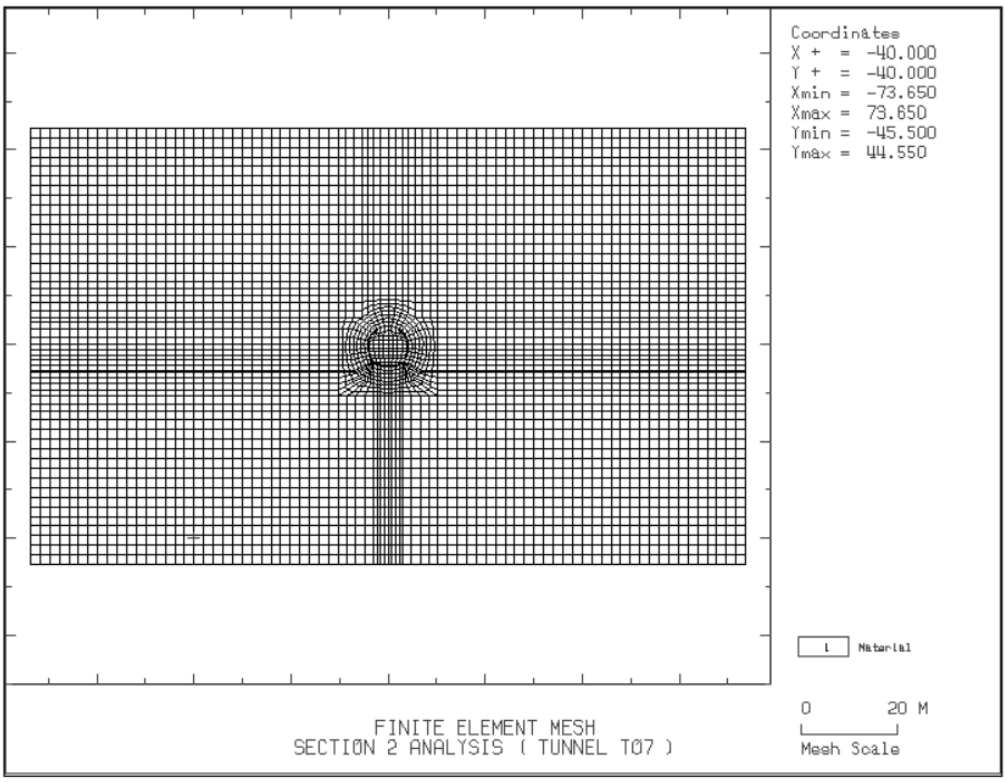

Figure 5-13 Finite Element Mesh Section 2

The finite element mesh presented showing the overburden of 20 m for Figure 5-12 (Section 4) and Figure 5-13 indicates overburden of 40 m for (Sections 5 and Section 2).

5.3 Excavation Tunnel Analysis

5.3.1 Description of the excavation load and lining subjected to external load steps.

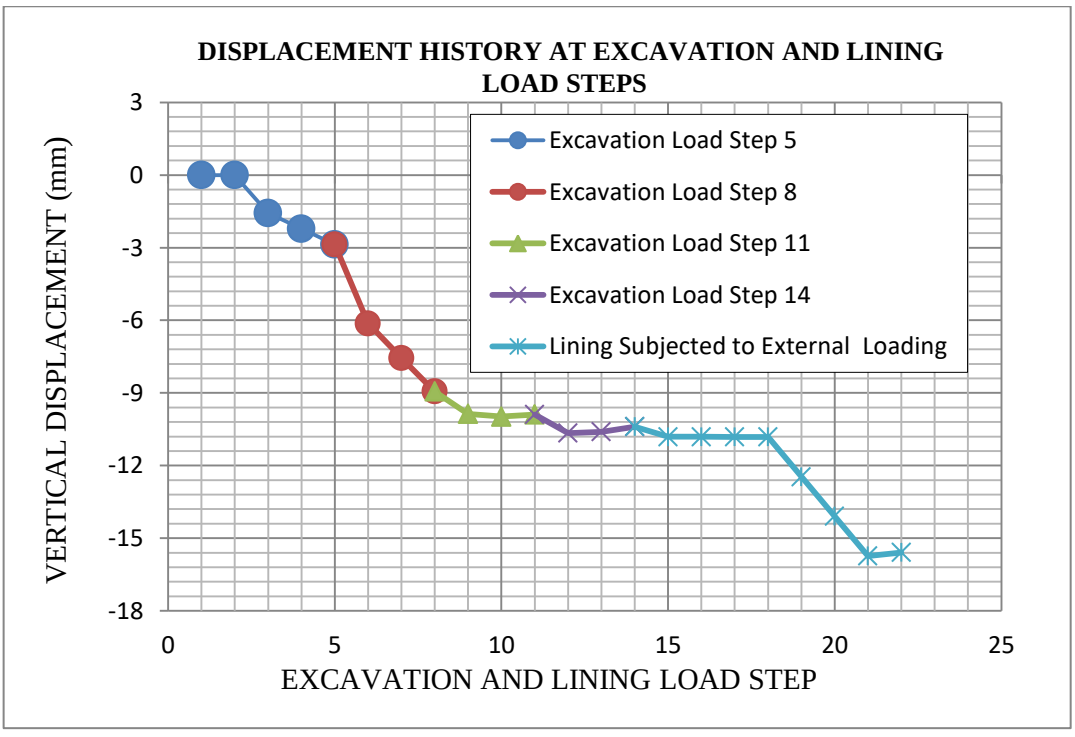

Figure 5-14 Description of Excavation and lining load Steps

5.3.2 Vertical and Horizontal Displacement History around the tunnel (Section 2)

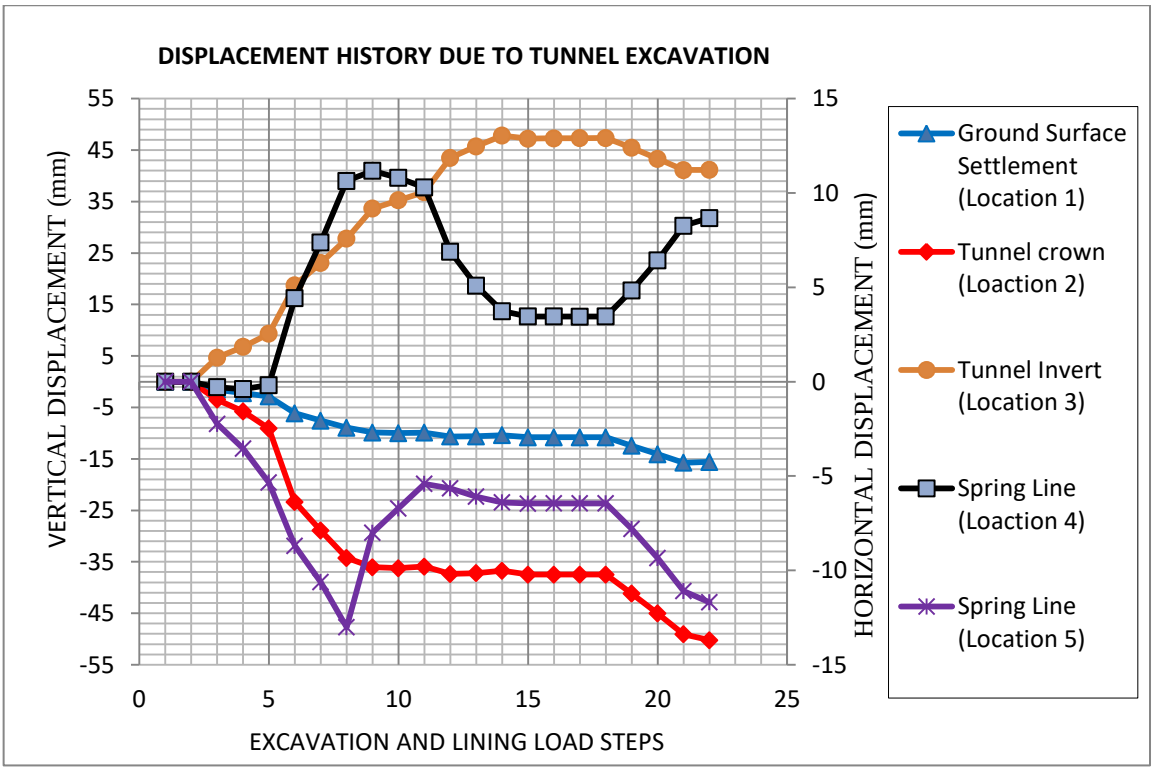

Figure 5-15 Vertical displacement at tunnel crown Section 4

5.3.3 Vertical and Horizontal Displacement History around the tunnel (Section 5)

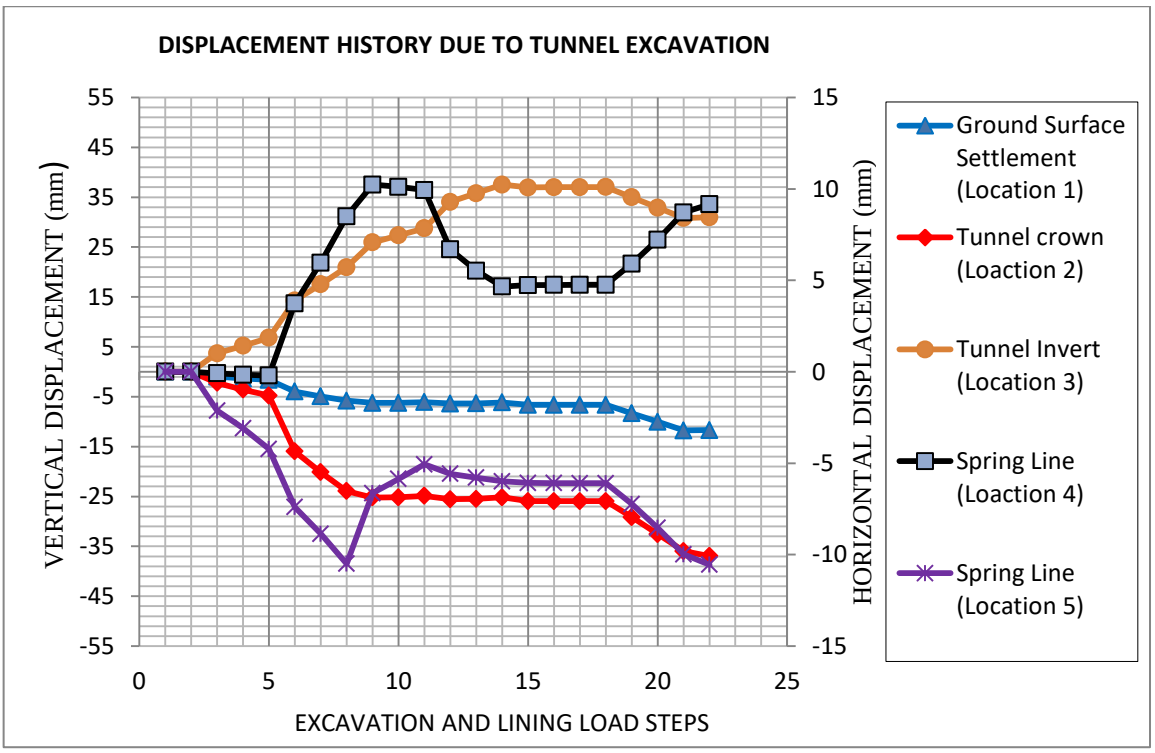

Figure 5-16 Vertical displacement at tunnel crown Section 5

5.3.4 Vertical and Horizontal Displacement History around the tunnel (Section 4)

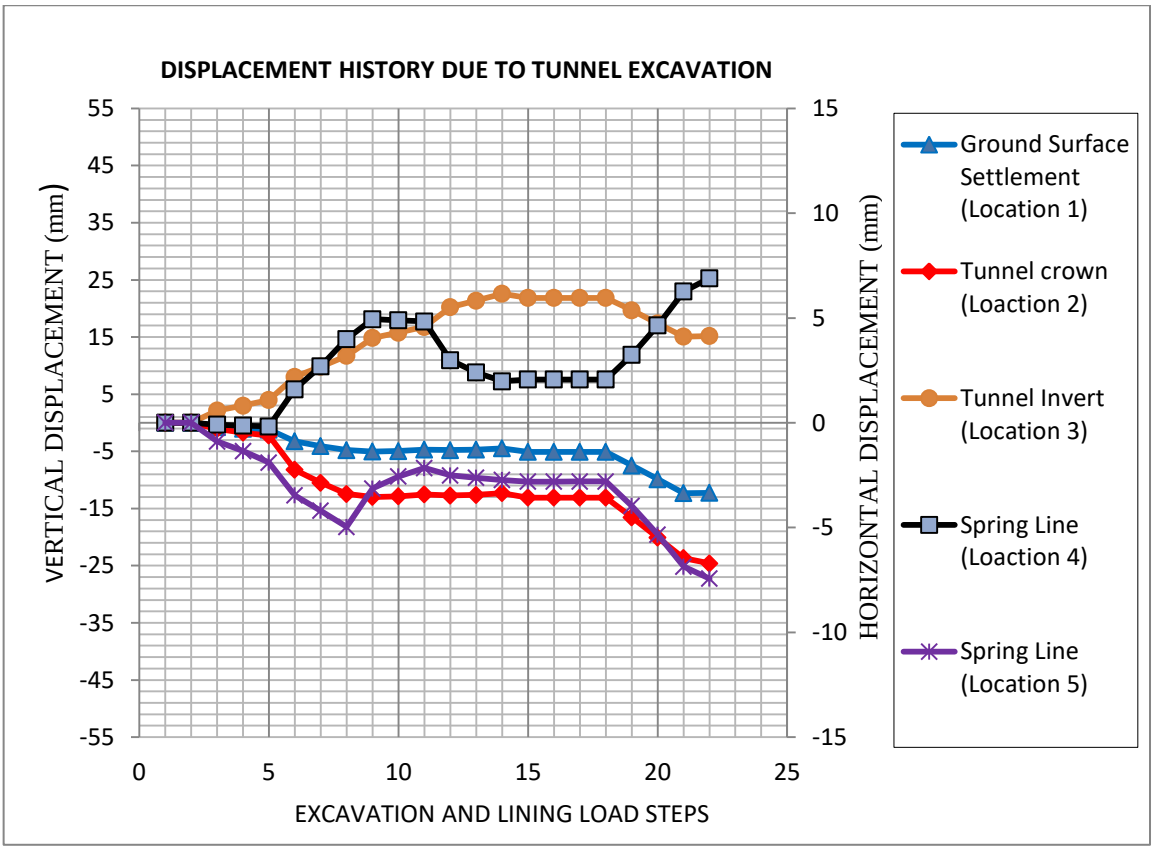

Figure 5-17 Vertical displacement at tunnel invert Section 4

Figure 5-15, Figure 5-16 and Figure 5-17 present the expected vertical displacements at the ground surface, around the tunnel crown, and tunnel invert due to tunnel excavation order induced load steps along the primary axis and the horizontal displacement about the spring line along the secondary axis. Table 5-17 below summaries all the displacements.

Table 5-17 Tunnel wall expected displacement history

LOCATION		Crown	Invert	Crown	Invert
Studied Sections	**Soil/Rock Type**	**Displacement at excavation load Step (mm)**		**Expected final displacement (mm)**	
Section 2	Rock C2 in fault zone (Highly fractured)	36.72	47.83	50.23	41.15
Section 4	Rock B-C rock in Transition to fault zone (Moderately fractured)	12.30	22.58	24.60	15.19
Section 5		25.18	37.52	36.97	30.98

From Table 5-17, the maximum vertical displacement of about 36.72 mm, at excavation load step and a maximum of 50.23 mm final displacement is predicted in the tunnel crown for highly fractured rock mass (Section 2). In Figure 5-16, the maximum vertical final displacement in the tunnel crown is 36.97 mm with is about 75 % less than the final expected displacement in Figure 5-15 (Section 2) under the same overburden of 40 m whereas the vertical displacements in Figure 5-17, show that a maximum vertical displacement 12.30 mm , and 24.60 mm both at excavation load and lining load subjected to external load. The induced displacements are larger at the tunnel crown. The presence of the external loading can increases the tunnel crown displacements by 26 % and 32 % in highly fractured rock mass (Section 2) and moderately fractured rock mass (Section 5) and about 50 % for moderately fractured rock mass (Section 4) at 20 m overburden. Thus the severity of the external is more critical on shallow tunnel excavations at lower over burden depth compared to those at high over burden.

As shown in Table 5-17, the vertical displacement in the tunnel at higher at final excavation load step but is lower even with presence of external load step from lining analysis as shown in the displacement history plots in all the studied sections. This due to minimum compression stresses expected at the provisional lining at the invert. The displacements in the tunnel invert is about 0.8 of the tunnel crown for studied section at 40 m overburdened compared to about 0.6 of the tunnel crown at 20 m over burden.

Therefore, it is concluded that the influence of overburden is related to the vertical displacement in a linear way as presented. The behavior of that highly fractured rock mass in a fault zone coupled with the influence of overburden indicates the highest displacement values, which is consistent with what, experience displays.

Table 5-18 Tunnel wall expected displacement at the spring line

Studied Sections	Soil/Rock Type	Displacement at Excavation Load Step (mm)		Expected final Displacement (mm)	
		LOC 4	LOC 5	LOC 4	LOC 5
Section 2	Rock C2 in fault zone (Highly fractured)	3.74	6.39	8.67	11.69
Section 4	Rock B-C rock in	1.98	2.73	6.90	7.44
Section 5	Transition to fault zone (Moderately fractured)	4.66	5.99	9.16	10.55

At spring line as shown in Table 5-18, the maximum horizontal displacements at the tunnel side walls are 3.74 mm and 8.67 mm (Section 2, Location 4) and 6.39 mm and 11.69 mm (Section 2, Location 5) at excavation load step and also lining subjected to external loading load step respectively. The maximum horizontal displacements at the tunnel side walls are 4.66 mm and 9.16 mm (Section 4, Location 4), 5.99 mm and 10.55 mm (Section 2, Location 5) at excavation load step and also lining subjected to external loading load step respectively. For lower overburden at 20 m , the maximum horizontal displacements at the tunnel side walls are 1.98 mm and 6.90 mm (Section 4, Location 4) and 2.73 mm and 7.44 mm (Section 4, Location 5) at excavation load step and also lining subjected to external loading load step respectively. However, rock B-C i.e. rock in transition to fault zone (Moderately fractured) for the different sections, the maximum horizontal expected 6.90 mm and 9.16 mm (Location 4) respectively.

Therefore, the lower the overburden the lower the expected displacements for the same surrounding rock mass and high overburdens thus high horizontal displacements expected at the tunnel excavations. It can therefore be explained that the effect of external load increases the expected horizontal displacements at most by nearly more than four times in the lower over burden at 20 m and about twice in higher over burdens at 40 m of those obtained at major excavation load steps. Thus, The influence of the external load combination induces an increased final horizontal displacement of about 11.69 mm (Section 2, location 5) with nearly 45 % increase in displacement. It can be concluded that the horizontal displacement can be influenced by the difference in the rock mass conditions and as well the overburden thus it is deemed vital to analyze the deformation expected around the tunnel excavation.

5.3.5 Ground settlement and Ground Surface displacement history

Table 5-19 Ground surface expected displacement history

Studied Sections	Soil/Rock Type	Expected Final Surface Displacement (mm)
Section 2	Rock C2 in fault zone (Highly fractured)	15.59
Section 4	Rock B-C rock in Transition to fault zone (Moderately fractured)	12.26
Section 5		11.71

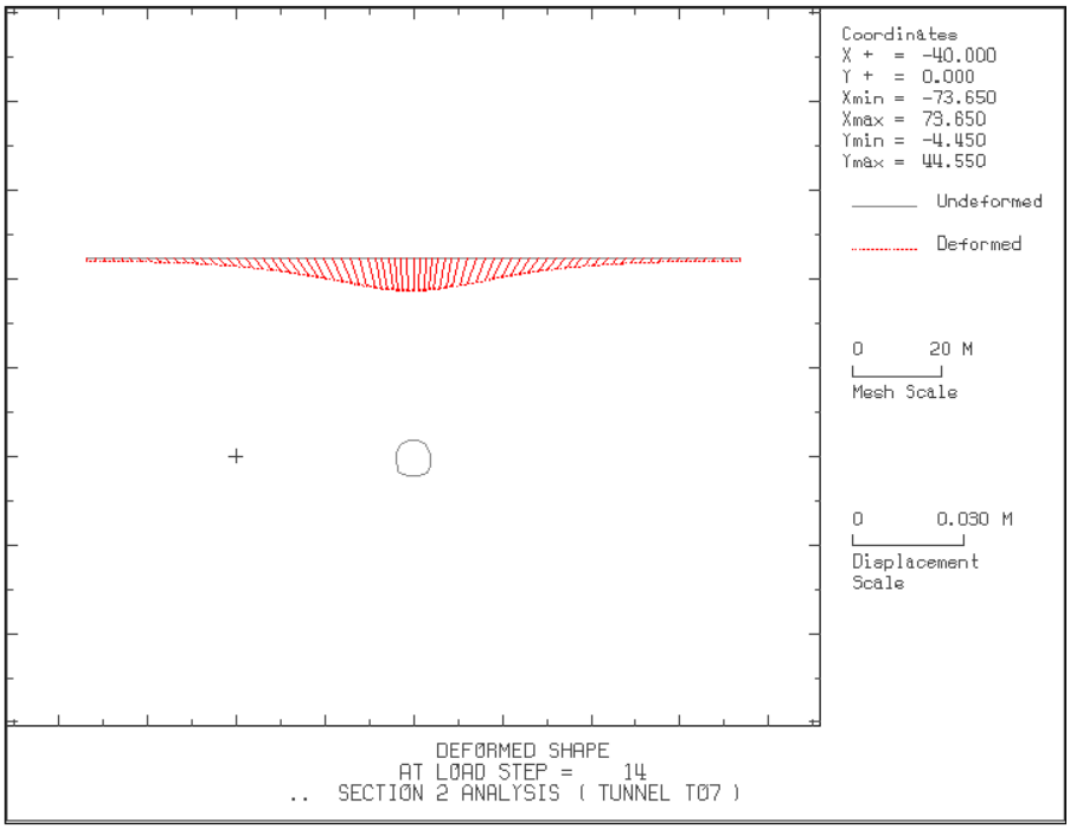

Figure 5-18 Ground surface deformed shape Section 2

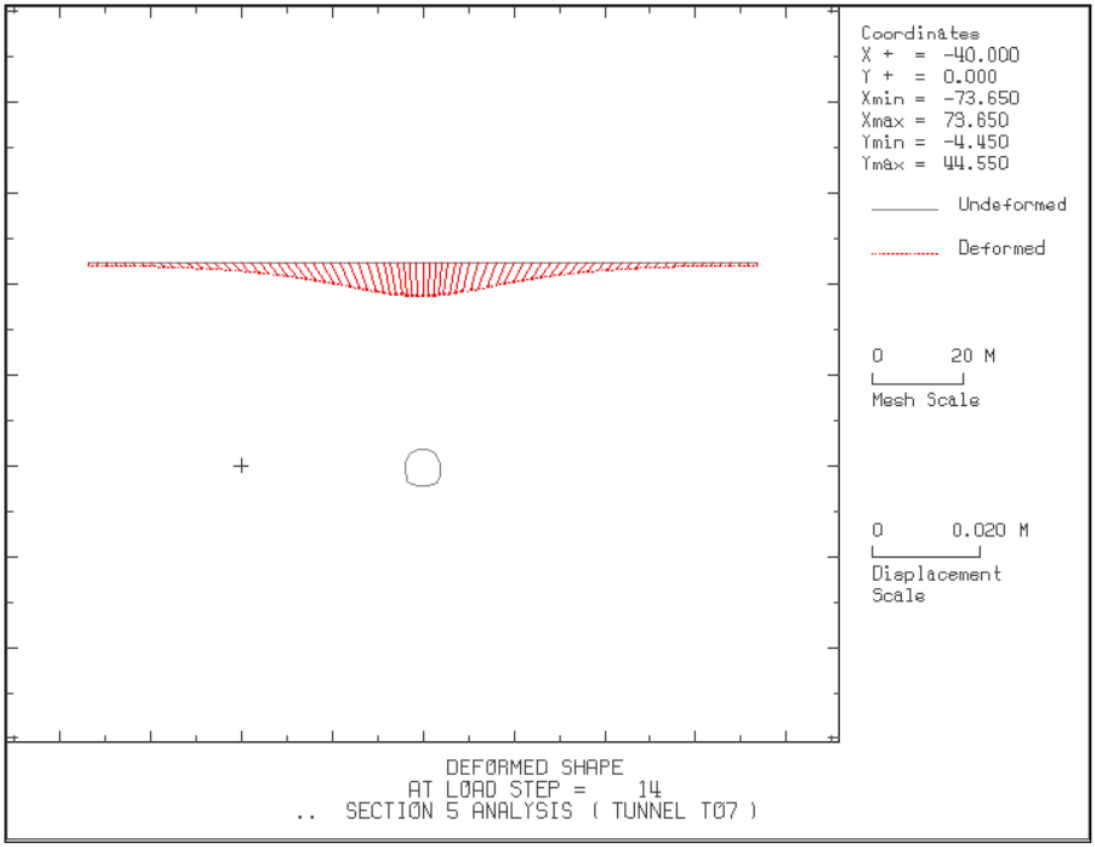

Figure 5-19 Ground surface deformed shape Section 5

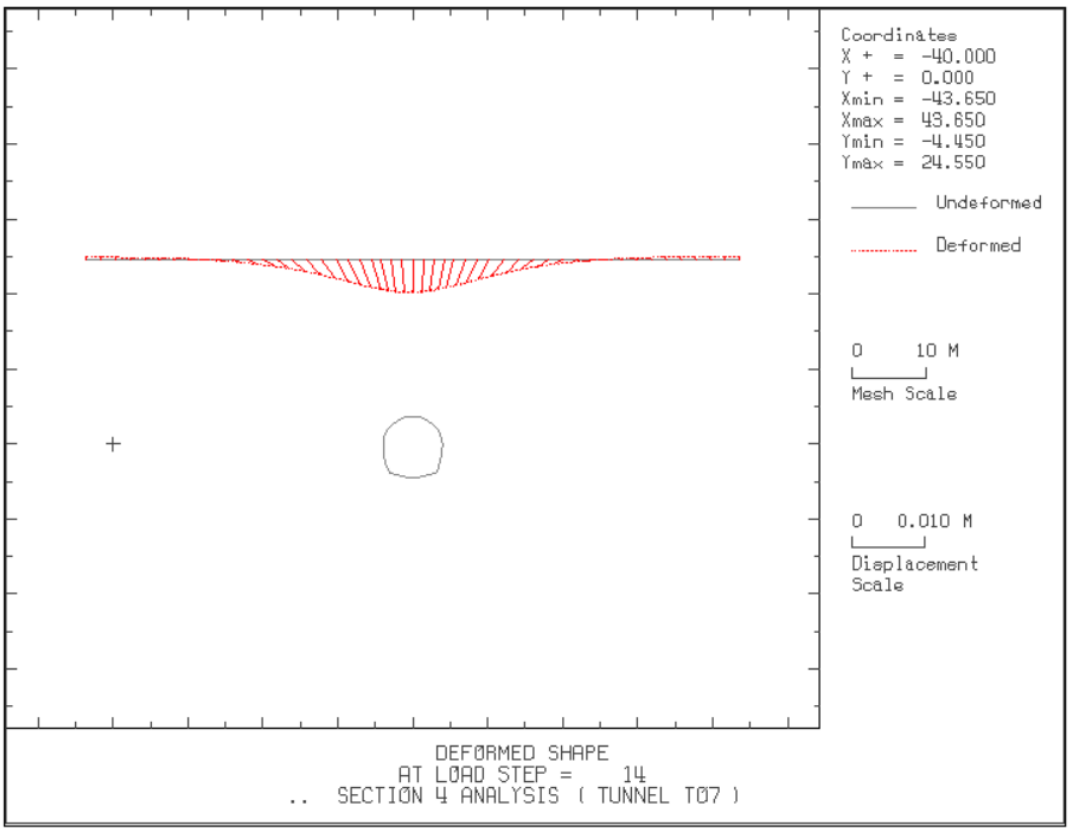

Figure 5-20 Ground surface deformed shape Section 4

Figure 5-18, Figure 5-19 and Figure 5-19 present the expected ground surface settlement in all the studied sections in different rock mass conditions and buried at different over burden depth. From Table 5-19, the vertical displacement at ground surface settlement of 12.26 mm for moderately fractured rock mass at 20 m overburden (Section 4) is about 5 % greater than a ground surface settlement of 11.71 mm for the rock mass condition at 40 m (Section 5). This due to the larger ground settlements expected at lower overburden depths especial in shallow tunnels compared to deep tunnel at higher over burden depths where there is limited expected surface settlements for homogenous rock mass conditions.

However, larger vertical displacement of 15.59 mm as shown in Table 5-19 is predicted in highly fractured rock mass (Section 2) in different rock mass compared to studied tunnel sections (Section 4 and Section 5) in moderately fractured rock mass. Thus the it can be noted that the ground settlement are highly influence by a difference in rock mass conditions. In addition, for deep tunnels the ground surface settlement is limited compare to shallow tunnel at lower overburdens but it is vital to also take into consideration the variation and change different rock masses the can highly influence the behavior of deformations in any underground excavation.

5.4 Stress distribution in the surrounding medium

5.4.1 Numerical simulation plot for Principal Stress Distribution Section 2

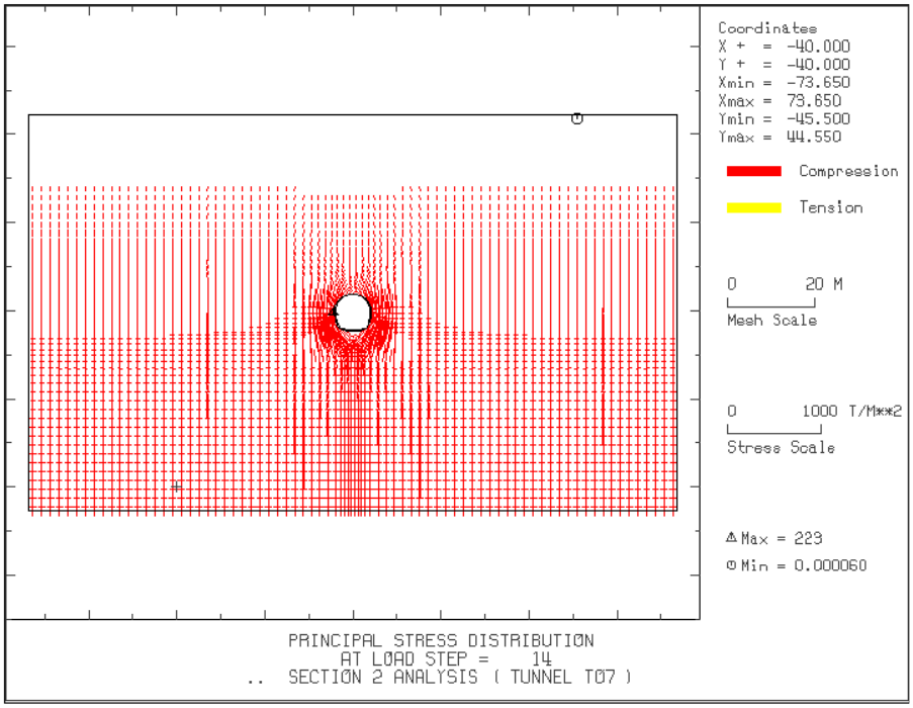

Figure 5-21 Principal stress at model boundary Section 2

5.4.2 Numerical simulation plot for Principal Stress Distribution Section 5

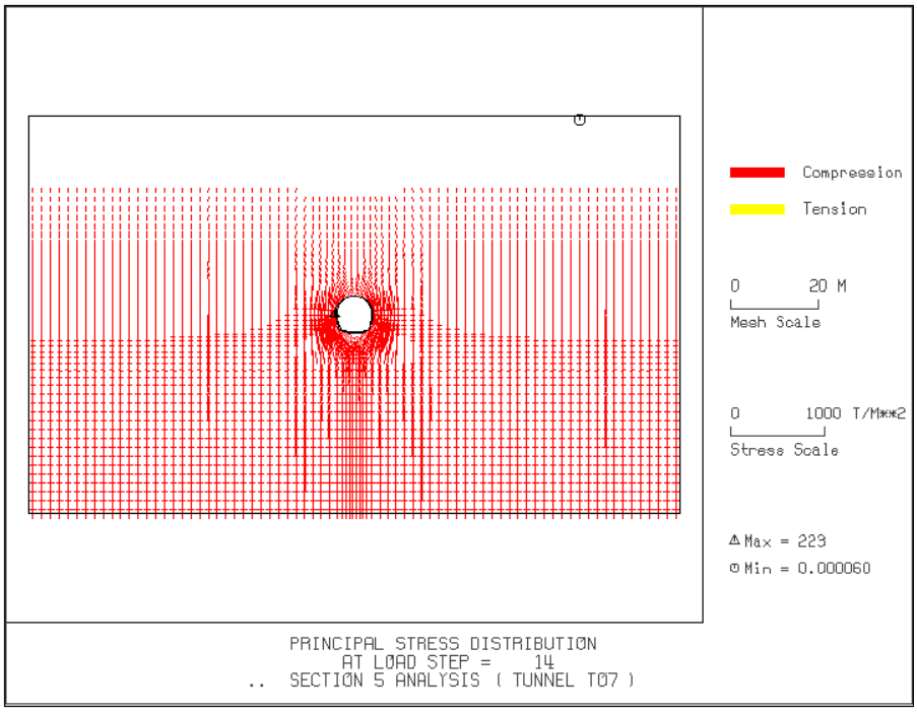

Figure 5-22 Principal stress at model boundary Section 5

Figure 5-21 the maximum principal stress in surrounding rock mass around the tunnel excavation is $229\ t/m^2$ $(2{,}245\ kN/m^2)$ and maximum at the tunnel sidewalls and

minimum at the tunnel crown and invert for highly fractured rock mass at 40 m overburden (Section 2).

5.5.3 Numerical simulation plot for Principal Stress Distribution Section 2

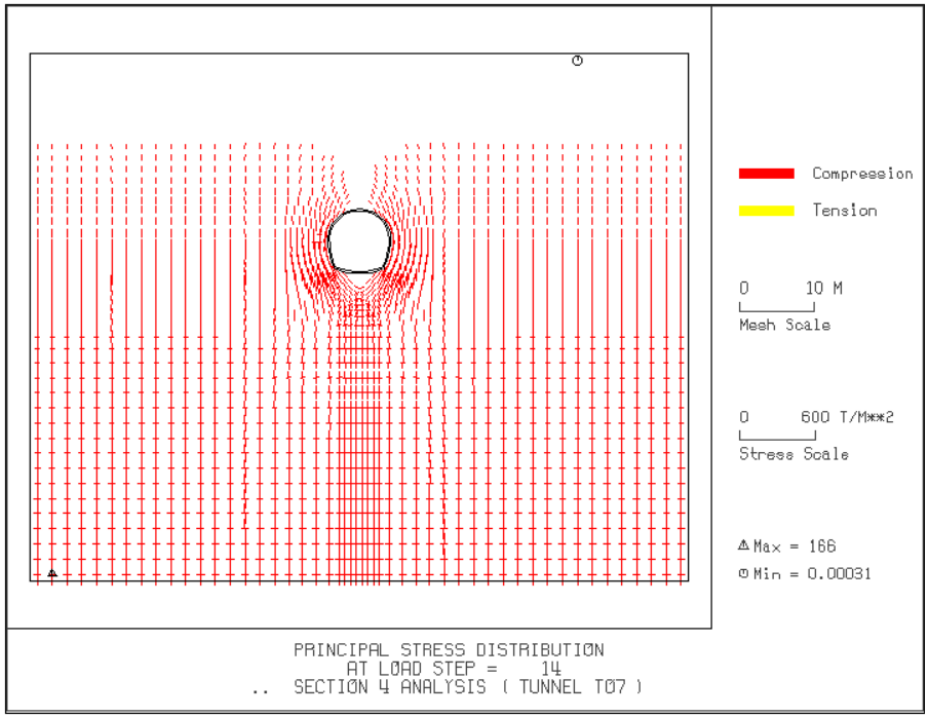

Figure 5-23 Principal stress at model boundary Section 4

In Figure 5-22, the maximum stress distribution is 223 t/m^2 (2,186 kN/m^2) expected at the curved sidewalls near the spring line. However, for the same rock mass type i.e. moderately fractured an increase in the principal stress distribution compared to the principal stress distribution of 166 t/m^2(1,628 kN/m^2) as shown in Figure 5-23 above. This is in agreement with the effect of a higher overburden for homogeneous rock mass conditions as shown in Table 5-20 below.

Table 5-20 Principal Stress Distribution in the surrounding medium

Studied Sections	Soil/Rock Type	Stress distribution (t/m^2)	Stress distribution (kN/m^2)
Section 2	Rock C2 in fault zone (Highly fractured)	229	2,245
Section 4	Rock B-C rock in Transition to fault zone (Moderately fractured)	166	1,628
Section 5		223	2,186

5.5 Major Principal Stress

Table 5-21 Major and Minor Principal Stresses around the tunnel excavation

Studied Sections	Soil/Rock Type	Major Principal stress	Minor Principal stress
Section 2	Rock C2 in fault zone (Highly fractured)	195 t/m^2 (**1,912 kN/m^2**)	50.41 t/m^2 (**494.22 kN/m^2**)
Section 4	Rock B-C rock in Transition to fault zone (Moderately fractured)	116 t/m^2 (**1,137 kN/m^2**)	30.50 t/m^2 (**299.02 kN/m^2**)
Section 5		206 t/m^2 (**2,020 kN/m^2**)	48.28 t/m^2 (**473.33 kN/m^2**)

5.5.1 Numerical simulation Plot for Major Principal Stress Section 2

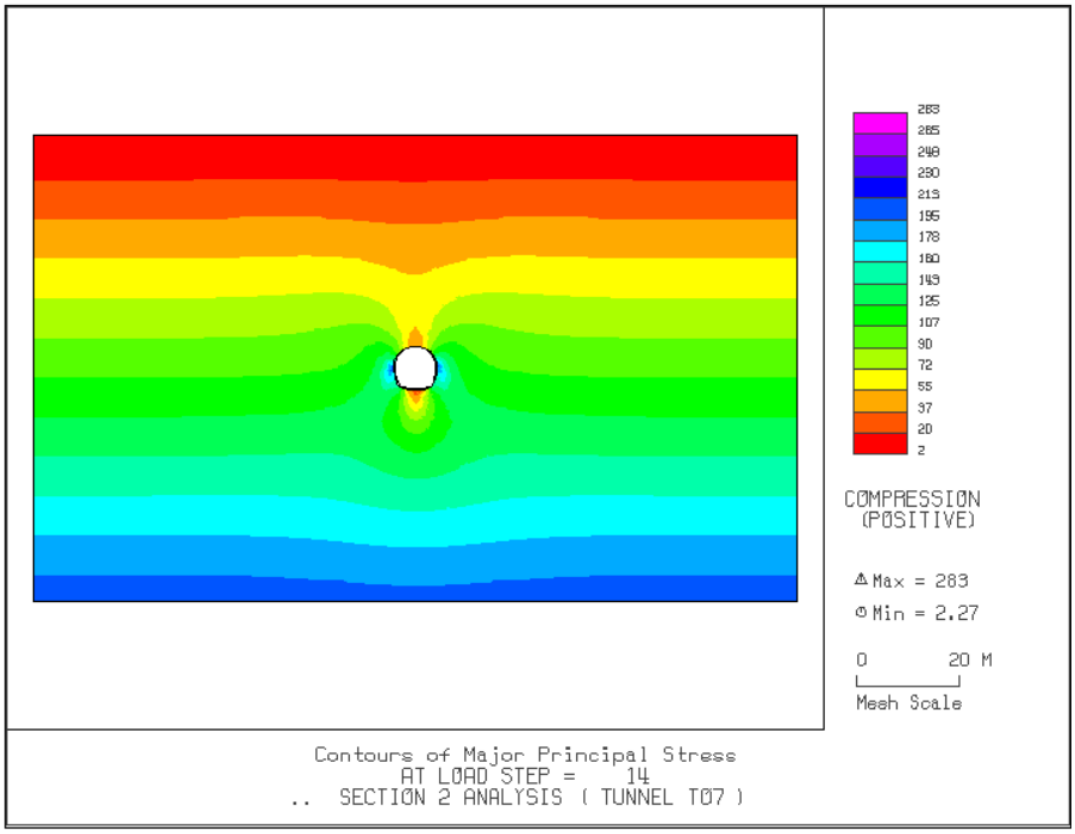

Figure 5-24 Color filled Major Principal Stress Section 2

Usually, three ground principal stresses are denoted in ascending order of magnitude they exist. Figure 5-24, the major principal stress of 198 t/m^2 (1,912 kN/m^2) is predicted within the vicinity of the tunnel side walls for highly fractured rock mass in overburden 40 m. The minimum stress 20 t/m^2 (196 kN/m^2) is expected at the tunnel invert whereas minimum major principal stress 2.27 t/m^2 located at the ground surface as expected as shown in the color contour option.

5.5.2 Numerical simulation plot for Major Principal Stress Section 5

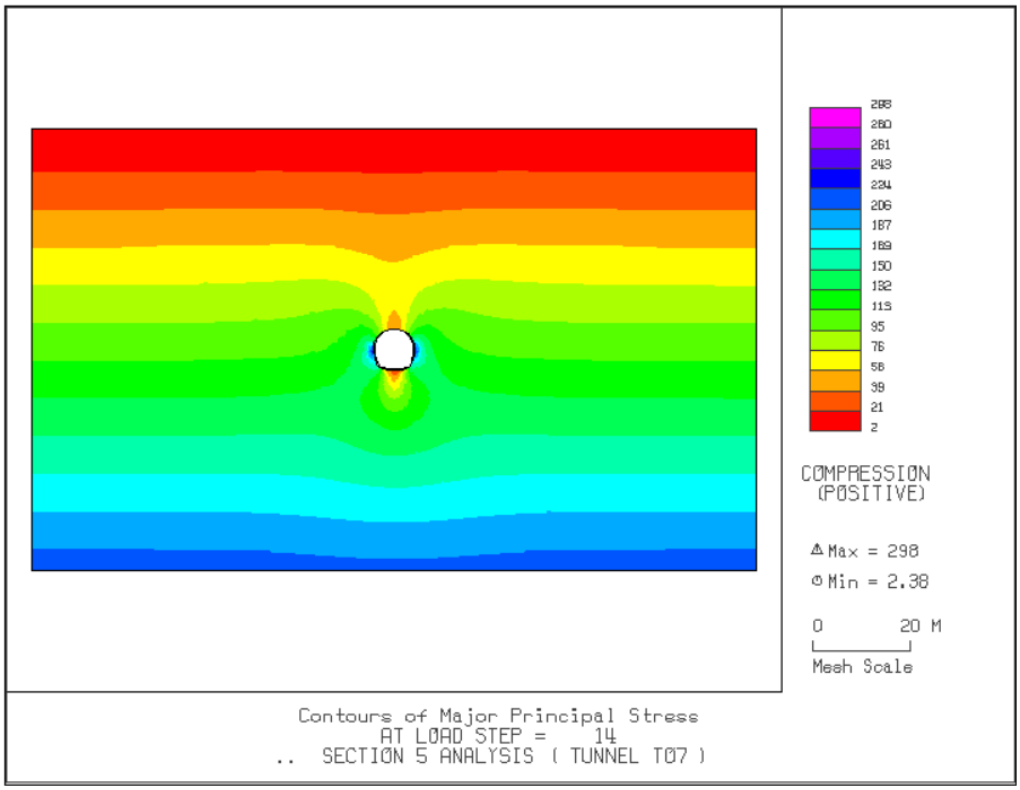

Figure 5-25 Color filled Major Principal Stress Section 5

5.5.3 Numerical simulation plot for Major Principal Stress Section 4

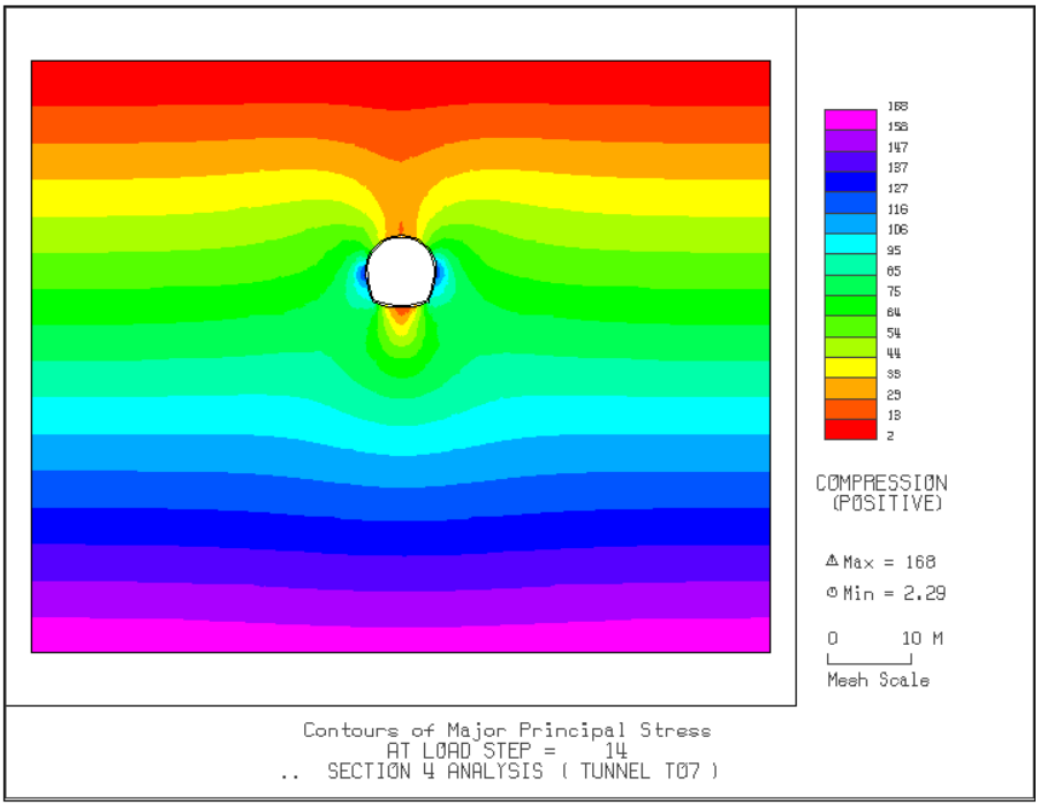

Figure 5-26 Color filled Major Principal Stress Section 4

In Figure 5-25, the major principal stress of $206\ t/m^2$ $(2{,}020\ kN/m^2)$ is predicted within the vicinity of the tunnel side walls for moderately fractured rock mass in overburden $40\ m$. The minimum major principal stress $2.38\ t/m^2$ located near the ground surface as expected as shown in the color contour option. However, From Table 5-21, higher values of major principal stress are predicted for the same rock mass condition as compared to those obtained in Figure 5-26 (Section 4). For rock B-C, moderately fractured an increase in the normal stresses at zero shear stress is due to the difference in the overburden of the same homogenous rock mass conditions. It is also noted that rock C2 type in fault zone i.e. highly fractured rock mass. The values of the principal stress are lower by about $5.6\ \%$ than in the obtained stresses in Figure 5-25 with the same overburden but different rock condition.

5.6 Minor principal stress

5.6.1 Numerical simulation plot for Minor Principal Stress Section 2

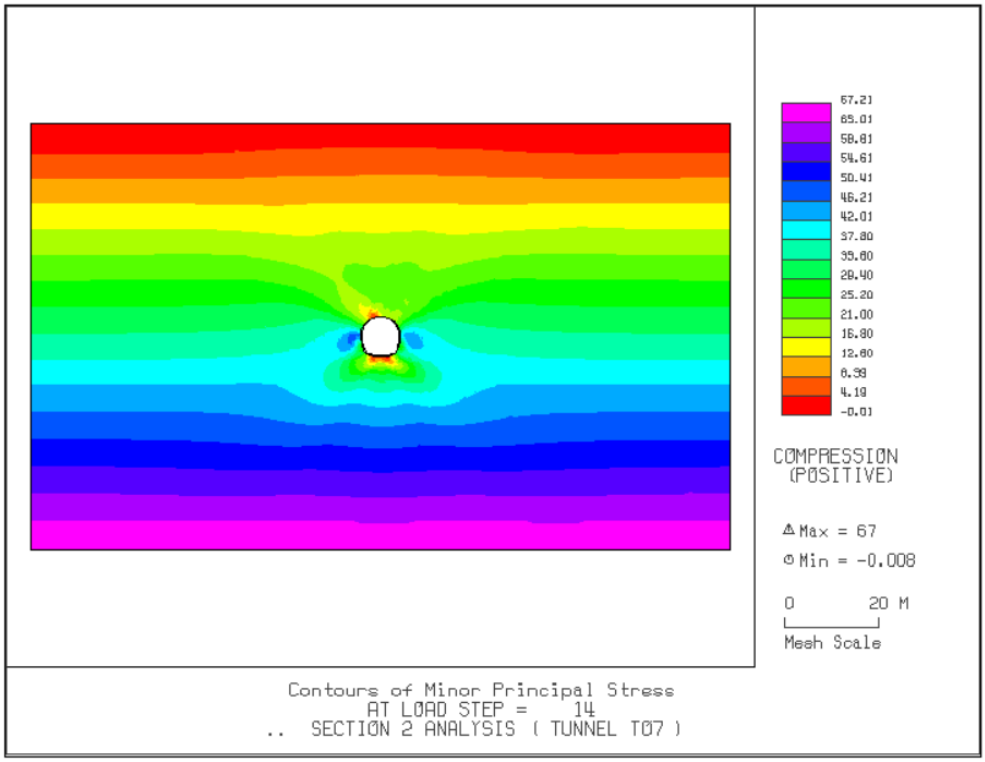

Figure 5-27 Color Contour of Minor Principal Stress Section 2

In Figure 5-27, the minor principal stress, σ_3 is $50.41\ t/m^2$ $(492.22\ kN/m^2)$ around the tunnel side walls is predicted. However, the maximum minor principal stress are locating a distance of about 5D from the tunnel center line and the minimum minor compressive stress is expected at the tunnel crown and invert this due to the arching even of the loads around circular underground excavations and also the loads are supported radially.

5.6.2 Numerical simulation plot for Minor Principal Stress Section 5

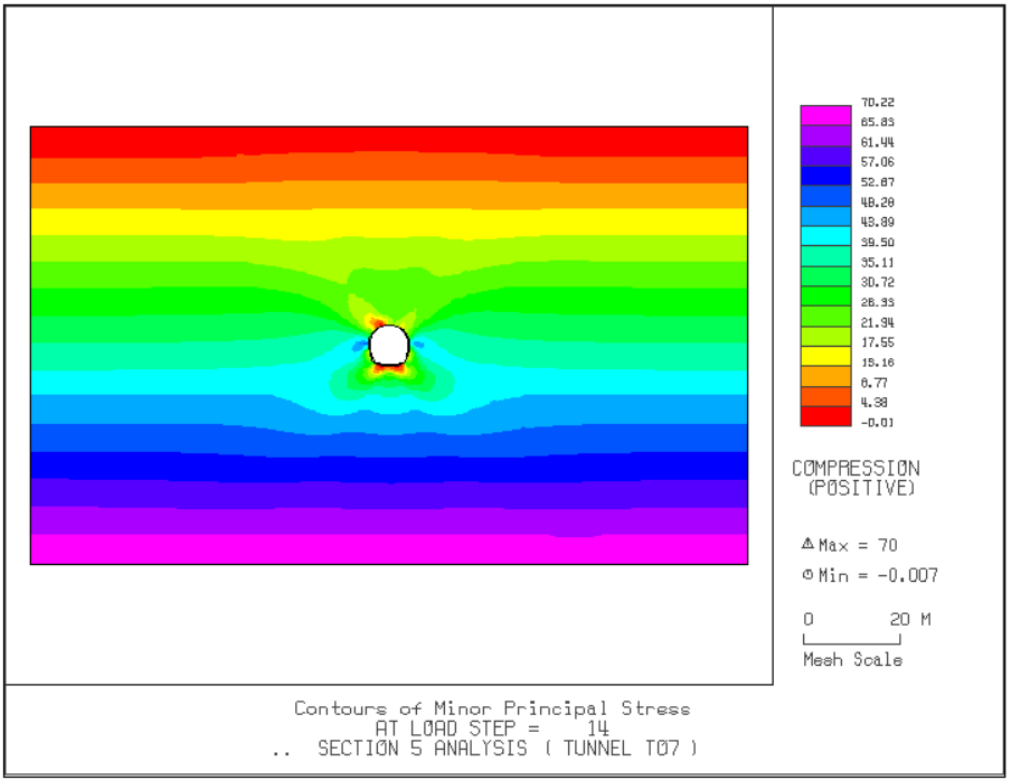

Figure 5-28 Color filled Minor Principal Stress Section 5

5.6.3 Numerical simulation plot for Minor Principal Stress Section 4

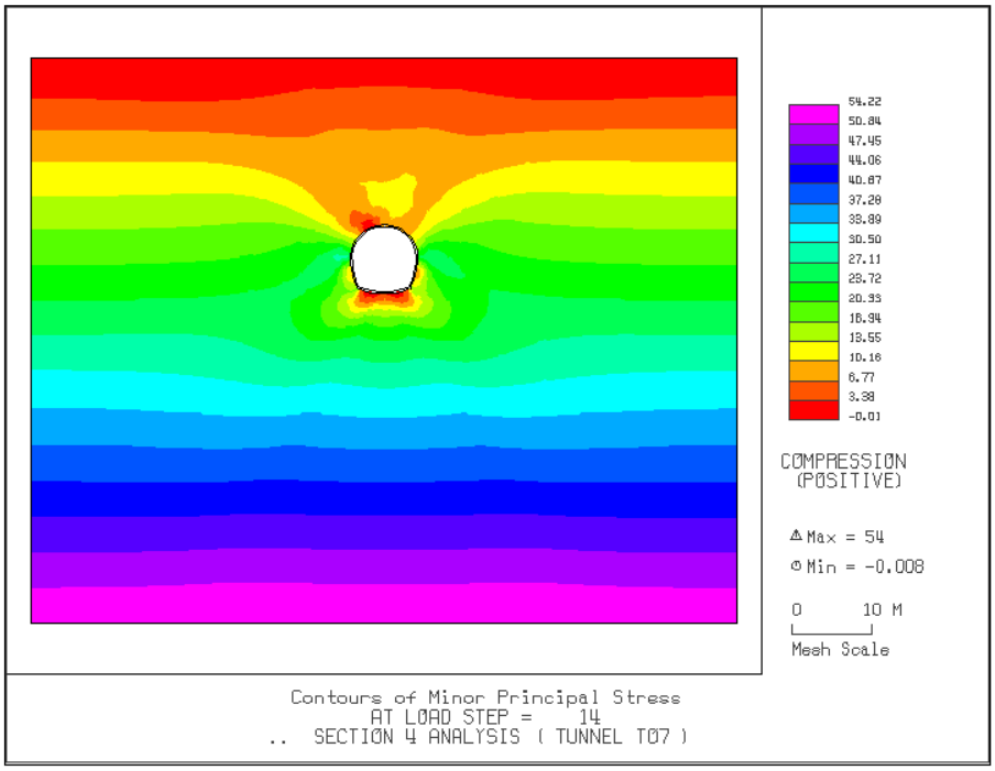

Figure 5-29 Color filled Minor Principal Stress Section 4

Considering the stability of any excavation, it's vital to understand the existence of the minor principal stresses. Figure 5-28, minor principal stress is 30.50 t/m^2 (473.33 kN/ m^2) and Figure 5-29 a value 48.28 t/m^2(299.02 kN/m^2) at the curved tunnel sidewalls for the same rock mass conditions in Section 5 and Section 4 respectively. However, maximum minor principal stress of is predicted for the surrounding rock mass at the lower bottom of the mesh boundary.

The overall major principal stress denoted, σ_1 yields the largest compressive stress around the tunnel sidewalls close to the spring line. It can be noted due to the arching effect of the loads the largest compressive major and minor stresses are also expected along the sidewalls since all loads are supported radially especially for deep tunnels at $H > [\text{span} \times (GSI/5)]$ whereas for shallow tunnels at depth $[H \leq \text{span} \times (50/(GSI)]$, according to Perri [38]. In addition, the rock mass overburden exerts pressure on the crown and horizontal loads bear on the sidewalls. Therefore, field stresses at any depth tend to confine the tunnel excavation hence stability to a certain degree is expected. Stability can be affected by overburden depth, the closeness of the excavation to the surface or how it's further inside the ground.

5.7 Principal stress distribution in the shotcrete

5.7.1 Numerical simulation plot Principal Stress Distribution Section 4

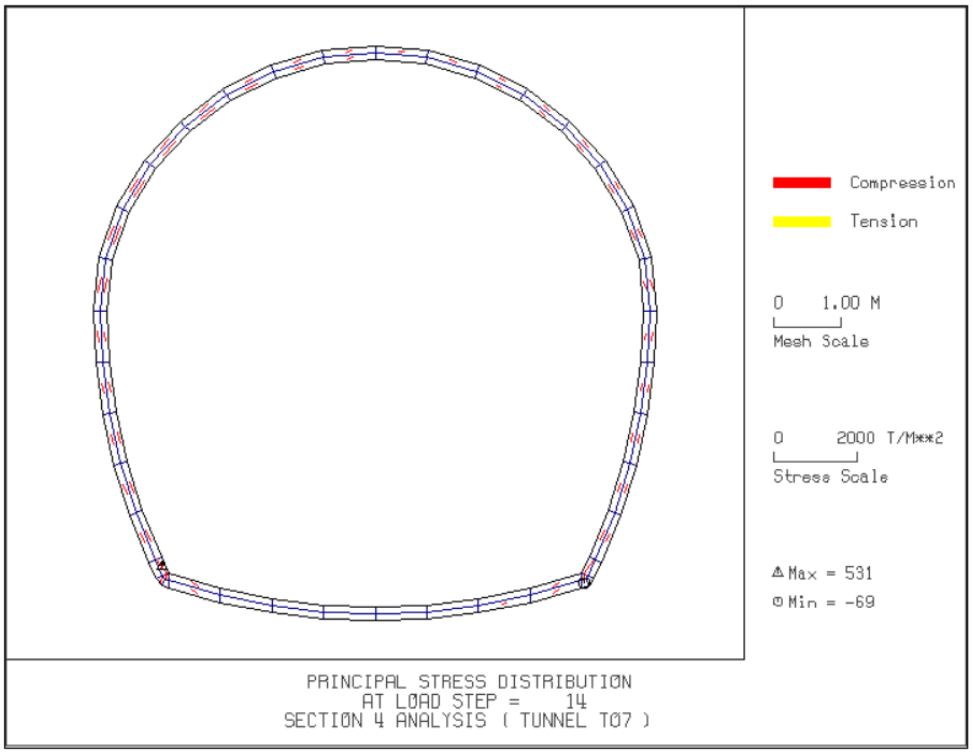

Figure 5-30 Principal Stress Distribution in Shotcrete Section 4

5.7.2 Numerical simulation plot Principal Stress Distribution Section 5

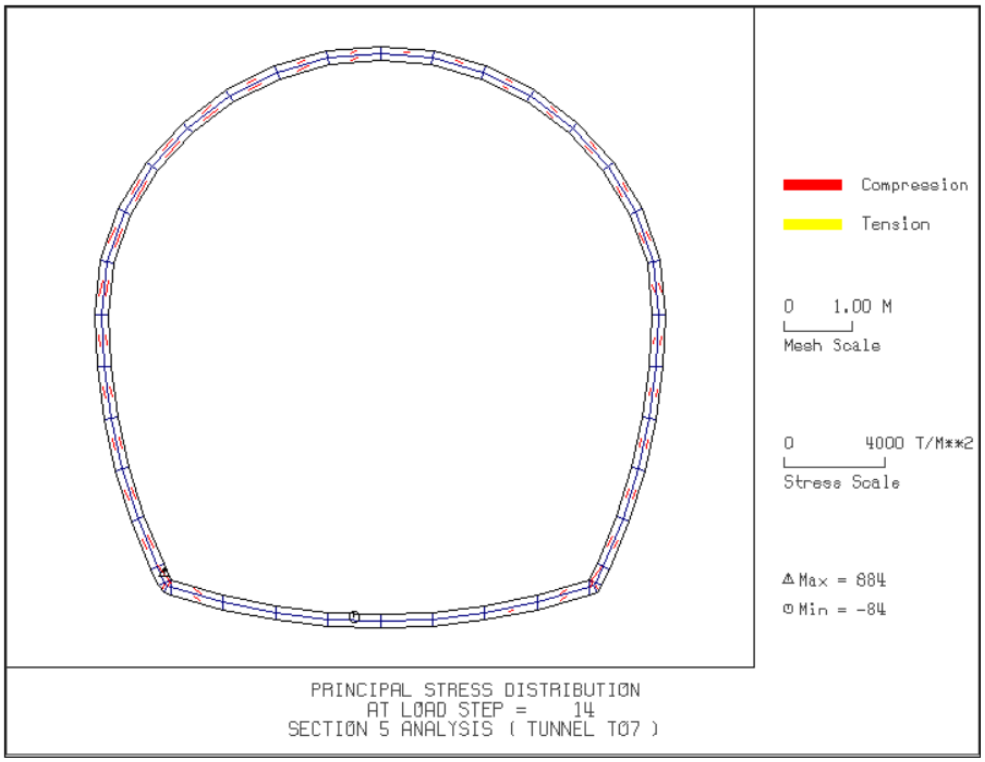

Figure 5-31 Principal Stress Distribution in Shotcrete Section 5

5.7.3 Numerical simulation plot Principal Stress Distribution Section 2

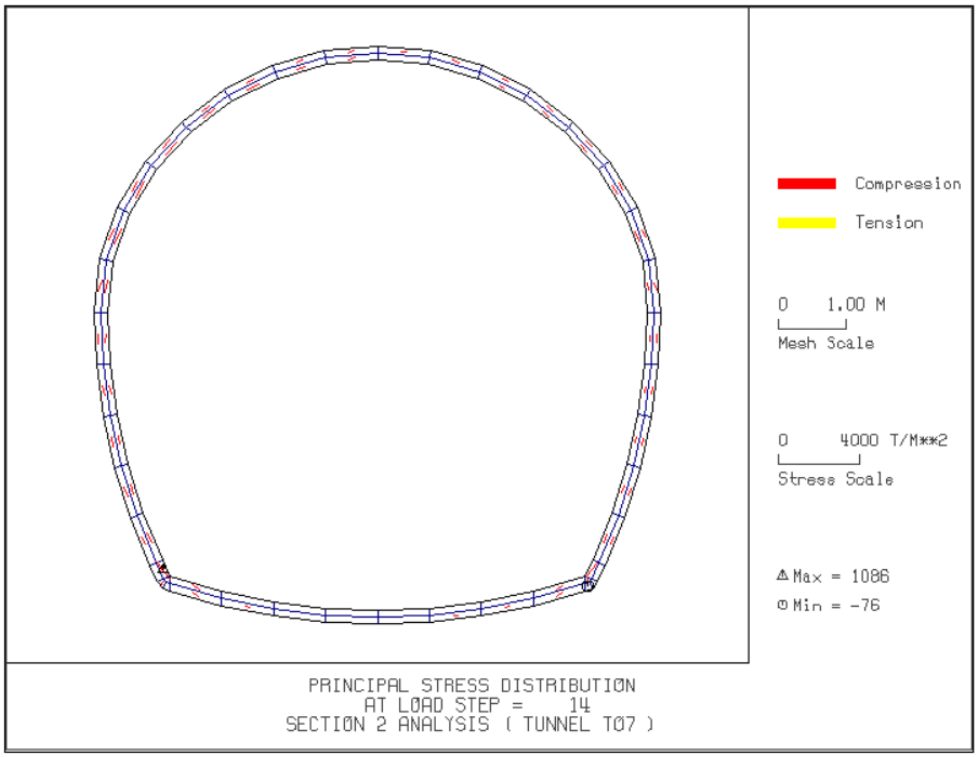

Figure 5-32 Principal Stress Distribution in Shotcrete Section 2

At full bench excavation, the stress distribution in the shotcrete increases due to stress release from the surrounding rock mass. In Figure 5-30, the induced maximum principal stress distribution in the shotcrete is $531\ t/m^2$ ($5{,}206\ kN/m^2$) compression and a minimum acting upward at the extreme bottom right at the tunnel invert with nearly no stress a the mid span of the shotcrete at the tunnel invert.

Figure 5-31, the maximum compressive stress distribution of $884\ t/m^2$ ($8{,}667\ kN/m^2$) is obtained at the far bottom left of the shotcrete tunnel side walls and minimum stress distribution value of is expected at the tunnel invert. However, the principal stress distribution in the shotcrete under different overburdens indicates higher value of principal stress distribution in high overburden $40\ m$ compared to the lower values of principal stresses expected in $20\ m$ overburden height for the same moderately fractured rock mass in Section 4 and Section 5 respectively. Thus, it can be concluded the for the same rock mass condition with influence of the rock mass overburden coupled with differences in rock mass parameters, the stress distribution expected in the shotcrete is dependent and varies to the above stated conditions. In Figure 5-32 the maximum principal stress distribution in the shotcrete is $1{,}086\ t/m^2$ ($10{,}647\ kN/m^2$) compression and a minimum acting upward at the extreme right bottom at the tunnel.

Therefore, in the highly fractured rock mass, the stress distribution in the shotcrete is increased by 22 % to that of moderately fractured rock mass at the same overburden $40\ m$. However, the design strength in the shotcrete of $0.20\ m$ thickness with characteristic compressive strength $25\ MPa$ is capable of withstanding the induced in situ stress from the surrounding rock masses.

5.8 Safety factor in the surrounding rock mass

Induced stress failure in the surrounding medium i.e. rock mass of tunnel T07 section under study, the failure potential is best estimated from the Strength Factor (SF). Table 5-22 shows a summary of contours of safety factor around the studied tunnel sections.

Table 5-22 Contours of Safety Factor around the tunnel excavation

Studied Sections	Soil/Rock Type	Actual of safety factors
Section 2	Rock C2 in fault zone (Highly fractured)	2.19
Section 4	Rock B-C rock in Transition to fault zone (Moderately fractured)	2.69
Section 5		2.69

5.8.1 Numerical simulation plot Safety Factor for Section 4

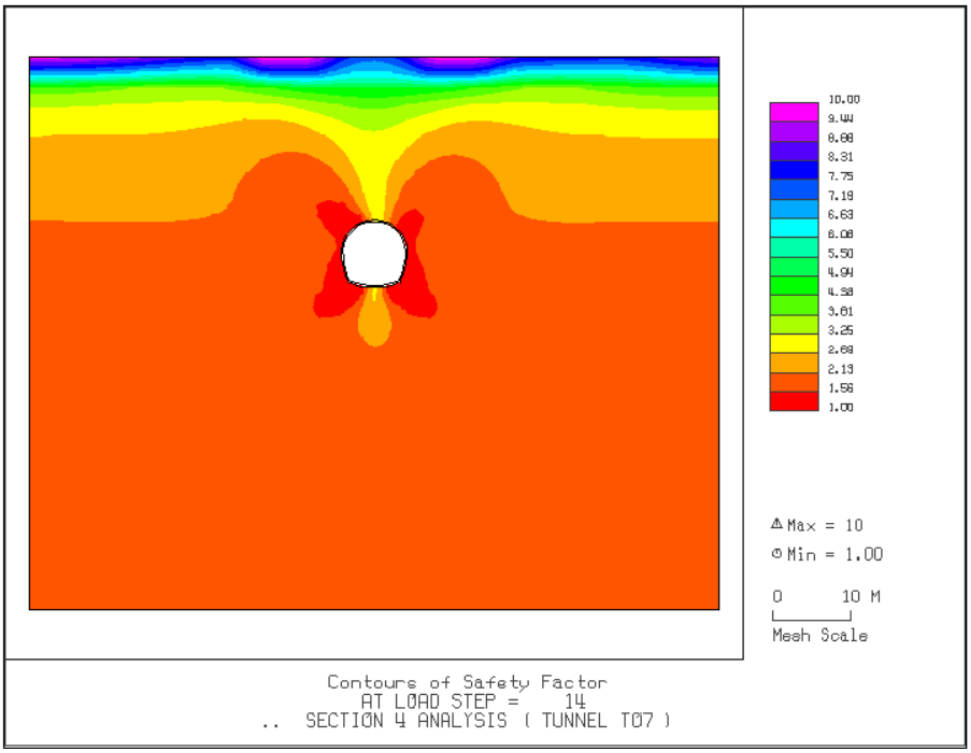

Figure 5-33 Color Contours of Safety Factor Section 4

5.8.2 Numerical simulation plot Safety Factor for Section 5

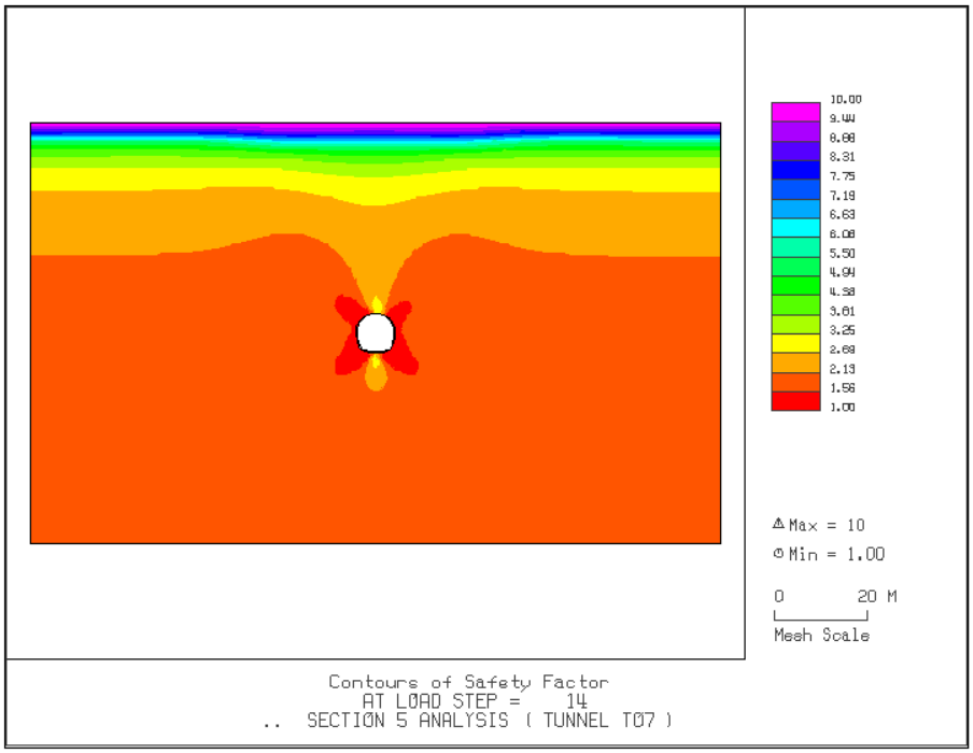

Figure 5-34 Color Contours of Safety Factor Section 5

5.8.3 Numerical simulation plot Safety Factor for Section 2

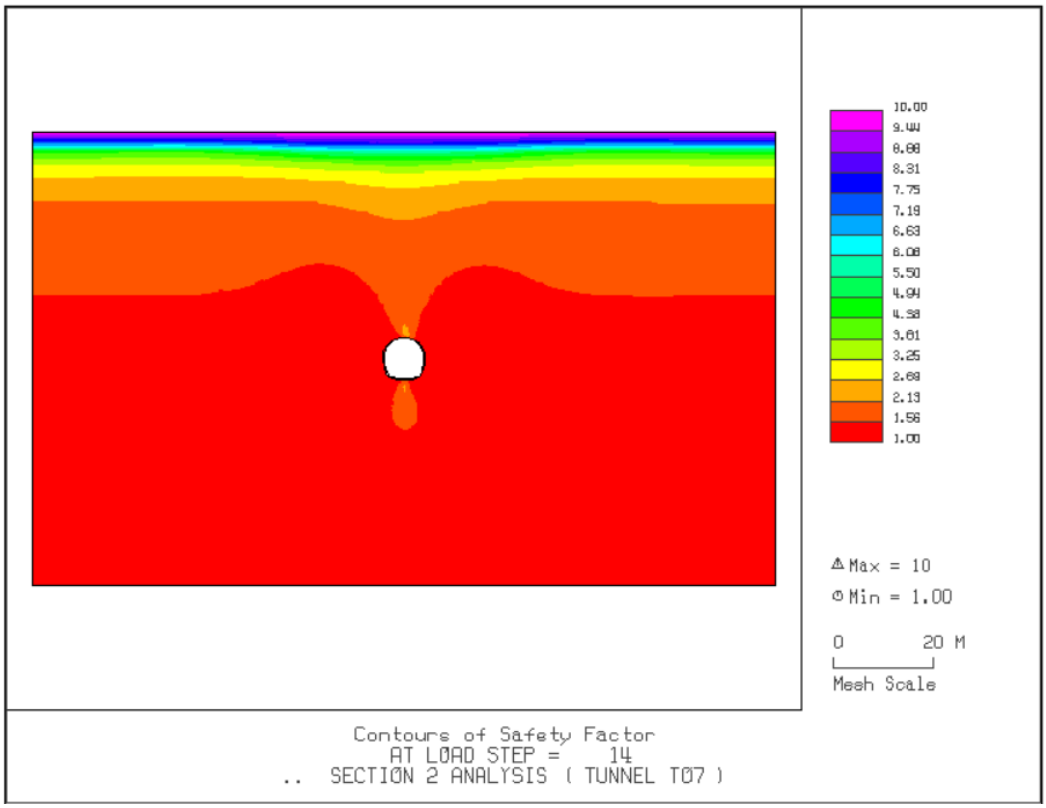

Figure 5-35 Color Contours of Safety Factor Section 2

The Safety Factor, SF against shear failure is the ratio of the strength of the rock mass to deviator stress. In table 5-21, the maximum Safety Factor is 2.69 near tunnel crown excavation as seen in Figure 5-33 and Figure 5-34 (Section 4 and Section 5) respectively. The maximum Safety Factor is 10 and is estimated at the top mesh boundary in the vertical at a distance greater than 4D to 5D measured from axis the tunnel about the spring line. In Figure 5-35, Section 2, the maximum SF is 2.19 in the vicinity of the tunnel excavation above the tunnel crown and the minimum SF is 1 at surrounding excavation side walls in both the highly fractured and moderately fractured rock mass.

It can be concluded that rock mass in terms of strength is greater than the computed stresses, thus there is no overstress in the rock mass. According to Greer, [39] the SF greater than 1.0 implies that the induced stresses less than the rock mass strength at all excavation load steps. When the SF is less than 1.0, the induced stresses are greater than the rock mass strength thus the rock mass surrounding the excavation is overstressed and highly susceptible to plastic rage behavior.

5.9 Axial Stress of Rock bolt

Table 5-23 Summary of Axial Stress on the Rock Bolts

Studied Sections	Soil/Rock Type	Axial stress on rock bolts (t/m^2)	Axial stress on rock bolt (kN/m^2)
Section 2	Rock C2 in fault zone (Highly fractured)	26,000	254,902
Section 4	Rock B-C rock in Transition to fault zone (Moderately fractured)	13,280	127,647
Section 5		25,480	249,804

Support capacity of rock bolting is assumed to be given by the capacity of each bolt divided by the area it has to support. The ultimate load capacity is $230\ \mathrm{kN/m^2}$, for diameter 26 mm rock bolts.

5.9.1 Numerical simulation plot Axial Stress of the rock bolts Section 4

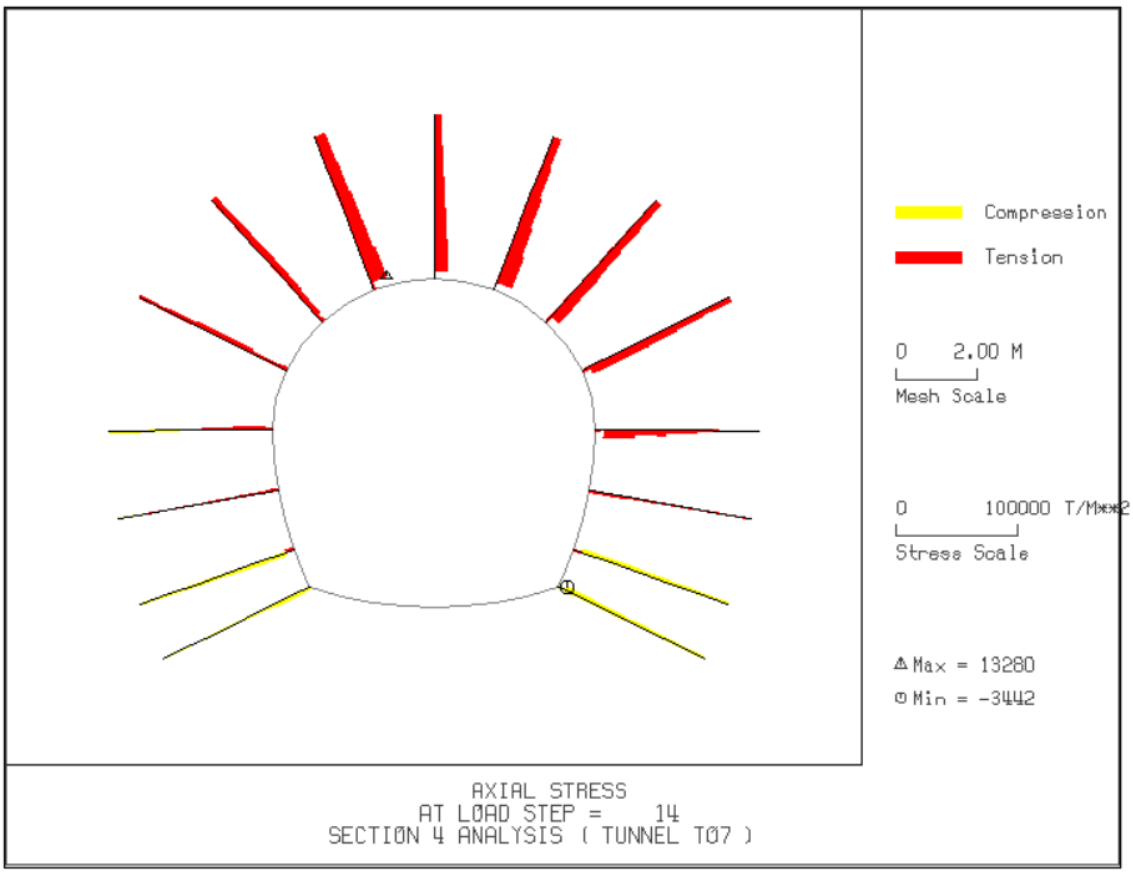

Figure 5-36 Axial Stress on the rock bolts Section 4

5.9.2 Numerical simulation plot Axial Stress of the rock bolts Section 5

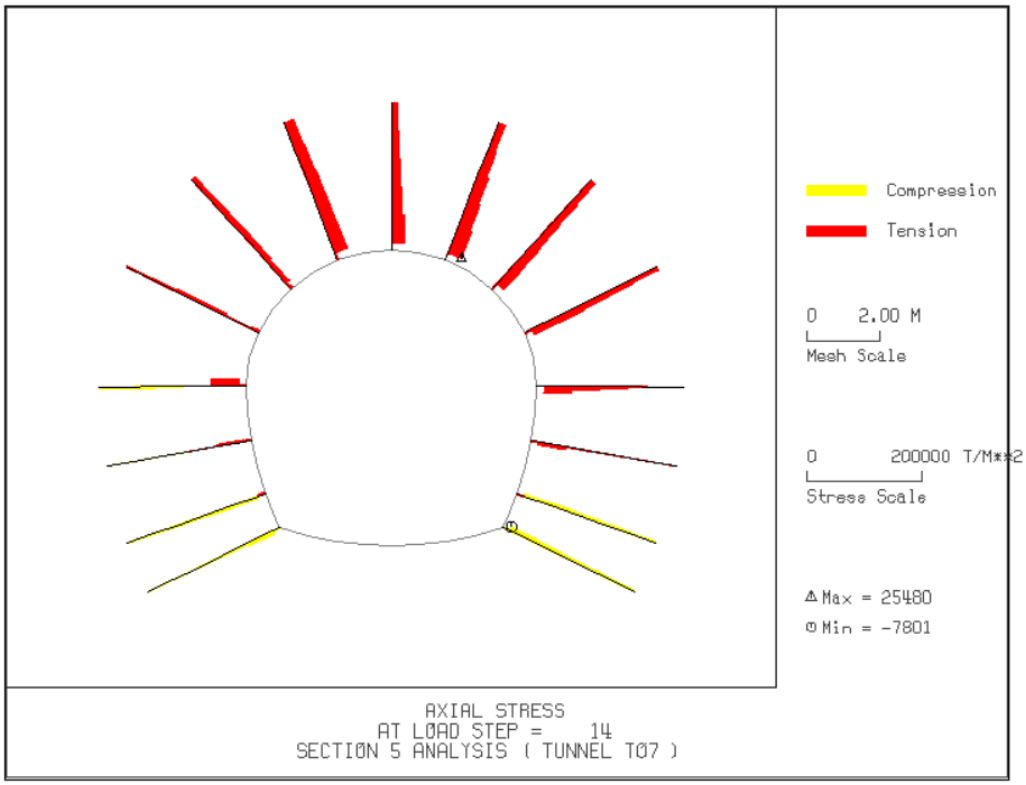

Figure 5-37 Axial Stress on the rock bolts Section 5

5.9.3 Numerical simulation plot Axial Stress of the rock bolts Section 2

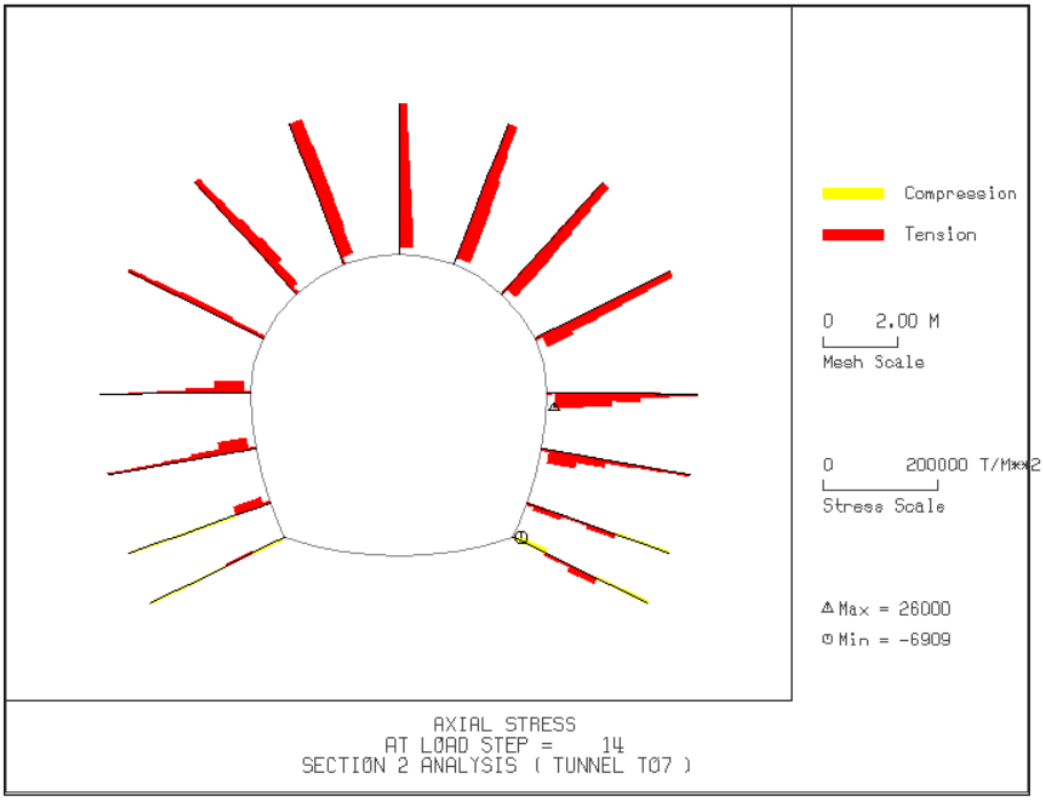

Figure 5-38 Axial Stress on the rock bolts Section 2

The axial stress on the rock bolts obtained from the finite element analysis is 249,804 kN/m^2 for highly fractured rock mass in Figure 5-38. Also, in case of high over burden 40 m, the axial stress on the rock bolt is higher than that in lower over burden 20 m for the same rock mass condition especially for moderately fractured rock in Figure 5-36 and 5-37 (Section 4 and Section 5) respectively. However, the maximum axial stress in the fully grouted rock bolts installed the tunnel crown since the over burden tend to exert much of the load at the crown.

5.9.4 Tunnel lining design and analysis

The evaluation of the ultimate limit state of the initial support considered partial factors 1.35 for the permanent loads and 1.5 for the variable loads according to the EuroCode2. The load combination used include the load due to the self-weight and loads due to the overburden. According to general practice, the loss of structural capacity of the supporting system is expected at long term, with the liner bearing ground and water pressure in the long term. The load combination is $[1.35 \times SW + 1.35 \times G + 1.35 \times GW]$ (where GW is the load due to the groundwater). No groundwater load is considered for the verification of the initial support and assumes that ground water level is not expected, thus, $GW = 0$. The following paragraphs describe the maximum thrust/axial forces; shear force, and bending moment (design values) computed in the Finite Element SMAP-S2 modelled as beam element (Final Lining). The ratio of the Young's modulus in degraded shotcrete to Young's modulus in hard shotcrete, REDH = 0.33

5.9.4.1 External Load for Lining Analysis

Table 5-24 External permanent load characteristics for lining Analysis

Property data	Lining Analysis		
	Section 2	**Section 4**	**Section 5**
Loosening load			
Horizontal pressure due to loosening load, HPRES (kN/m^2)	89.93	78.24	82.16
Vertical pressure due to loosening load, VPRES (kN/m^2)	269.79	234.73	246.48
Number of Load steps for loosening, (Max = 400)	3	3	3

5.9.4.2 Bending Moment in the lining

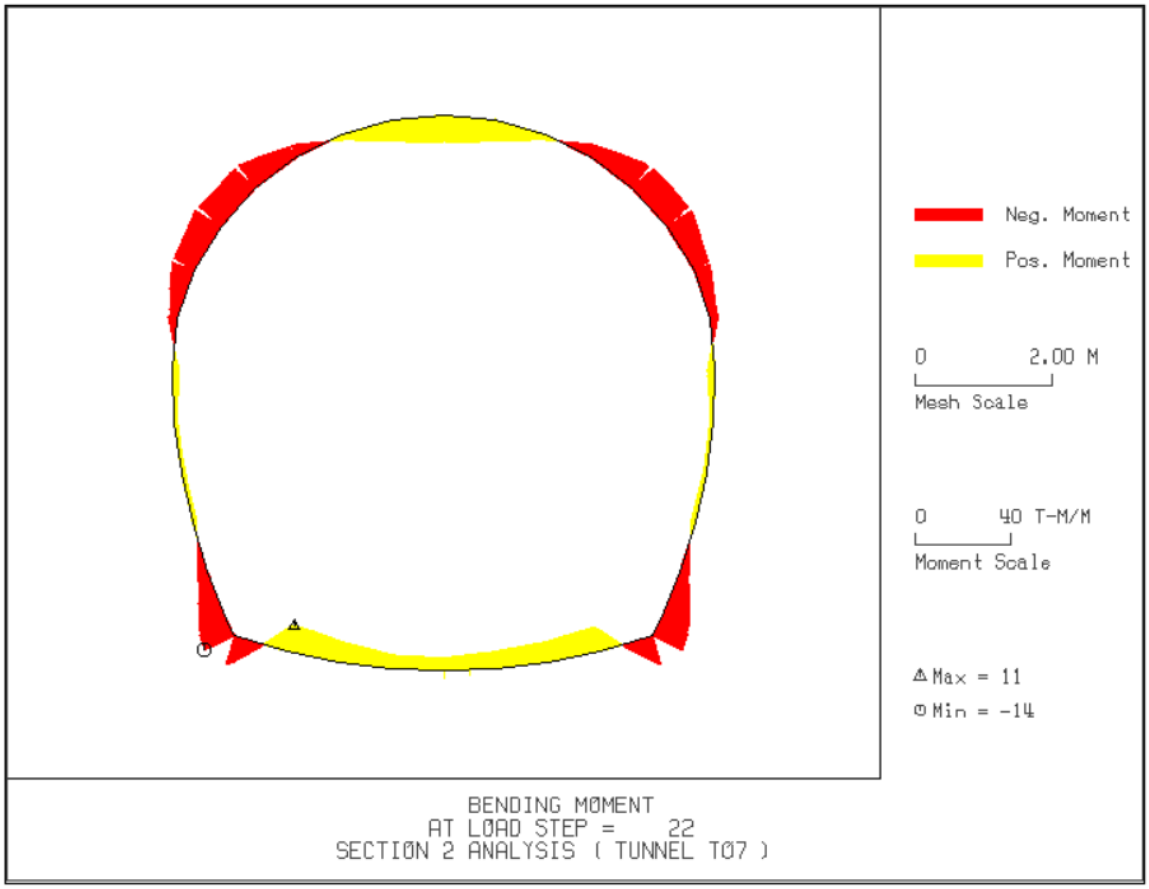

Figure 5-39 Bending Moment in lining Section 2

5.9.4.2.1 Tunnel lining resulting bending moment Validation

a) Moment capacity on the compression face is the lining is as follows

$$\emptyset M_{nc} = \emptyset 0.65 \cdot f_{ck} \cdot S \qquad (5.2)$$

M_{nc} = Nominal resistance of the compression face of concrete section, S = Section modulus of the lining section based on gross un-cracked section. f_{ck} = Characteristic compressive strength of the 28 days of plain concrete.

Calculating for section modulus as follows:

$$S = \frac{b_w \cdot h^2}{6} = \frac{1.0 \times 0.3^2}{6} = 0.015\ m^3,$$

$f_{ck} = 25$ Mpa,

$$\emptyset M_{nc} = (0.55 \times 0.85 \times (25 \times 000) \times 0.015)$$

$$= 175.31\ kNm/m$$

$$M_{nc} = \frac{175.31}{0.55} = 318.75\ \text{kNm/m} > M_d = 107.84\ \text{kNm/m}$$

Where: -$M_d = 11\ \text{tm/m}$ the maximum design bending moment.

Therefore, Moment capacity, i.e. the factored moment strength $\emptyset M_{nc}$ should be greater than the moment M_d caused by factored loads. For beams, being serviceable implies that the deformation, primarily the vertical deflection, must be limited.

b) Compressive strength of the lining is as follows

$$\emptyset P_c = \emptyset 0.6 \cdot f_{ck} \cdot A \qquad (5.3)$$

Where: -

P_c = Normial resistance of lining in compression, $\emptyset = 0.55$ for plain concrete, f_{ck} = characteristic compressive strength of the 28 days of plain concrete, and A = Cross sectional area section.

$$\emptyset P_c = [0.55 \times 0.6 \times (25 \times 1000) \times (1.0 \times 0.3)]$$
$$= 2{,}475\ \text{kN/m}^2$$

$$P_c = \frac{2475}{0.55} = 4{,}500\ \text{kN/m}^2$$

c) Check for compression face as follows: -

$$Q_A/_{\emptyset P_c} + Q_M/_{\emptyset M_{nc}} \leq 1.0 \qquad (5.4)$$

Where: Q_A = Axial load force (thrust in the lining) effect, $Q_M = M_T$ the moment force effect

$$\left(\left(\frac{129}{0.102}\right)/_{(2475)}\right) + \left(\left(\frac{11}{0.102}\right)/_{(175.31)}\right) \leq 1.0$$

$$(0.511) + (0.615) \leq 1.0$$

$$\mathbf{1.1 \cong 1.0}$$

Therefore, it can be concluded that the proposed final lining is safe from compression forces. It also expected that lining is checked for the tensile strength of the plain concrete.

5.9.4.3 Thrust and Shear in the lining

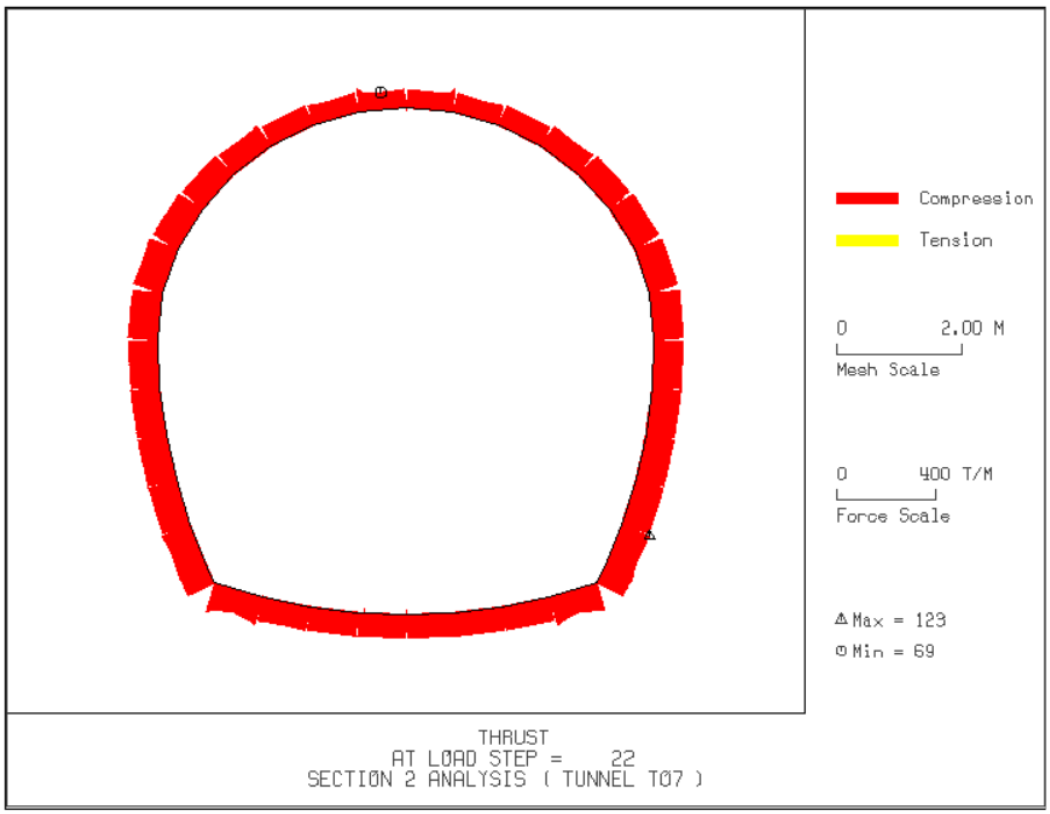

Figure 5-40 Line Thrust in lining Section 2

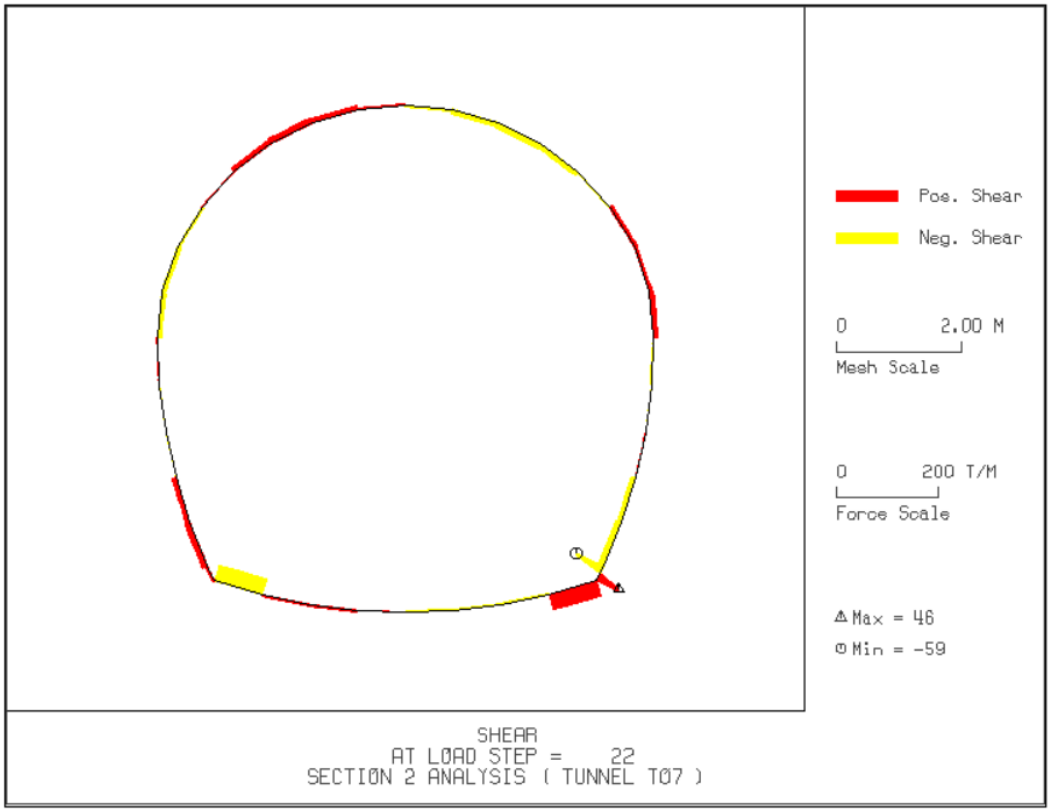

Figure 5-41 Shear in lining Section 2

5.9.4.3.1 Tunnel lining axial force/thrust Validation

Ultimate limit State: - Design resistance N_{Rd} to axial failure for the lining rectangular section under study. The design resistance in terms of axial force lining in plain concrete is calculated as follows; -

$$N_{Rd} = b_w \cdot h \cdot f_{cd} \cdot \emptyset \tag{5.5}$$

Where:- N_{Rd} = Thrust/Axial resistance, b_w = Overall width of the cross-section, h = overall depth of the cross-section and $\emptyset$ = is the factor taking into eccentricity, including second effects that take into account where they are likely to affect the overall stability of the lining structure significantly and for the attainment of the ultimate limit state at critical section according to EC2 5.8, for case used eccentricity 0.95 of a column which is usually less than 1 on the cross section.

$$N_{Rd} = (1.0 \times 0.3 \times (25 \times 1000) \times 0.95)$$

$$N_{Rd} = 7{,}125\ \text{kN/m}^2 \text{ But } N_d = 1{,}206\ \text{kN/m}^2$$

$$N_{Rd} > N_d$$

The thrust $N_d = 123\ \text{t/m}^2$ ($1206\ \text{kN/m}^2$) is less than the axial resistance, this is because the resistance is based on assumptions for purely plain concrete whereas the design axial force by SMAP simulation using FE analysis takes into consideration the presence of reinforcement bar that are important to increase the axial resistance of the entire lining section as they are able to withstand the imposed confining pressure.

Therefore, for plain concrete where the design value of the axial compressive is greater than the axial resistance, reinforcement bars placed in the lining. This phenomenon is true for horseshoe type of tunnel since they are prone to high stresses at the bottom edges/corner and thus the maximum axial/thrust is concentrated at such locations.

5.9.4.3.2 Tunnel lining Shear Resistance Validation

Shear design value under which no shear reinforcement is necessary for the final lining unreinforced in shear. The design value for shear resistance $V_{Rd,c}$ and according to the Euro code 2 for concrete structures under ULS or EN 1992: 1-1

$$V_{Rd,c} = \left[C_{Rd,c}\, k(100\rho_1 f_{ck})^{\frac{1}{3}} + k_1 \sigma_{cp}\right] \cdot b_w \cdot d \tag{5.6}$$

The minimum value for $V_{Rd,c}$ based on the V_{min} (N/mm^2) can be selected from the Equation 4.9 below

$$V_{Rd,c} = V_{min} \cdot b_w \cdot d \tag{5.7}$$

For $k = \left[1 + \left(\sqrt{200/d}\right)\right] = 1.89$ and $f_{ck} = 25$ MPa

$$V_{min} = 0{,}035 \cdot k^{3/2} \cdot f_{ck}^{1/2}$$

$$\mathbf{V_{min} = 0.4547\ N/mm^2}$$

Check for minimum value for $V_{Rd,c}$ gives for $b_w = 1000$ mm and $d = 250$ mm

$$V_{Rd,c} = 113{,}676.5183\ N$$

$$V_{Rd,c} = 113.676\ kN$$

$$\mathbf{V_{Rd,c} \approx 11.595\ t}$$

For validation, the effective height $d = 250$ mm for the lining of thickness $h = 300$ mm and shotcrete 0.2 m with 15 rock bolts at $S_c = 1.5$ m and $S_l = 1.0$ m in the supporting system for permanent condition.

The maximum shear force acting on the lining is $\mathbf{V_{ed}} = 46$ t/m from SMAP lining analysis which is approximately 450.98 kN/m.

Where: - $\mathbf{V_{ed} \leq V_{Rd,c}}$, no calculated shear reinforcement is necessary. Form the result, $\mathbf{V_{ed}}$ is the design shear force in the section simulated and resulting from external loading for the considered load combination.

$\boldsymbol{\gamma_C}$ = Partial safety factor for concrete	**1.5**
$\mathbf{C_{Rd,c}}$ = Coefficient derived from the tests (recommend 0.12) = $(\mathbf{0.18/\gamma_C})$ for NDC (normal density concrete)	0.12
$\mathbf{k}$ = size factor = $\left[\mathbf{1} + \left(\sqrt{\mathbf{200/d}}\right)\right]$	1.89
$\boldsymbol{\rho_1}$ = longitudinal reinforcement ration (<0.02) = $(\mathbf{A_{st}/A_c})$	0.0015
$\mathbf{A_{st}}$ = longitudinal reinforcement area considering wire mesh area = $(\mathbf{mm^2})$	442.44

$\mathbf{f_{ck}}$ = Characteristic concrete compressive strength =25 **Mpa**	25
$\mathbf{b_w}$ = smallest lining section width in the tensile area ($\mathbf{mm}$)	1000
$\mathbf{N_d}$ = Compressive force (Maximum Thrust) ($\mathbf{kN}$)	1206
$\boldsymbol{\sigma_{cp}}$ = concrete compressive stress at the centroid axis due to axial loading = $(\mathbf{N_d/A_c})$ $(\mathbf{N/mm^2})$	4.02
$\mathbf{k_1}$ = Coefficient , with recommend value	0.15
$\mathbf{A_c}$ = Concrete lining Cross section area ($\mathbf{mm^2}$)	300000
$\mathbf{V_{Rd,c}}$ ($\mathbf{kN}$)	**238.3**
$\mathbf{V_{Rd,c}}$ ($\mathbf{t}$)	23.86

Therefore, since $\mathbf{V_{ed} > V_{Rd,c}}$, according to EC2, sufficient shear reinforcement is required, thus tension reinforcement bars provided to resist any additional tensile force caused by shear. The following page presents the summary results for the analysis result/ output.

5.9.4 Summary of SMAP Numerical Solution, Analytical Validation Solution and AKH design Solution for Tunnel T07.

No.	Result/ Output	Studied Sections	Soil/Rock Type	Tunnel Stability Solution			Remark
				SMAP Numerical	Analytical	AKH design	
1	Maximum Vertical displacement	Section 2	Rock C2	50.23 mm	51.0 mm	50.0 mm	Maximum stress agrees well with other methods
		Section 4	Rock B-C	24.60 mm	12.0 mm	18.5 mm	
		Section 5		36.97 mm	29.8 mm	32.5 mm	
3	Maximum Major Principal Stress	Section 2	Rock C2	1,912 kN/m^2	920 kN/m^2	2000 kN/m^2	Displacements agree with AKH design
		Section 4	Rock B-C	1,137 kN/m^2	480 kN/m^2		
		Section 5		2,020 kN/m^2	960 kN/m^2		
4	Rock Bolt Axial Force	Section 2	Rock C2	254,902 kN/m^2	n/a.	500 MPa Characteristic yield strength of Steel	Axial stress is less than the yield strength.
		Section 4	Rock B-C	127,647 kN/m^2			
		Section 5		249,804 kN/m^2			
5	Maximum Safety Factor	Section 2	Rock C2	2.19	$SF \geq 1$	5.28 - 8.52	Tunnel excavation is reported safe
		Section 4	Rock B-C	2.69			
		Section 5		2.69			
6	Liner Bending Moment	Section 2	Rock C2	107.84 kNm/m	175.31 kNm/m	80 kNm/m	200 mm Shotcrete, 300 mm liner class 25 MPa, fitted using 6.5 mm diameter, 150 mm *150 mm, fyk = 500 MPa wire mesh
7	Liner Thrust/Axial Force	Section 2	Rock C2	1,265 kN/m	7,125 kN/m	1,860 kN/m	
8	Liner Shear Force	Section 2	Rock C2	450.98 kN/m	238.3 kN/m	180 kN/m	

CHAPTER 6 CONCLUSIONS AND RECOMMENDATIONS

6.1 Introduction

The following conclusions, recommendations, and future works are presented.

6.1.1 Conclusion

The following conclusions were made from the study: -

1. The solution for ground surface dispalacments varies depending on rock mass condition and is higher in lower over burden rock mass compared to that of main tunnel section in high rock mass over burden but in the same rock mass conditions.
2. Numerical solution by FEM for computed displacements around the tunnel is higher in maximum rock mass overburden and varies depending on the rock mass conditions.
3. In this study, an ultimate compressive major principal stress of $2{,}020\ \mathrm{kN/m^2}$ was comuputed for the main tunnel and the corresonding supporting system design forces in the final lining i.e liner bending moment of 107.84 kNm, thrust/axial force of 1,265 kN and Shear force of 450.98 kN was simulate for Tunnel T07 rock mass and the rock bolt pattern for each rock bolt with an ultimate load capacity of $230\ \mathrm{kN/m^2}$, for diameter $26\ \mathrm{mm}$ diameter and fully grouted rock bolts was estimated numerically.

6.1.2 Recommendation

This research provides a thorough knowledge of estimated tunnel deformations and simplification of a list of assumptions used in the analysis. However, 2-D static analysis was employed in the study. Recommendations on future works are as follows: -

- A study on the seismic analysis on tunnel excavation and perform the 3-D analysis in fault zones to understand the overall deformations induced during tunneling.
- An investigation into the fore poling umbrella foreseen in case of soil conditions and when crossing critical sections
- Numerical Analysis for initial stress on natural ground condition prior to tunneling excavation and comparison between site exploration by monitoring.
- Precast concrete lining analysis and design of rock support for tunnels in weak rock mass based on Norwegian Method of Tunneling (NMT).

REFERENCES

[1] Mihalis, I.K; Kawadas, M.J.; Anagnostopoulo, A.G., Tunnel Stability Factor - A new parameter for weak rock tunneling, Greece, 2008.

[2] Michaela, Kavvadas; Dimitrisa, Litsas; Ioannisb, Vazaios; Petrosc, Fortsakis, "Development of a 3D finite element model for shield EPB tunnelling," pp. 22-34, May 2017.

[3] L. Sousa, "Risk Analysis for Tunneling Projects," 2010.

[4] Thomas Konstantis., Spyridon Konstantis; Panagiotis Spyridis, Tunnel Losses: Causes, Impact, Trends and Risk Engineering Management, 2016.

[5] Mohammed, J., "Underground structures Support, Stress and Strain of Tunnel," 2015.

[6] Johansson, F., Bjureland, W.; Spross, J., "Application of reliability-based design methods to underground excavation in rock," Stockholm:BeFo., In press.

[7] Stille, H.; Eriksson, M.; Nord, G., "Kompendium i bergmekanik.," Stockholm, 2005a..

[8] Ongodia E.J, "Geotechnical engineering design of a tunnel support system," 2017.

[9] Basarir, H., Ozsan, A., Karakus, M., Analysis of support requirements for a shallow diversion tunnel at Guledar dam site, 2005, pp. P.131-145..

[10] Zhu, Weishen, Li, Shucai, Li, Shuchen, et al., Systematic numerical simulation of rock tunnel stability considering different rock conditions and construction effects, 2003, pp. P.31-536.

[11] Beaver, P, "A History of Tunnels the Citadel Press.," 1972.

[12] Megaw and Barlett, "Tunnels: Planning, Design, Construction," West Sussex, Ellis Horwaod limited, 1981, pp. pp.11-18.

[13] Terzaghi, K., Rock Deffects and Loads on Tunnel Supports., The Commercial Shearing & Stamping Co., 1946.

[14] Sinha, R., Undergriund Structures Design and Instrumenation, Amsterdam: Elsevier, 1989, pp. pp 17-19.

[15] Kastner, H., Statik does Tunnel - and Stollen Baues, 1962.

[16] Marie, J., "Tunneling: Mechanics and Hazards.," 1998. [Online]. Available: http://www.umich.edu/~gs265/tunnel.html. [Accessed 9 October 2018].

[17] Palmstrøm_et.al., "Proper extent of site investigations for under- ground excavations," Report R&D project “Tunnels for the Citizens”. Publication No. 101, p. 116, 2003.

[18] Rønning, J., "Newer pre-investiagtions methods for tunnels," 2003.

[19] Nilsen, A. and Palmstrom, B. "Engineering Geology and Rock Engineering”.," Norwegian Group for Rock Mechanics, Handbook, p. 249, 2000.

[20] Barton, R. Lien and Lunde, "Engineering classification of rock masses for design of tunnel support," 1974, pp. 189-236.

[21] Bieniawski, Z.T, Geomechanics Classification of Rock Masses and its Application in Tunneling., vol. Vol.IIA, Denver, 1974, pp. 27-32.

[22] Geol, R. K., Status of tuneling in and underground construiton activites and technologies India, 2001, pp. 63-75.

[23] NEH, "Engineering Classification of Rock Materials , National Engineering Handbook (NEH)," 2012.

[24] Hoek, E. Practical Rock Engineering, Vancouver: Evert Hoek Consulting Engineer, 2007.

[25] Herget, G. Stresses in Rock, Rotterdam: A.A Balkema, 1988.

[26] Chen, W.F., Limit Analysis and Soil Plasticity, Developments in Geotechnical in Geotechnical Engineering, Amsterdam.: Elsevier Scientific,, 1975.

[27] Perri, G., Behavior Category and Design Loads for Conventionally Excavated Tunnels, 2007.

[28] Gunnar Arnar., Rock Mass Classification and Reinforcement Strategies for Tunnels in Iceland, 2008.

[29] Singh B. and Goel, R. K."Tunnelling in Weak Rocks," vol. 5, J. A. H. FREng, Ed., Elsevier Ltd, 2006, pp. 183-195.

[30] Kacar Onur., 3D Finite Element Modelling of Surface Excavation and Loading over Existing Tunnels, 2007, p. 114.

[31] Potts, D. and Zdravkovic, Finite element analysis in geotechnical engineering-theory, Thomas Telford, London, 2001, pp. 135-167.

[32] Jing, L and Hudson, J. "Numerical methods in rock mechanics," International Journal of Rock Mechanics & Mining Sciences, vol. Vol. 39, pp. 409-427, 2002.

[33] Comtec Research TUNA, TUNA. TUNnel Analysis Software, 2018.

[34] AFTES Recommendation., The Convergence-Confinment method, 2001.

[35] Yapi Merkezi., "Tunnel T07 - Excavation and Support Design Report," Yapi Merkezi, Addis Ababa, 2015.

[36] Moller, S. C., Tunnel induced settlements and structural forces in linings, Stuttgart, Germany, 2006.

[37] Perri, G.,, Behavior Category and Design Loads for Conventionally Excavated Tunnels, 2007.

[38] Greer, A.J, Finite Element Modeling and Stress Analysis of Unferground Rock Cavern, University of California., California: ProQuest Dissertations Publishing, 2012, 2012.

[39] Euro Code 2., EN 1992 -1-1:2004 - Euro Code 2 - Design of Concrete Strucutres Part 1-1 General Rules and Rules for Building., 2004.

[40] Meißner, H., Tunnelbau unter tage–empfehlungen desarbeitskreises 1.6 “numerik in der geotechnik” abschnitt 2,”, vol. 19, 1996, p. 99–108.

APPENDIX 1

Calculation regarding R4 for ISTYPE = 1 in TUNA Plus,

Normally, they assume R4 by trials.

Here, I solved for exact R4 given Invert Depth (d)

Step 1.

Compute k = d / h

where h is Invert Half width

Refer to TUNA Plus Example Problem 1

Step 2.

Solve Equation (5) to get angle A4

Step 3.

Get R4 from Equation (1).

Note:

TUNA Plus Example problem 1 assumes Invert Depth of d = 0.4328 m

Computing R_4, given Invert Depth d
For ISTYPE = 1 ($A_1 + A_2 = 90°$)

2019.04.30 1/2
K.J. Kim

Figure 1.

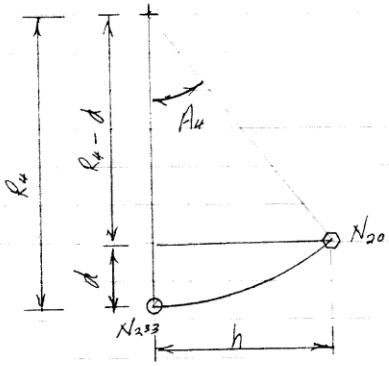

$$R_4 \sin A_4 = h \quad (1)$$

$$R_4 (1 - \cos A_4) = d \quad (2)$$

From (1) and (2)

$$\sin A_4 = k \cdot (1 - \cos A_4), \quad k = (h/d) \quad (3)$$

$$\rightarrow (1 - \cos^2 A_4) = k^2 (1 - 2\cos A_4 + \cos^2 A_4)$$

$$\rightarrow (k^2 + 1)\cos^2 A_4 - 2k^2 \cos A_4 + k^2 - 1 = 0 \quad (4)$$

Solving Equation (4) for $\cos A_4$

$$\boxed{\cos A_4 = \frac{k^2 - 1}{k^2 + 1}} \quad (5)$$

For given h, assume Invert Depth d, then $k = h/d$
Solve Equation (5) for A_4
Then get R_4 from Equation (1).

ibi

TUNA plus Example Problem 1

$$\begin{bmatrix} A_1 = 60^\circ & R_1 = 5.24\ m \\ A_2 = 30^\circ & R_2 = 4.24\ m \\ A_3 = 19.781^\circ & R_3 = 9.86\ m \end{bmatrix}$$

X Coordinate of Spring Line (Node No 14)

$$\begin{aligned} X_{14} &= X_2 + R_2 \\ &= (R_1 \sin A_1 - R_2 \cos A_2) + R_2 \\ &= (5.24 \sin 60^\circ - 4.24 \cos 30^\circ) + 4.24 \\ &= 5.1060\ m \end{aligned}$$

Invert Half Width (h) $\longrightarrow$ (Node No 20)

$$\begin{aligned} h &= R_3 \cos A_3 - (R_3 - (X_2 + R_2)) \\ &= R_3 \cos A_3 - (R_3 - X_{14}) \\ &= 9.86 \cos 19.781^\circ - (9.86 - 5.1060) \\ &= 4.5242\ m \end{aligned}$$

Assume Invert Depth (d) $\longrightarrow$ (Node No 233)

$$d = 0.4328\ m$$

Now compute k and A_4 from Equation (5)

$$\begin{aligned} k &= h / d \\ &= 4.5242 / 0.4328 \\ &= 10.4533 \end{aligned}$$

$$\begin{aligned} A_4 &= \cos^{-1}((k^2-1)/(k^2+1)) \\ &= \cos^{-1}((10.4533^2-1)/(10.4533^2+1)) \\ &= 10.929^\circ \end{aligned}$$

Finally Compute R_4 from Equation (1)

$$\underline{\underline{R_4}} = h / \sin A_4 = 4.5242 / \sin 10.929^\circ$$

$$= \underline{\underline{23.8628\ m}}$$

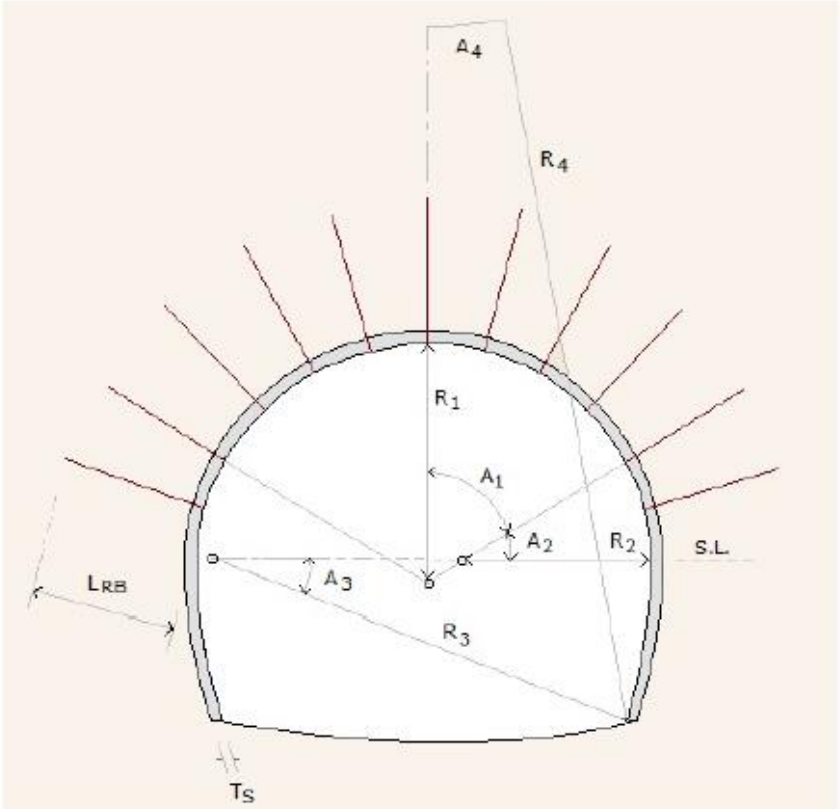

R_1	=	5.24 M	A_1	=	60°
R_2	=	4.24 M	A_2	=	30°
R_3	=	9.86 M	A_3	=	19.781°
R_4	=	23.86 M			

Number of Rock Bolts (NUMRB)	=	11
Length of Rock Bolts (LRB)	=	3.0 M
Spacing of Rock Bolts (TSPACING)	=	1.2 M
Thickness of Shotcrete (TS)	=	15 Cm
Thickness of Liner (TL)	=	30 Cm
Reinforcing Bar Area (ASI)	=	22 Cm^2
Reinforcing Bar Area (ASO)	=	22 Cm^2

Figure 6.1 Tunnel dimensions for Example 1

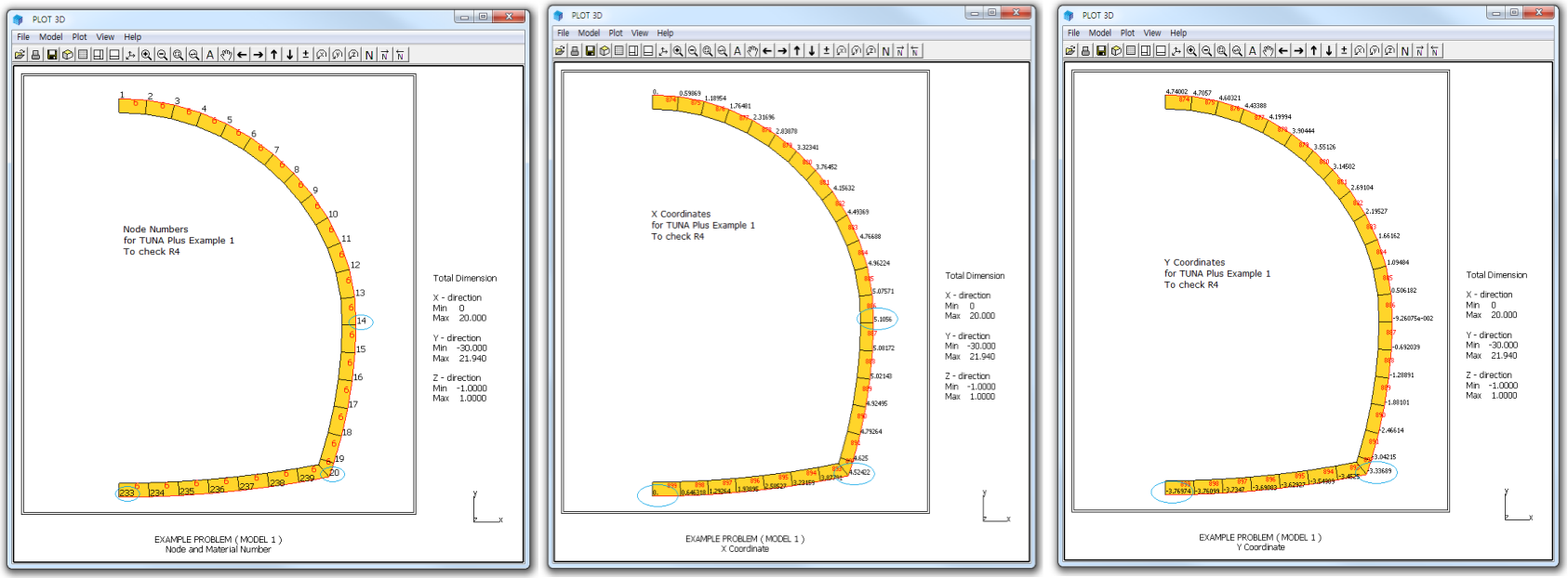
PLOT 3D
File Model Plot View Help
Node Numbers
for TUNA Plus Example 1
To check R4
Total Dimension
X - direction
Min 0
Max 20.000
Y - direction
Min -30.000
Max 21.940
Z - direction
Min -1.0000
Max 1.0000
EXAMPLE PROBLEM (MODEL 1)
Node and Material Number
PLOT 3D
File Model Plot View Help
X Coordinates
for TUNA Plus Example 1
To check R4
Total Dimension
X - direction
Min 0
Max 20.000
Y - direction
Min -30.000
Max 21.940
Z - direction
Min -1.0000
Max 1.0000
EXAMPLE PROBLEM (MODEL 1)
X Coordinate
PLOT 3D
File Model Plot View Help
Y Coordinates
for TUNA Plus Example 1
To check R4
Total Dimension
X - direction
Min 0
Max 20.000
Y - direction
Min -30.000
Max 21.940
Z - direction
Min -1.0000
Max 1.0000
EXAMPLE PROBLEM (MODEL 1)
Y Coordinate

APPENDIX 2

Parameter description of RMR, rock mass rating

Table 4.4: Rock Mass Rating System (After Bieniawski 1989).

A. CLASSIFICATION PARAMETERS AND THEIR RATINGS									
Parameter			Range of values						
1	Strength of intact rock material	Point-load strength index	>10 MPa	4 - 10 MPa	2 - 4 MPa	1 - 2 MPa	For this low range - uniaxial compressive test is preferred		
		Uniaxial comp. strength	>250 MPa	100 - 250 MPa	50 - 100 MPa	25 - 50 MPa	5 - 25 MPa	1 - 5 MPa	< 1 MPa
	Rating		15	12	7	4	2	1	0
2	Drill core Quality RQD		90% - 100%	75% - 90%	50% - 75%	25% - 50%	< 25%		
	Rating		20	17	13	8	3		
3	Spacing of discontinuities		> 2 m	0.6 - 2 . m	200 - 600 mm	60 - 200 mm	< 60 mm		
	Rating		20	15	10	8	5		
4	Condition of discontinuities (See E)		Very rough surfaces Not continuous No separation Unweathered wall rock	Slightly rough surfaces Separation < 1 mm Slightly weathered walls	Slightly rough surfaces Separation < 1 mm Highly weathered walls	Slickensided surfaces or Gouge < 5 mm thick or Separation 1-5 mm Continuous	Soft gouge >5 mm thick or Separation > 5 mm Continuous		
	Rating		30	25	20	10	0		
5	Ground water	Inflow per 10 m tunnel length (l/m)	None	< 10	10 - 25	25 - 125	> 125		
		(Joint water press)/ (Major principal σ)	0	< 0.1	0.1, - 0.2	0.2 - 0.5	> 0.5		
		General conditions	Completely dry	Damp	Wet	Dripping	Flowing		
	Rating		15	10	7	4	0		

B. RATING ADJUSTMENT FOR DISCONTINUITY ORIENTATIONS (See F)						
Strike and dip orientations		Very favourable	Favourable	Fair	Unfavourable	Very Unfavourable
Ratings	Tunnels & mines	0	-2	-5	-10	-12
	Foundations	0	-2	-7	-15	-25
	Slopes	0	-5	-25	-50	

C. ROCK MASS CLASSES DETERMINED FROM TOTAL RATINGS					
Rating	100 ← 81	80 ← 61	60 ← 41	40 ← 21	< 21
Class number	I	II	III	IV	V
Description	Very good rock	Good rock	Fair rock	Poor rock	Very poor rock

D. MEANING OF ROCK CLASSES					
Class number	I	II	III	IV	V
Average stand-up time	20 yrs for 15 m span	1 year for 10 m span	1 week for 5 m span	10 hrs for 2.5 m span	30 min for 1 m span
Cohesion of rock mass (kPa)	> 400	300 - 400	200 - 300	100 - 200	< 100
Friction angle of rock mass (deg)	> 45	35 - 45	25 - 35	15 - 25	< 15

E. GUIDELINES FOR CLASSIFICATION OF DISCONTINUITY conditions					
Discontinuity length (persistence)	< 1 m	1 - 3 m	3 - 10 m	10 - 20 m	> 20 m
Rating	6	4	2	1	0
Separation (aperture)	None	< 0.1 mm	0.1 - 1.0 mm	1 - 5 mm	> 5 mm
Rating	6	5	4	1	0
Roughness	Very rough	Rough	Slightly rough	Smooth	Slickensided
Rating	6	5	3	1	0
Infilling (gouge)	None	Hard filling < 5 mm	Hard filling > 5 mm	Soft filling < 5 mm	Soft filling > 5 mm
Rating	6	4	2	2	0
Weathering	Unweathered	Slightly weathered	Moderately weathered	Highly weathered	Decomposed
Ratings	6	5	3	1	0

F. EFFECT OF DISCONTINUITY STRIKE AND DIP ORIENTATION IN TUNNELLING**			
Strike perpendicular to tunnel axis		Strike parallel to tunnel axis	
Drive with dip - Dip 45 - 90°	Drive with dip - Dip 20 - 45°	Dip 45 - 90°	Dip 20 - 45°
Very favourable	Favourable	Very unfavourable	Fair
Drive against dip - Dip 45-90°	Drive against dip - Dip 20-45°	Dip 0-20 - Irrespective of strike*	
Fair	Unfavourable	Fair	

* Some conditions are mutually exclusive . For example, if infilling is present, the roughness of the surface will be overshadowed by the influence of the gouge. In such cases use A.4 directly.
** Modified after Wickham et al (1972).

APPENDIX 3

Guidelines for excavation and support rock tunnels in accordance with the RMR system

Rock Mass Class	Excavation	Support		
		Rock Bolts (20-mm Dia, Fully Grouted)	Shotcrete	Steel Sets
Very good rock I RMR:81–100	Full face 3-m advance	Generally, no support required except for occasional spot bolting		
Good rock II RMR:61–80	Full face 1.0–1.5-m advance Complete support 20 m from face	Locally, bolts in crown 3 m long, spaced 2.5 m, with occasional wire mesh	50 mm in crown where required	None
Fair rock III RMR: 41–60	Top heading and bench 1.5–3-m advance in top heading Commence support after each blast Complete support 10 m from face	Systematic bolts 4 m long, spaced 1.5–2 m in crown and walls with wire mesh in crown	50–100 mm in crown and 30 mm in sides	None
Poor rock IV RMR: 21–40	Top heading and bench 1.0–1.5-m advance in top heading. Install support concurrently with excavation 10 m from face	Systematic bolts 4–5 m long, spaced 1–1.5 m in crown and wall with wire mesh	100–150 mm in crown and 100 mm in sides	Light to medium ribs spaced 1.5 m where required
Very poor rock V RMR: <20	Multiple drifts 0.5–1.5-m advance in top heading. Install support concurrently with excavation. Shotcrete as soon as possible after blasting	Systematic bolts 5–6 m long, spaced 1–1.5 m in crown and walls with wire mesh. Bolt invert	150–200 mm in crown, 150 mm in sides, and 50 mm on face	Medium to heavy ribs spaced 0.75 m with steel lagging and fore-poling if required. Close invert

(After Bieniawski 1989).

APPENDIX 4

General chart for GSI estimates from geological observations.